2015

Hybrid Electronic Materials: Characterization and Thin-film Deposition

Kalyan Chakravarthy Kanakamedala
Louisiana State University and Agricultural and Mechanical College

HYBRID ELECTRONIC MATERIALS: CHARACTERIZATION AND THIN-FILM DEPOSITION

A Dissertation

Submitted to the Graduate Faculty of the
Louisiana State University and
Agricultural and Mechanical College
in partial fulfillment of the
requirements for the degree of
Doctor of Philosophy

in

Division of Electrical and Computer Engineering
The School of Electrical Engineering and Computer Science

by
Kalyan Chakaravarthy Kanakamedala
B.Tech, Jawaharlal Nehru Technological University, 2008
August 2015

Dedicated to

Kanakamedala Rajeswari
Kanakamedala Nageswara Rao
Kanakamedala Sowmya
Kanakamedala Senaka Krishna
and rest of the family

ACKNOWLEDGEMENTS

I would like to express my deep gratitude to many people that made this work possible:

Dr. Theda Daniels-Race: This work would not have been possible without your constant encouragement and unwavering belief in me throughout my tenure here at LSU. You have always inspired me with your scientific temper, never-quitting attitude towards science and life. I am indebted for your valuable guidance, caring nature that made this tedious journey easier.

Doctoral research committee: Dr. Martin Feldman, Dr. Georgios Veronis, Dr. Cristiana Sabliov and Dr. Yuri Antipov for your valuable time and suggestions that contributed towards this work. Dr. Georgios Veronis was always approachable to discuss any scientific problems.

Dr. Martin Feldman: Your nonchalant way of approach to scientific problems has always inspired me and working as your teaching assistant taught me the importance of patience and forgiveness.

Dr. Pratul Ajmera: For your encouragement to pursue research in my initial years at LSU that helped me start my journey down this path.

Dr. Cristiana Sabliov: Encounters with you started with taking your nanotechnology course and which turned into part of my research work. Your constant encouragement throughout years, also providing with valuable advice and research materials was very helpful.

Mr. Christopher E O' Loughlin: For being not just a lab manager but being a good friend. Also for taking interest in my research, helping me around the clock and being there for me to rely upon in research endeavors and otherwise.

Mr. Golden Hwaung: Helping me in the initial years to survive LSU and looking after me all the time.

Dr. Anirban Sarkar: For always extending a helpful hand when needed and providing with your valuable advice that proved very helped in later years of PhD.

Ms. Lori Patternson: Working for you have taught me that little kindness and encouragement can go far.

Colleagues: Would like to thank Dr. Pradeep Pai, Dr. Naga Korivi, Madhavi Divakar, Naveen Naryan Jagadish, Subhodip Maulik, Sean Hou and Kim Jeonghwan for helpful disscussions and constant support.

Family and Friends: You guys (you know who you are) has been the invisible net that has supported me through all these years to get me through the up and downs of the graduate life. Also Rachatigers for making this journey a tad bit easier and fun.

I would also like to thank the Louisiana Board of Regents for their partial financial support of this work. Also would like to thank Dr. Kristina Johnson of Enduring Hydro for her generous financial support. We are also grateful for Electronic Material and Device Laboratory (EMDL) within the Division of Electrical & Computer Engineering (LSU) for providing with various research facilities to pursue this work.

TABLE OF CONTENTS

ACKNOWLEDGEMENTS iii

LIST OF TABLES viii

LIST OF FIGURES ix

ABSTRACT xiii

CHAPTER 1: BRIEF DESCRIPTION OF CHAPTER CONTENT 1

CHAPTER 2: INTRODUCTION AND LITERATURE REVIEW 3
2.1: Electronics at the Nanoscale 3
2.2: Hybrid Electronic Materials 5
2.3: Thin-film deposition methods 7
2.3.1: Electrospraying 9
2.3.2: Needle electrospraying 11
2.3.3: Electrospraying parameters 13
2.4: Analytical Methods and Instruments Used 14
2.4.1: Atomic Force Microscopy 14
2.4.2: Conductive Probe Atomic Force Microscopy (CP-AFM) 21
2.4.3: Scanning Electron Microscopy 23

CHAPTER 3: MOTIVATION AND RESEARCH GOALS 25

CHAPTER 4: NANOGUMBOS: CHARACTERIZATION AND THIN-FILM DEPOSITION 26
4.1: Introduction 26
4.2: Group of Uniform Materials Based on Organic Salts (GUMBOS) 26
4.2.1: Synthesis of GUMBOS: General Techniques 28
4.2.2: Synthesis of nanoGUMBOS: Specific Species 30
4.3: Experimental setup 37
4.3.1: Substrate preparation 37
4.3.2: Atomic Force Microscopy (AFM) imaging 37
4.3.3: Conductive Probe Atomic Force Microscopy (CP-AFM) 38
4.3.4: Sample preparation of [R6G][TPB] nanoparticles 38
4.3.5: Test structure for characterization of [R6G][TPB] nanowires 39
4.3.6: Sample preparation of [PIC][BETI] and [PIC][NTf_2] 43
4.3.7: Sample preparation of [TC2][BETI] nanoGUMBOS for vapor sensing 43
4.3.8: Test structure for characterization of [TC2][BETI] nanoGUMBOS for vapor sensing 43
4.4: Results and Discussion 50
4.4.1: [R6G][TPB] nanoparticles: Imaging and I-V Characterization 50
4.4.2: [R6G][TPB] nanowires: Imaging and I-V Characterization 52
4.4.3: [PIC][BETI] and [PIC][NTf_2] nanoGUMBOS: Imaging and I-V Characterization. 55

4.4.4: [TC2][BETI] nanoGUMBOS: Direct analyte injection method 57
4.4.5: [TC2][BETI] nanoGUMBOS: Carrier gas method 58
4.5: Conclusions 61

CHAPTER 5: STUDY OF ELECTROSPRAY ASSISTED ELECTROPHORETIC DEPOSITION OF CARBON NANOTUBES ON NON-CONDUCTIVE SUBSTRATES 62
5.1: Introduction 62
5.1.1: Electrophoretic Deposition 63
5.1.2: Electrospray Deposition 64
5.2: Experimental Procedure: 66
5.2.1: Acid-refluxing of the carbon nanotubes 66
5.2.2: Preparation of electrospray and EPD CNT solution 66
5.2.3: Substrate preparation 67
5.2.4: Deposition of initial CNT layer by electrospraying 67
5.2.5: Electrophoretic deposition of CNTs 68
5.3: Results and Discussion 69
5.3.1: Resistivity measurements 72
5.3.2: Comparison of Raman spectra of different CNT samples: 76
5.4: Conclusions 78

CHAPTER 6: FARADAY ELECTROSPRAYING 79
6.1: Introduction 79
6.1.1: Porous electrospinning method 79
6.1.2: Multiple spikes electrospinning method 79
6.2: Faraday Electrospraying 80
6.2.1: Experimental setup 81
6.2.2: Results and Discussion 83
6.2.3: Conclusions 84

CHAPTER 7: SUMMARY AND RECOMMENDATIONS FOR FUTURE WORK 85
7.1: Summary of results 85
7.2: Recommendations for future work 87
7.3 Final Remarks 90

REFERENCES 91

APPENDIX A: PERMISSION TO REPRINT FROM ACS PUBLICATIONS 103

APPENDIX B: PERMISSION TO REPRINT FROM ROYAL SOCIETY OF CHEMISTRY 107

APPENDIX C: PERMISSION TO REPRINT FROM ELSEVIER 109

APPENDIX D: PERMISSION TO REPRINT FROM SPRINGER 115

APPENDIX E: LETTERS OF PERMISSION 117

APPENDIX F: PUBLICATIONS, TECHNICAL DISCLOSURES, AND PRESENTATIONS 118

VITA 120

LIST OF TABLES

Table 4-1: Table showing the calculated volume of VOC to be injected into the chamber 46

Table 5-1: I_G/I_D ratio for Pristine CNTs, CNTs in EPD solution, Electrospray Solution..... 76

LIST OF FIGURES

Figure 2-1: Number of publications since 1996 based on a literature search (Web of Science) using the keywords "hybrid materials" and "electronic."..... 8

Figure 2-2: Surface tension as a function of applied potential (Reprinted with permission from[45]. Copyright (1987) Elsevier)..... 10

Figure 2-3: Pendant drops of hexadecane at increasing potential, showing distortion of the drop due to the applied field a) 0 kV b) 1.0 kV c) 2.0 kV d) 3.0 kV e) 4.0 kV and f) 4.5 kV. (Reprinted with permission from[45]. Copyright (1987) Elsevier)..... 11

Figure 2-4: Schematic of Needle Electrospraying..... 12

Figure 2-5: Various modes of electrospraying (Reprinted with permission from[42]. Copyright (2008) Elsevier)..... 13

Figure 2-6: Schematic of the essential components of an Atomic Force Microscope..... 15

Figure 2-7: Topographic image generated by the AFM tip..... 18

Figure 2-8: Graphical construction of an AFM force-displacement curve. In panel (a) the curve F(D) represents the tip-sample interaction and the lines 1, 2, and 3 represent the elastic force of the cantilever. At each distance the cantilever deflects until the elastic force equals the tip-sample force and the system is in equilibrium. The force values f_a, f_b, and f_c at equilibrium are given by the intersections a, b, and c between lines 1, 2, and 3 and the curve F(D). (Reprinted with permission from[63] . Copyright (2011) American Chemical Society)..... 21

Figure 2-9: Schematic of a Conductive Probe Atomic Force Microscopy system..... 23

Figure 4-1: Commonly used anions and cations of Ionic Liquids (Reprinted with permission from [75]. Copyright (2011) American Chemical Society)..... 27

Figure 4-2: (as quoted from [65]) Micro quench emulsion method (A) Solid [bm2Im][PF6] in water at room temperature; (B) molten-state [bm_2Im][PF_6] phase separated from water at 70 ^oC; (C) o/w emulsion containing [bm2Im][PF6] as the inner phase; (D) [bm_2Im][PF_6] nanoparticle crop suspended in water at room temperature. In these images, [bm2Im][PF6] was stained with a water-insoluble dye (Nile Red) for visualization purposes. (Reprinted with permission from [65]. Copyright (2008) American Chemical Society)..... 29

Figure 4-3: Basic processes for nanoparticle formation within reverse micelles. Individual reverse micelles are shown without free surfactants: (a) [Bm_2Im][BF_4] nanoGUMBOS; (b)[Bm_2Im][$FeCl_4$] magnetic GUMBOS particles. (Reprinted with permission from[68] . Copyright (2011) Royal Society of Chemistry)..... 30

Figure 4-4: Chemical structure of [R6G][TPB] (Reprinted with permission from [85]. Copyright (2011) Royal Society of Chemistry)..... 31

Figure 4-5: Fabrication of [R6G][TPB] nanowires and nanoarrays by AAO templating. (Reprinted with permission from [85]. Copyright (2011) Royal Society of Chemistry)..... 32

Figure 4-6: Synthesis of [PIC][BETI] (Reprinted with permission from[86]. Copyright (2012) Royal Society of Chemistry)..... 33

Figure 4-7: a) TEM and b) SEM micrographs of the [PIC][BETI] nanoGUMBOS (Reprinted with permission from[86]. Copyright (2012) Royal Society of Chemistry)..... 34

Figure 4-8: Synthesis of [PIC][NTf_2] (Reprinted with permission from[86]. Copyright (2012) Royal Society of Chemistry)..... 35

Figure 4-9: a) TEM and b) SEM micrographs of the [PIC][NTf_2] nanoGUMBOS (Reprinted with permission from[86]. Copyright (2012) Royal Society of Chemistry)..... 35

Figure 4-10: Chemical structure of TC GUMBOS (Reprinted with permission from [88]. Copyright (2012) American Chemical Society) 36

Figure 4-11: SEM micrographs of (A) [TC0][BETI], (B) [TC1][BETI], and (C) [TC2][BETI] aggregates (Reprinted with permission from [88]. Copyright (2012) American Chemical Society) 37

Figure 4-12: Schematic of the dropcasting of nanoparticles suspended in solution on the gold coated glass substrate 38

Figure 4-13: Schematic of nanowires dropcasted on interdigitated structure..... 39

Figure 4-14: (a) Schematic of the Isolation chamber with electrical characterization system (b) Bell jar vacuum chamber with electrical connections 40

Figure 4-15: a) Schematic b) actual mask of the interdigitated structure with inter-finger distance of 10μm. 41

Figure 4-16: Spin curve for photoresist Shipley 1813 41

Figure 4-17: a) Optical microscope image of gold interdigitated structure, b) A pair of fingers of the interdigitated structure 42

Figure 4-18: Schematic of the direct injection method..... 44

Figure 4-19: Direct injection vapor sensing experimental setup 45

Figure 4-20: Schematic of the vapor sensing using carrier gas method 47

Figure 4-21: Needle electrospraying setup 48

Figure 4-22: SEM images of the [TC2][BETI] nanowires deposited with electrospraying for carrier gas method..... 49

Figure 4-23: Atomic Force Microscopy (AFM) images of [R6G][TPB] nanoGUMBOS, topographic image of the dropcasted [R6G][TPB] nanoparticles on gold surface 50

Figure 4-24: I-V characteristics of [R6G][TPB] nanoparticles with CP-AFM. Each colored trace is representative of the I-V characteristics for various test sites along the sample (Reprinted with permission from Springer [93]). 51

Figure 4-25: a) Atomic force microscopy images of the [R6G][TPB] nanowires, b) Red line represents the height profile line scan (shown below the topographic images) of the nanowires. 53

Figure 4-26: Current voltage characteristics of [R6G][TPB] nanowires swept from 0 to 1V. Each trace shows data acquired from each of several [R6G][TPB] nanowire samples. Inset showing leakage current on the order of 10^{-11}A through the Au on glass substrate devoid of nanowires.. 54

Figure 4-27: Atomic Force Microscopy images of (a) [PIC][NTf_2] and (b) [PIC][BETI] nanoGUMBOS on gold substrate (Reprinted with permission from Springer[97]). 56

Figure 4-28: Log plot of Current-voltage (I-V) curves of [PIC][NTf_2] and [PIC][BETI] nanoGUMBOS obtained by conductive probe atomic force microscopy (CP-AFM) (Reprinted with permission from Springer [97]). 57

Figure 4-29: Normalized current response of test structure to various analytes..... 58

Figure 4-30: Response of [TC2][BETI] nanowires to an increasing volume of aniline injected into the gas containment chamber..... 58

Figure 4-31: Carrier gas method used for detection of aniline vapors at different flow rates. 59

Figure 4-32: Maximum sensor currents for different aniline flow rates..... 60

Figure 5-1: Schematic diagram of the electrospray-assisted electrophoretic deposition strategy 65

Figure 5-2: Schematic diagram of the electrospray deposition 68

Figure 5-3: Schematic diagram of the electrophoretic deposition 68

Figure 5-4: Electrospraying coating results on non-conducting glass substrates with an applied constant voltage of 8.5 kV and constant flow rate of 50 µL/min for (a) for 5 min showing poor CNT coating, (b) for 10 min showing improved coating, (c) for 20 min, and (d) SEM imaging with 20 min deposition duration showing high quality surface coating. 69

Figure 5-5: Thickness of CNT coating electrosprayed on glass substrates as a function of deposition time for an applied E-field of 8.5 kV and flow rate of 50 µL/min..... 70

Figure 5-6: EPD (performed with E-field = 60 V/cm, deposition time = 3 min) results on electrosprayed samples (a) for 5 min showing poor CNT coverage, (b) for 10 min showing improved surface coverage, (c) for 20 min, and (d) SEM imaging with 20 min electrospraying

time showing dense CNT packing without microstructural dis-continuity. The results substantiate the effect of underlying coating on the final CNT film growth. 71

Figure 5-7: Thickness values of the CNT films (a) with varying E-field during EPD with constant deposition time of 3 min on samples electrosprayed for 20 min, and (b) varying electrospraying deposition time with constant EPD parameters (E-field= 60 V/cm and time= 3 min). 73

Figure 5-8: (a) Variation in sheet resistance of the electrosprayed CNT films as a function of deposition time from 10 min to 60 min, and (b) variation of sheet resistance values of the final CNT coating by EPD in relation to varying electrospraying deposition time from 10 min to 60 min (EPD was performed at a constant applied E-field of 60 V/cm with 3 min of deposition on the underlying CNT coating). 75

Figure 5-9: Raman spectra of (a) pristine MWCNTs, (b) acid refluxed and ultrasonicated CNT solution in ethanol, (c) ultrasonicated electrospray CNT-IPA for EPD, (d) electrosprayed CNT coating on glass substrate, and (e) final CNT coating obtained by EPD. All of the spectra displayed signature Raman peaks of MWCNTs at 1336 cm^{-1}, 1587 cm^{-1} and 2648 cm^{-1} wavenumber. 77

Figure 6-1: Schematic of the multiple spikes electrospraying method 80

Figure 6-2: Disturbances on the liquid surface due to sound waves. 81

Figure 6-3: Application of high potential to the free surface of the liquid causing electrospraying. 82

Figure 6-4: Schematic of electrospraying with sound waves setup 82

Figure 6-5: Liquid wave patterns on the free surface generated by the sound waves 83

Figure 6-6: Electrospray of ethanol with Faraday waves 84

ABSTRACT

Hybrid Electronic Materials (HEMs), as defined for this dissertation, are combinations of organic and inorganic materials as may be used to fabricate active device components in "beyond the transistor" electronics. However, the use of organics is often limited by issues such as thermal stability, compatibility with traditional (semiconductor) materials, and current processing technology. Thus, we began our exploration of HEMs with a "new" class of materials called GUMBOS (Group of Uniform Materials Based on Organic Salts) as derived from ionic liquids. For this first segment of our work, we investigated selected species of GUMBOS and nanoGUMBOS via their current-voltage characteristics, electronic sensing capabilities, and amenability to thin-film formation using the technique of electrospraying.

For the next segment, and primarily thin-film portion of this research, we elected to include the now more "traditional" material of carbon nanotubes (CNTs). Although reasonably well-characterized, CNTs still offer a significant challenge in terms of thin-film deposition, particularly upon non-conductive substrates. Electrophoretic deposition (EPD) is a solution-based technique that we have previously researched for the deposition of CNT thin-films onto metal and semiconductor substrates. However, EPD is limited by its need for conductive electrodes. We eliminate the latter through an electrospray-assisted form of EPD which accomplishes the twofold task of successfully depositing CNT thin-films onto non-conductive material while increasing the utility of EPD as it applies to HEMs. We also characterized the effect of our electrospray-assisted EPD technique upon CNT film thickness, quality, and morphology.

Our investigation concludes with the prototype development of a new method of electrospraying based upon Faraday waves. In conjunction with characterization and thin-film

deposition, this prototype demonstrates a means by which to scale HEMs to feasible commercial utilization.

CHAPTER 1: BRIEF DESCRIPTION OF CHAPTER CONTENT

This chapter gives a brief description of the chapters 2 to 7 of this work.

Chapter 2 ("Introduction and Literature Review") gives a brief introduction to hybrid materials and their applications. It describes several methods used in the literature for developing hybrid materials and discusss the methods used for thin-film deposition. Electrospraying as a method of thin-film deposition is reviewed. Several modes of the electrospraying phenomenon are described in addition to the needle electrospraying method used in this work. Atomic force microscopy as it is used in for imaging and as a conductive probe for understanding the electrical properties of nanomaterials is reviewed. Several modes of AFM operation are discussed, and the operation of CP-AFM is described. Scanning electron microscopy as technique used for studying the morphology of thin-films is also briefly described.

Chapter 3 ("Motivation and Research Goals") describes the motivation of the work and the goals to which this research as aspired. Motivation behind characterization of a new class of nanomaterials and thin films deceptions is discussed. The chapter also includes reasons for the deposition of CNTs on non-conductive substrates and motivation for the development of new electrospraying methods using Faraday waves.

Chapter 4("NanoGUMBOS: Characterization and Thin-film deposition") describes various methods of synthesizing nanoGUMBOS in general and also discusses the methods used for the synthesis of specific nanoGUMBOS candidates used in this work. This chapter also gives a detailed account of experiments conducted for electrical characterization of [R6G][TPB] nanoparticles, [R6G][TPB] nanowires, [TC2][BETI] nanowires, [PIC][BETI] and [PIC][NTf_2] nanostructures. Electrical characteristics obtained using AFM imaging, CP-AFM, and the fabrication details interdigitated structure used for electrical measurements are discussed in detail. Deposition of thin-films of [TC2][BETI] using electrospraying are discussed. Further,

detailed account of the use of [TC2] [BETI] nanowires and its thin-films for chemical vapor sensing is discussed.

Chapter 5 ("Study of Electrospray Assisted Electrophoretic Deposition of Carbon Nanotubes on Insulator Substrates") describes a unique method of deposition for multi-walled carbon nanotubes on non-conductive substrates using electrospraying and electrophoretic deposition as it was specifically developed for this work. Experimental account of the deposition of the initial layer of CNTs using electrospraying and further use of this initial layer for electrophoretic deposition of thicker CNTs layer is covered. Further, several parameters of electrosprayed thin-film on the final CNTs film are investigated and discussed in detail. Raman spectrograph results indicating the morphological changes in CNTs structures throughout the process are also discussed.

Chapter 6 ("Faraday Electrospraying") discusses the design and development of a new technique for electrospraying using Faraday waves. Brief review of techniques for electrospraying from the open-solution surface is discussed. Experimental setup developed to study Faraday electrospraying is discussed.

Chapter 7 ("Summary and Recommendations for Future work") is as stated by its title.

CHAPTER 2: INTRODUCTION AND LITERATURE REVIEW

2.1: Electronics at the Nanoscale

According to the National Nanotechnology Initiative, "Nanotechnology is the ability to control and restructure the matter at the atomic and molecular levels in the range of approximately 1–100 nm, and exploiting the distinct properties and phenomena at that scale as compared to those associated with single atoms or molecules or bulk behavior"[1]. Due to the shift in physical and chemical properties of materials of these dimensions, great interest has developed around all things nanotechnological. A characteristic as straightforward as the surface-to-volume ratio of these nanostructures enhances physical properties such as absorption wavelength, chemical reactivity; and oftentimes the exhibition of electrical properties when compared to their bulk counterparts. For example, the physical manifestation of the reduction in the size of gold from the bulk to nanoparticles is a change in color due to scattering of light in the nanoscale [2]. In conjunction with tools of molecular and atomic level imaging and manipulation such as Scanning Tunneling Microscopy (STM)[3-5], Atomic Force Microscopy (AFM)[6], and Dip-Pen Nanolithography (DPN)[7], to name a few, the now seminal Feynman talk entitled "There's Plenty of Room at the Bottom" has become a discussion of pragmatic rather than prophetic applications [8]. In short, the "nano"-scale has opened up "big" opportunities in the next-generation of electronics[9].

In order to understand the context in which nanoscale effects in electronic materials are addressed in this dissertation, a brief review of electronic devices is in order. Historically, electronics has come a long way since the invention of the solid-state point contact transistor by John Bardeen, William Shockley, and Walter Brattain in 1947[10, 11]. Without exaggeration, it can be stated that solid state electronics, especially based on silicon, has exponentially transformed everyday life[1, 12-14]. The trend of doubling the number of transistors every

eighteen months, as was predicted by Dr. Gordon Moore in 1975[15, 16] has driven the computer industry and all functions with which it can be associated[17]. Even as Moore's law holds true to-date with state-of-the-art technology for next generation processors based on, for example, a 15 nm channel length, the key challenging issue is not just the scale but improving both the reliability and versatility of these devices.

To address next-generation device and circuit challenges, researchers have typically taken one of two paths—either the "top down" or the "bottom up" approach. Manipulating larger size materials using physical and chemical processes to fabricate nanoscale structures is known as the top-down approach. This approach relies heavily upon the precision and the ability of macroscale equipment to resolve nanoscale features[18-20]. Although excellent progress has been made in electronics as devices have progressed from micron, submicron, and the aforementioned nanometer ranges, the demand for smaller feature sizes has been accompanied by an almost prohibitive increase in fabrication cost from this top-down perspective[21]. With the practical motivation of such economic issues alongside the scientific curiosity-driven research of nanoscale phenomena, industrial technologists and researchers are now taking the "bottom-up" approach as well. The latter takes its inspiration, at least in part, from biology which uses physical and chemical forces such as self-assembly to create a plethora of biological organisms as extensive as the human genome[22]. Thus, the aptly named field of molecular electronics falls under the umbrella of the bottom-up approach[23, 24]. Self-assembly of nanomaterials to form desired structures without any external manipulation shows a great deal of potential as an alternative to the current top-down approach, and, several nanoscale structures have been demonstrated[25-28]. However, for bottom-up production at the commercial level, there are several challenges in terms of integration, scale of self-assembly, ease of production,

and environmental effects. Insomuch as "materials" are the basis for the successful and ultimately commercial exploitation of nanoscale phenomena, this dissertation presents original research aimed at addressing select aspects of the above challenges. Through the characterization of electronic properties, in addition to the exploration of techniques for thin-film deposition, a study of a series of unique or "hybrid" (organic-inorganic) combinations of materials will be described in the discussion to follow.

2.2: Hybrid Electronic Materials

Recent years have seen an increase in the use of non-traditional materials in electronics. Organic materials are being increasingly integrated into solar cells, organic LED's, and opto-electronics[29-31], and it was less than twenty years ago that the Nobel prize in chemistry was awarded for research on conductive polymers[32]. A material which includes two or more of moieties combined at the molecular scale to create a new material is called a "hybrid material." Usually these include organic and inorganic materials. The nature of interaction between organic and inorganic material determines the kind of hybrid material it creates[33-36]. These interactions can be loosely classified into Class I and Class II materials. Class I materials show weak interaction between the organic and inorganic matrix. These interactions include van der Waals, hydrogen bonding, and electrostatic forces. Class II materials show strong interactions between the organic and inorganic matrix. These interaction include covalent, ionic, and coordinative interactions. Hybrid materials are also synthesized to improve structural properties of materials like elasticity, thermal stability, and refractive index and also to improve surface properties of the materials like hydrophobicity, permeability, and surface energy. Several methods for synthesis of hybrid materials are used. The most common methods are discussed here.

i) Formation of components by in-situ technique

In this process the formation of hybrid materials is solely dependent on the chemical transformation of the precursors involved throughout the preparation of the materials. New molecules of the precursors get a total makeover and exhibit completely different properties from the original precursors involved. The reaction conditions and composition of the precursors decides the final properties of the resulting material. Control over the reaction conditions are of immense importance due to their effect on the properties of the final material obtained.

ii) Formation of inorganic materials by in-situ technique

In this process in-situ formation of inorganic materials require covalent bond in solutions. This low-temperature process employed most often yields thermodynamically stable structures. Often inorganic materials formed by this method are amorphous in nature while crystallinity only exists in the nanoscale of its structure. The main techniques for in-situ formation of inorganic materials are the—a) Sol-gel process, b) Non-hydrolytic Sol-gel process, and c) Sol-gel reaction of non-silicates.

iii) Formation of organic polymers by pre-formed inorganic materials

To make organic monomers compatible with inorganic materials, the inorganic surface can be treated with surfactants. Here Class I materials are formed if the inorganic component does not interact or interacts very weakly with the organic polymer. If the inorganic component interacts very strongly with the organic polymer, Class II materials are formed.

iv) Synthesis by forming both components simultaneously

Homogeneous types of interpenetrating networks are formed by simultaneous formation of the organic and inorganic polymers. For organic polymerization, the monomers are mixed with the precursor of a Sol-gel process, and all the steps are done simultaneously in the presence

or absence of a solvent. This method of synthesizing creates increases the reaction rate for the following processes:

- The rate of chemical reaction of the polymerization of the organic phase
- The rate of chemical reaction of the hydrolysis and condensation creating the inorganic phase
- Phase separation thermodynamics between two phases

v) Building block approach

In this method, the building blocks will react with one another forming a final hybrid structure in which the precursor will partially keep its structure. These building blocks could be molecular or nano-sized to form the nano-composites. Thus, the structure of the initial materials used will be present in the final hybrid structure. This approach has one major advantage over the in-situ process as the hybrid material will partially keep the property of one of the building blocks. Therefore, structure-property prediction is possible to a certain extent. Recently there has been increased interest in use of hybrid materials for electronic applications. Figure 2-1 shows the increase in publications (using keywords "hybrid materials" or "electronic") from 1996 to 2015(June). The ease of chemical modification and large scale economic production are key factors driving interest in these materials. Towards this end, combinations of both organic and inorganic materials, dubbed "hybrid electronic materials" (HEMs) show great promise in terms uniting the bottom-up approach with traditional microfabrication techniques [22, 25, 37].

2.3: Thin-film deposition methods

Since the development of materials for electronic devices and circuits, a range of techniques have been used to obtain thin-films[38, 39]. Planar processing relies on the deposition of layers of materials which can be selectively placed one after another. Each layer is used to build what will become device components through, for example, photolithographic

techniques[40, 41]. In nanoelectronics one focus is upon the reduction of device feature sizes. However, for applications beyond experimental curiosity, it is necessary to find ways to quickly and reproducibly deposit thinfilms which, for hybrid electronic materials, may be newly synthesized materials (i.e.-GUMBOS, Chapter 4) or nanostructures (i.e.-carbon nanotubes, Chapter 5). Of the many methods of thin film deposition, one promising technique for meeting the aforementioned criteria is that of electrospraying, the particulars of which are introduced below.

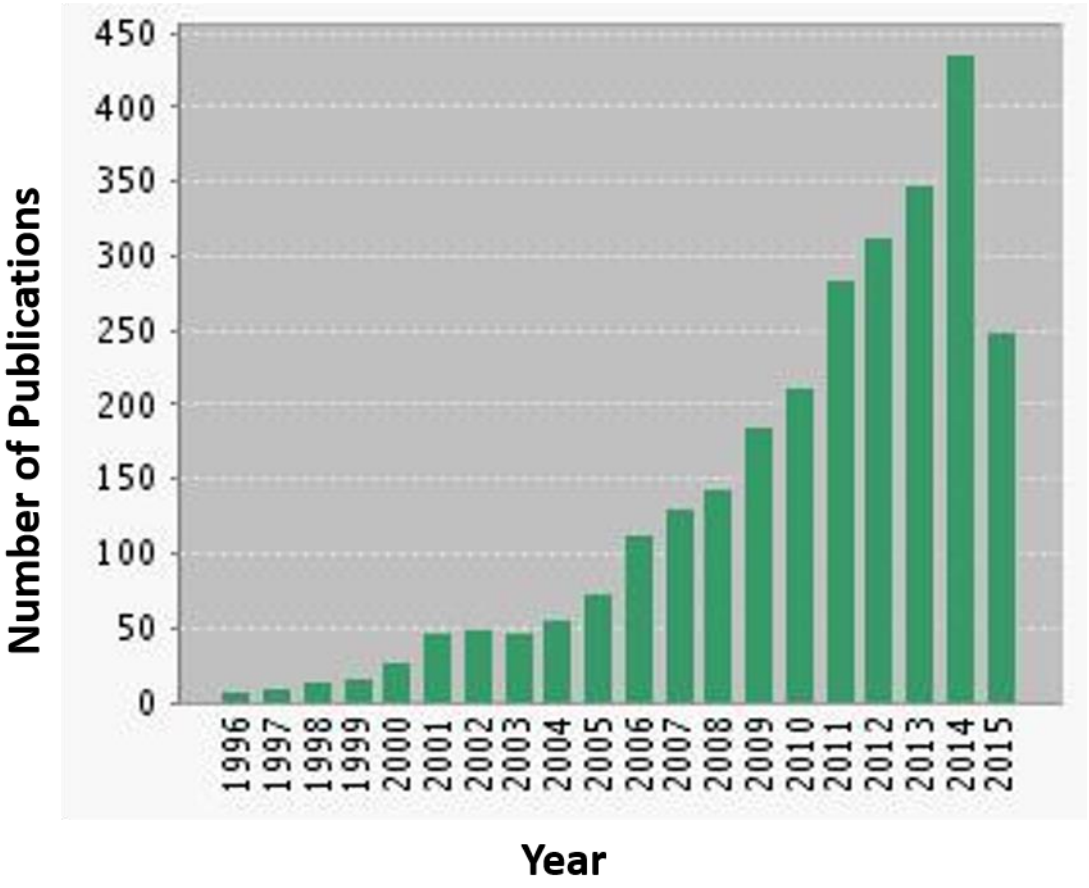

Figure 2-1: Number of publications since 1996 based on a literature search (Web of Science) using the keywords “hybrid materials” and “electronic.”

2.3.1: Electrospraying

Intense research into the economical production of nanoparticles and nanofibers in recent years has driven the search for new technologies. Electrospraying, a century old technique for producing fibers, has generated newfound interest as a means of producing various nanostructures [42-51]. Most notably, electrospraying is used in nano-electronics[42], tissue engineering[52], and the deposition of carbon nanotubes[53]. Our long-term interest in electrospraying stems from the desire to generate thin-films of nanoGUMBOS and carbon nanotubes as may be used in the development of hybrid electronic devices. Words such as "electrospraying" and "electrospinning" are often used interchangeably, although a distinction may be made depending on the type of deposition *i.e.*, a viscoelastic solution (polymer, electrospinning) or otherwise (electrospraying). Moreover, depending on the nature of the applied electric field, electrospraying is considered to be of the direct current (DC) or of the alternating current (AC) type. DC electrospraying has been extensively used in laboratory and industrial settings due to its simplicity and was the method of choice for our work.

The effect of high electrostatic force on a liquid drop is of immense importance in electrospraying. When a liquid droplet is subjected to high electrostatic force, there is a decrease, albeit nonlinear, in the net surface tension of the droplet.

$$\Upsilon = \Upsilon_0 - E_0 \qquad (2\text{-}1)$$

A simple relation for the following can be given as equation (2-1), where Υ and Υ_0 are the net and initial surface tension on the droplet, respectively, in a constant electric field (E_0). The graph in Figure 2-2 depicts the change in droplet net surface tension with respect to an increasing potential difference.

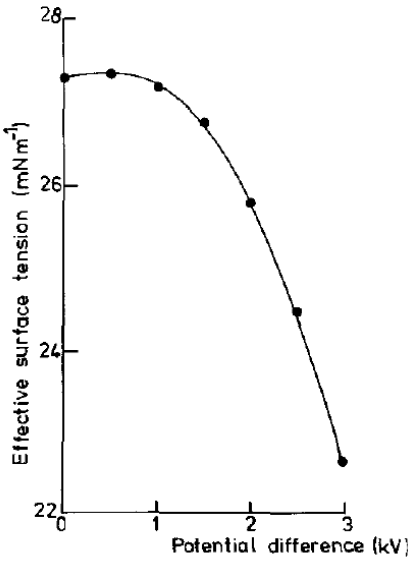

Figure 2-2: Surface tension as a function of applied potential (Reprinted with permission from[45]. Copyright (1987) Elsevier)

As the potential difference between the nozzle and the target is increased from 0 kV to 4.5 kV (Figure 2-3, left to right) on a hexadecane pendant droplet, shape distortion of the droplet can be observed[45]. If the potential across the droplet is further increased, an electro-hydrodynamic (EHD) force overcomes the surface tension ($E_0 > \Upsilon_0$), thus causing the droplet to split apart into several smaller droplets. In a uniform electric field, this process is repeated until the electrostatic field is smaller than the surface tension of the droplets, in turn, causing the droplets to become smaller in diameter.

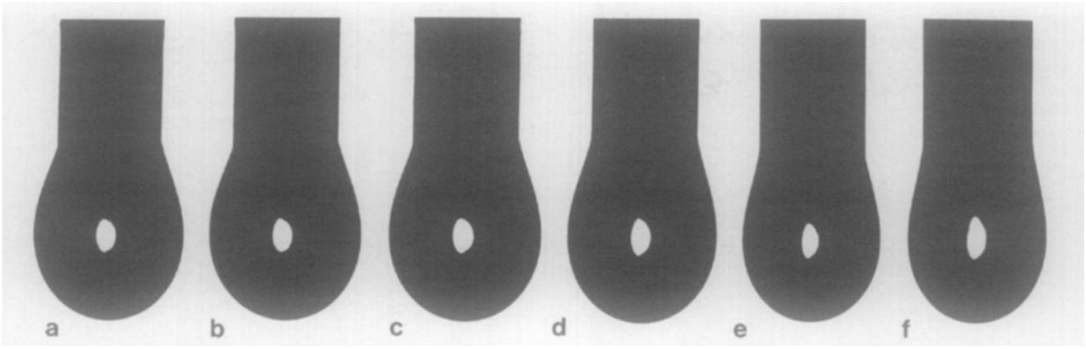

Figure 2-3: Pendant drops of hexadecane at increasing potential, showing distortion of the drop due to the applied field a) 0 kV b) 1.0 kV c) 2.0 kV d) 3.0 kV e) 4.0 kV and f) 4.5 kV. (Reprinted with permission from[45]. Copyright (1987) Elsevier)

2.3.2: Needle electrospraying

Needle electrospraying is a widely used electrospraying technique. A schematic of needle electrospraying is shown in Figure 2-4. As the potential on the needle is increased, the resultant spraying broadly operates in three modes as follows: i) dripping mode, ii) pulsating mode, and iii) jetting modes.

2.3.2.1: Dripping mode

When no potential is applied between nozzle and grounded collector, liquid pumped through the nozzle drips down in the form of large droplets. As the potential is increased, gradually EHD forces emerge causing deformation of the droplets. In 1882 Lord Rayleigh, L. *et al.* investigated the theoretical limit of charge density on a droplet, after which the original droplet splits into smaller ones. This phenomenon is called the Rayleigh Limit[54]. Droplets are drawn towards the collector depending on the applied potential and the drop size. In fact, as droplets emerge from the end of the capillary, electrostatic force pulls them, thus increasing the dripping rate. This is the basis for the "dripping mode."

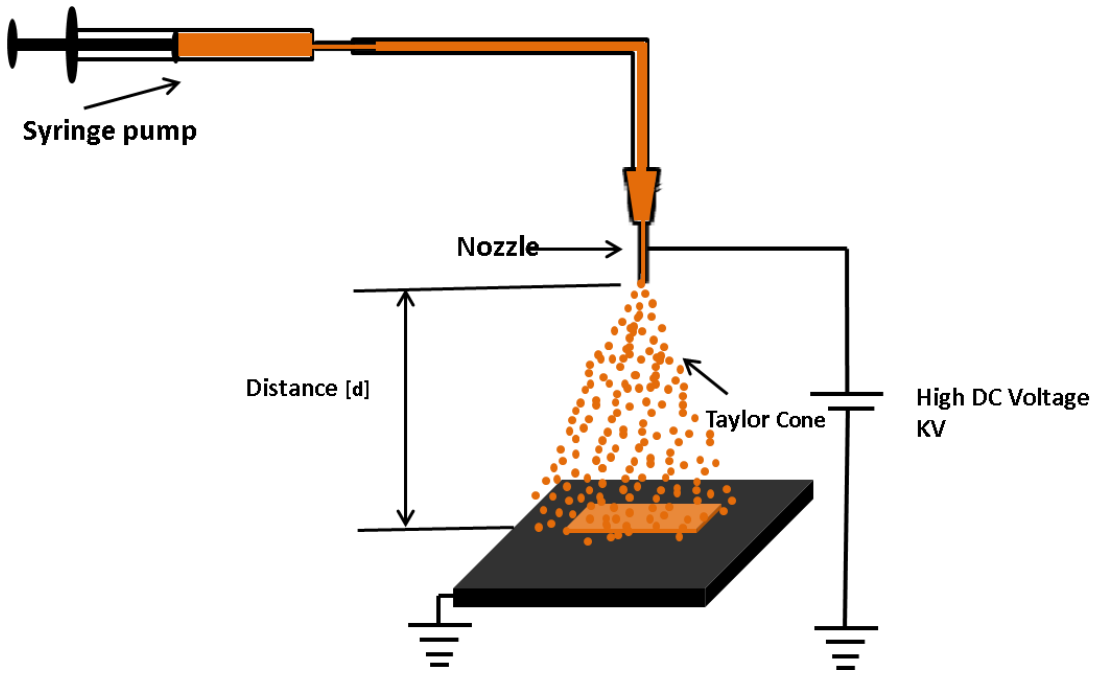

Figure 2-4: Schematic of Needle Electrospraying

2.3.2.2: Pulsating mode

As the voltage is slightly increased from the dripping mode, charge density on the droplets increases. This induces instability in the droplets which, in turn, causes them to eject even smaller droplets or long filaments. As filaments are formed, they break down into a burst of droplets. This is repeated in cycles and is known as "pulsating mode."

2.3.2.3: Jetting modes

As the voltage (and electrostatic field) is further increased above pulsating mode, liquid from the filament formed in pulsating mode is split up into fine droplets with narrow diameter distribution. A series of jetting modes are formed, starting with a stable cone jet mode, and a conical structure is observed at the apex of the nozzle (as shown in Figure 2-5). Oscillating and precession modes are caused by induced instability in the cone jet mode due increased electric field. Further increases in potential create multiple jets along the perimeter of the capillary. This

leads to the stabilizing of these jets and the formation of a multi jet mode. Figure 2-5 depicts the series of modes of electrospraying using the capillary method. As electric field is increased even further, depending on the solution properties, a steady and stable jet is formed.

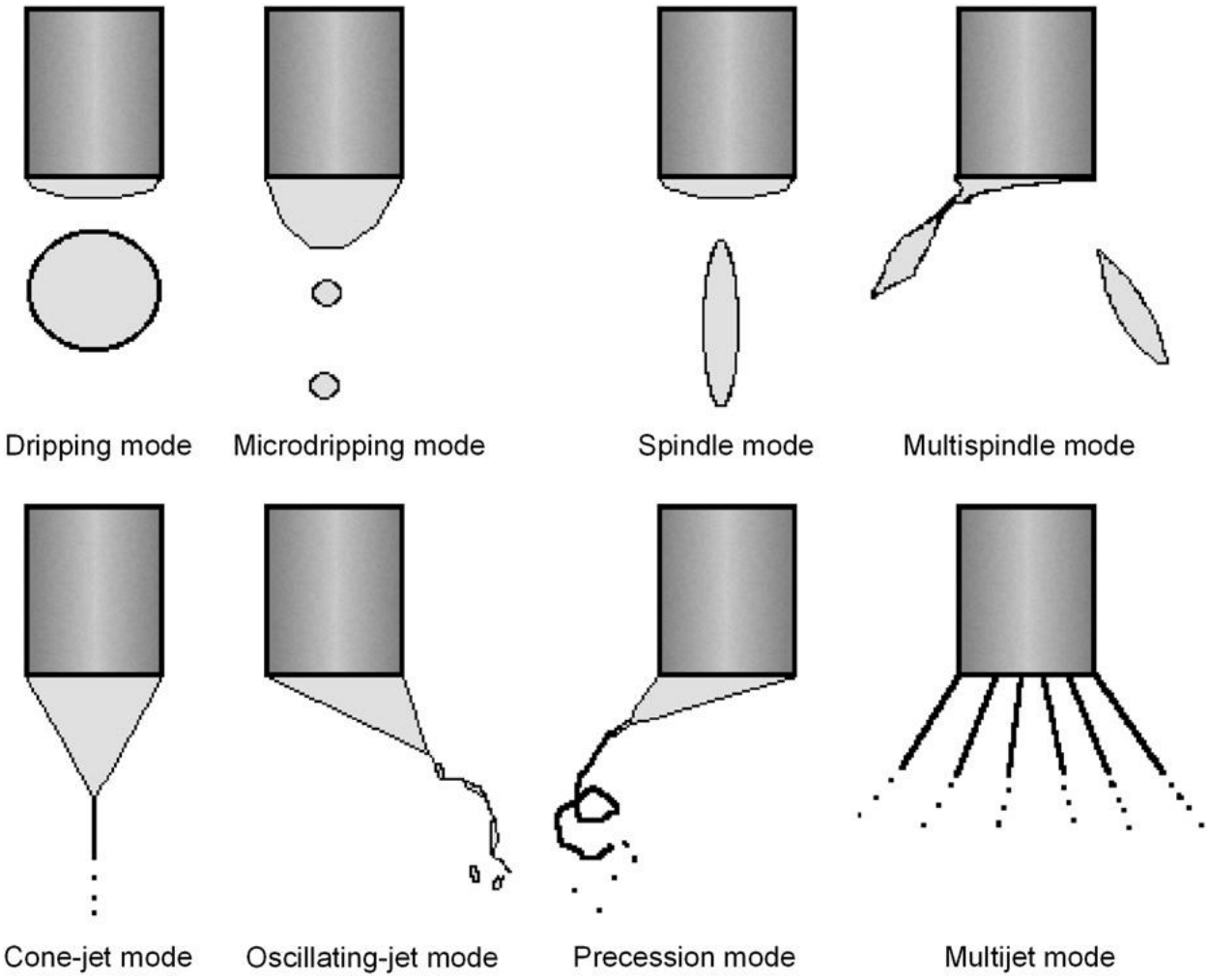

Figure 2-5: Various modes of electrospraying (Reprinted with permission from[42]. Copyright (2008) Elsevier)

2.3.3: Electrospraying parameters

The size of the droplets or fiber formation depends on several factors including solution properties, distance between the capillary and collector, potential applied, flow rate, shape of the

collector, and the assumption that temperature and the ambient (air) are constant. The versatility of electrospraying lies in its ability to tune several of the aforementioned to achieve the desired droplet or fiber size. Ultimately, size distribution can be controlled using these parameters as well [43, 55-57].

2.4: Analytical Methods and Instruments Used

Several analytical methods are used in this work to characterize and analyze the materials we studied. This section gives a brief overview of methods and instruments used in this work.

2.4.1: Atomic Force Microscopy

Since the 1980s, the development of practical instrumentation for various forms of scanning probe microscopy has opened up an entirely new era of understanding with respect to the surface properties of materials[3-5]. A case in point would be the realization of Atomic Force Microscopy (AFM) in 1986 by Binning, Quate, and Gerber[6]. AFM uses a sharp tip whose radius at its widest point is in the nanometer range to scan the topography of a sample. Likewise, surface forces with high precision, on the order of 10^{-18} N/m, can be measured using AFM. The imaging resolution of this technique is in the range of nanometers, also due to the sharp tip, and is not limited by wavelength like other optical or electron-based instruments. The dependence of AFM on physical interaction with a surface provides ample data in terms of surface forces, viscoelasticity, and Van der Waals forces. AFM is also one of the few instruments that can give three dimensional images of surfaces at the nanoscale.

For our work we used a Pacific Nanotechnology (now Agilent) NanoR AFM. A schematic of the essential components of this instrument is shown in Figure 2-6. As indicated, the tip (attached to a cantilever) is rastered across the surface of a sample. As the tip is moved

along the surface, light from a laser is reflected off of the back of the cantilever onto a photodetector resulting in the transfer of the mechanical motion of the tip-cantilever combination to that of an optical signal received by a photodetector. This detector serves as the source of an electrical signal to a highly sensitive and precise controller and feedback system. As the tip interacts with the surface, via van der Waals attraction or even direct physical contact with the particles, the feedback system directs the tip to respond in the Z-direction, depending on the amount of deflection in the cantilever. Simultaneously, the tip follows the envelope of the surface line-by-line, as controlled by an X-Y motion generator, which guides the direction and speed of the raster scan. Ultimately, each scan line of data is added to form an image matrix which itself can be manipulated and analyzed by the AFM system software. Both two and three dimensional images of the scanned surface can be generated.

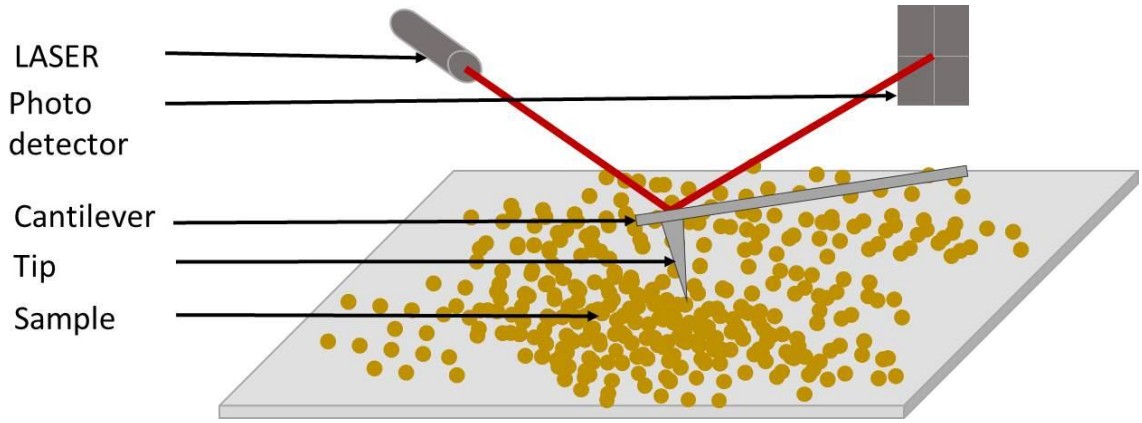

Figure 2-6: Schematic of the essential components of an Atomic Force Microscope

2.4.1.1: Feedback Control

The feedback control for an AFM consists of force sensors, a feedback control circuit, and error signal generation. The feedback control circuit continuously monitors the force sensors and compares their data to a set point. The difference between these sensors and set point

generates a corresponding error signal. A proportional Z displacement generated results in a new error signal. This is a form of negative feedback which is repeated to minimize the overall error signal by moving the Z Piezo accordingly. For a regular scan, XY movement in the form of a raster scan, is achieved by feeding saw-tooth waveforms of different widths.

2.4.1.2: Piezoelectric transducers

Materials which change their physical size due to the application of charge are called piezoelectric materials. Their accuracy and reproducibility of size are critical to controlling the AFM tip at the nanometer scale. Piezoceramics have a natural resonance frequency that depends on their size and shape. Electronically, piezoelectric materials act as capacitors that, when charged, change dimensions and remain at that size and shape until they discharge. Circuits driving piezoelectrics are usually large capacitor driving circuits. The direction and magnitude of change depends on several factors such as the material, crystal orientation, and applied voltage. Piezoelectric materials have hysteresis and creep. Creep occurs due to the application of voltage impulses across the crystal. However, the relationship between crystal dimensions and the applied voltage is usually not linear, exhibiting an undesirable hysteresis, drift, creep and other nonliearlities in the tip operation. Inherent nonlinearity, hysteresis, creep and drift are compensated for by a combination of software and hardware modifications [58-60]. Mokaberi *et al* have investigated the elimination of creep and hysteresis by using an in-situ computation of compensation factors[61]. Inverse model parameters are used to generate a desired input signal to correct the creep, drift and hysteresis. The application of a compensation factor results in high accuracy and predictability of the piezoelectric transducers.

2.4.1.3: Force Sensor

A force sensor measures the van der Walls forces between the tip and the surface. This sensor is very sensitive to any changes down to the picoNewton range. Light-lever AFM force sensors are the most widely used as shown in Figure 2-6. When light from a diode laser shines on the back of the cantilever, this light is deflected and impinges upon a photo-detector array. Typically, the light must be aligned manually when a new cantilever is installed to optimize reflection from the cantilever into the photo-detector. Ultimately, changes in the topography of a sample are reproduced in this light-lever sensing arrangement. Thus, mechanical motion is translated to an opto-electronic signal which can be processed to produce an AFM image.

2.4.1.4: Image processing

Movement of the tip up and down as it scans along the line causes deflection of the incident laser signal. This deflection is measured by the photodetector, which generates a proportional electric signal. A continuous acquisition of the deflection caused by the tip is recorded to generate the topography of the observation as shown in Figure 2-7. The acquired line images are stored and stitched together by the software to generate a three dimensional image. Since, all of the experiments are conducted with a NanoR model Pacific Nanotechnlogy (now Agilent) AFM, Nanorule software is used for the post-processing of the images. The latter includes application of image processing techniques to remove artifacts generated by the AFM. Nanorule software is also used for measurements on the images to estimate height, width, and area of the three dimensional structures.

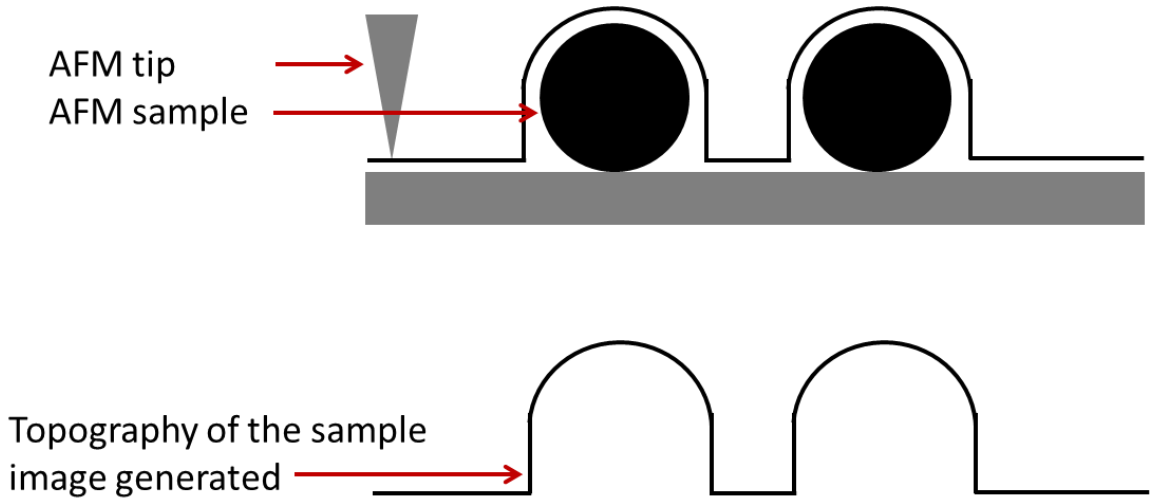

Figure 2-7: Topographic image generated by the AFM tip

2.4.1.5: Modes of AFM operation

AFM is used to measure several physical properties such as topography, viscoelasticity, and surface roughness and can be used for surface modification as may be needed in conjunction with lithographic processing. Determination of this wide range of properties requires operating the AFM in several modes, depending on the material type and the property to be measured. These operating modes have been widely divided into two categories of Contact Mode and Vibrating mode as follows:

a. Contact Mode

In contact mode, the tip is in contact with the sample surface. This contact is actually with the thin layer of water vapor and contaminants that coat the sample in an ambient room temperature AFM operation. (However, the latter is not an impediment to imaging the nanoscale topology of the sample.) To obtain an image a constant force is applied as the AFM tip is rastered across the sample. Negative feedback from the force sensor is used to maintain a constant force; any deviation from the setpoint is used to determine the actual topography of the sample. Several lines generated in this way are stitched together by the software to generate a

topographical image. Contact mode is used for “hard” (solid) as opposed to “soft” (biological, highly malleable, or liquid) materials. High resolution images on the order of <1 nm have been reported using this method[62]. Contact mode tips typically have a resonant frequency of less than 50 kHz and a lower Young's modulus to allow for the degree of flexibility needed to follow the topography of rough surfaces. A typical contact tip can dynamically adapt up to several microns of variation in height in this mode of operation.

b. Vibration Mode

Scanning over soft and semi-elastic samples is difficult using contact mode AFM. Contact mode is typically used to provide information on sample topography or for surface potential mapping. However, to know the viscoelastic and friction properties of a material AFM is operated in vibration mode. In this mode the AFM tip is oscillated at a high frequency on the order of 170 kHz. As the tip vibrates over the surface, there is a change in tip frequency due to interaction with surface forces (i.e.-attractive, repulsive, van der Walls). The change in frequency compared to the initial frequency is used to generate a proportional voltage. This proportional voltage is measured to estimate the actual topography of the sample. Deviation from the actual frequency due to attractive and repulsive forces is recorded to generate an image in this mode. Vibrating mode tips are stiff (high Young’s modulus) and have a high resonant frequency (several hundreds of kHz). Depending upon how closely the tip is oscillated with respect to the surface, vibration mode is categorized into two types i) close contact and ii) intermittent contact. In close contact mode the tip oscillates inside the natural “contamination layer” that resides on any material exposed to the atmosphere. Scans taken in close contact mode yield high resolution images. In intermittent mode the tip is oscillated just outside of the contamination layer. This mode requires a greater amplitude of oscillation to overcome surface capillary forces. The risk

of damaging the tip is higher in the intermittent mode. Close contact is the more frequently used of the vibrational operating modes.

2.4.1.6: Force-Distance Curves

The precise control of vertical distance in an atomic force microscope down to 0.1 nm and force sensitivity of 1 pN makes it an ideal instrument for measuring the surface forces of materials. When an AFM tip in contact with a surface is raised at a constant velocity, the surface forces on the tip cause a change in the tip's velocity and shape (low Young's modulus). These changes in shape and velocity can be monitored and recorded using the Z force sensor of the AFM. The change in shape or displacement of the tip is proportional to surface forces which are reflected in the deflection of the cantilever. Hooke's law equation (2-2) of proportionality is used to convert the Z displacement obtained from the AFM to force data.

$$F = kx \tag{2-2}$$

where k is the force constant and depends on the Young's modulus of the tip. A typical force-distance curve as obtained from an AFM is shown in Figure 2-8. Force distance curves provide information about the tip-sample interaction, F(D), and the elastic force of the cantilever. Figure 2-8(a) represents the tip-sample interaction force. The lines 1-3 represent the elastic force of the cantilever. Each point on (b) represents an equilibrium reached by the tip, due to the cantilever deflection, caused by the inherent elastic force of the cantilever and the tip-sample interaction. Plotting the force-distance curves of a material can provide information about properties such as viscoelasticity, surface charge densities, and the hydrophobicity of the material[63].

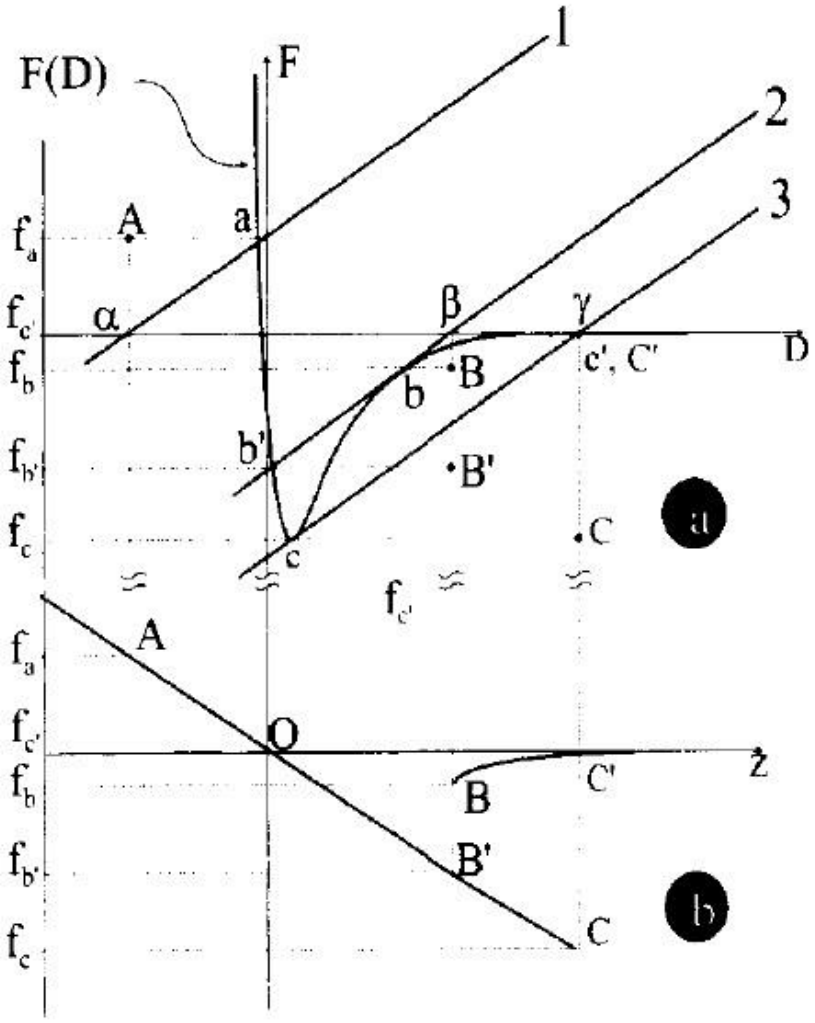

Figure 2-8: Graphical construction of an AFM force-displacement curve. In panel (a) the curve F(D) represents the tip-sample interaction and the lines 1, 2, and 3 represent the elastic force of the cantilever. At each distance the cantilever deflects until the elastic force equals the tip-sample force and the system is in equilibrium. The force values f_a, f_b, and f_c at equilibrium are given by the intersections a, b, and c between lines 1, 2, and 3 and the curve F(D). (Reprinted with permission from[63] . Copyright (2011) American Chemical Society)

2.4.2: Conductive Probe Atomic Force Microscopy (CP-AFM)

Conductive Probe Atomic Force Microscopy converts an AFM into an instrument from which nanoscale electronic properties can be obtained and characterized. As per its name, CP-AFM uses a conductive tip as an electrode. Typical CP-AFM tips consist of silicon nitride

coated with gold (Au) or platinum (Pt). The extra layer of conductive material coating increases the diameter of the tip and its force constant, thus resulting in stiffer tips. Therefore, higher resolution imaging is sacrificed in lieu of electronic characterization.

Parametric current-voltage (I-V) characteristics can be measured using this method. Figure 2-9 shows the schematic of a CP-AFM where the conductive Pt coated probe acts as one electrode and a gold coated conductive substrate acts as another electrode, thereby forming a metal (Pt)-particle(nanowire or nanoparticle)-metal (Au) junction. Current is applied through the sample via the tip, and the corresponding voltage is measured. In order to limit the possibility of a short circuit, external limiting resistors are placed in series. A Keithley 4200 Semiconductor Characterization System (SCS) was used in our experiments in the process of obtaining electronic material sample data and as a protective device. For example, the SCS can be programmed to limit the amount of current, thereby preventing damage to the tip. The conductive tips were obtained from MikroMasch. Our typical tip of choice is MikroMasch model DPE 14 /no Al. It is made from etched silicon with a 30 nm Pt coating. The radius is less than 40 nm and the height is approximately 20-25 μm with a cone angle below 40^{o} and a resonant frequency of approximately 160 kHz. The DPE14 with Pt coating has a force constant of approximately 5.7 N/m. As is necessitated by CP-AFM measurements, lower force constant tips are used in the contact mode (section 2.4.1.5:a) now required for electrical characterization.

Using the aforementioned contact mode, images of CP-AFM samples can be obtained, albeit with less than the highest possible resolution (due to the coating on the tip). Therefore, for this work, prior to the I-V measurements, AFM images were obtained. We used a Pacific Nanotechnology tip (Model: P-MCU-SICT-O) in contact mode. Our images were processed using our instrument's manufacturer supplied NanoRule post processing software for the

removal of artifacts and imaging errors. The tips used for all of the imaging and CP measurements were chosen carefully to minimize delamination or adsorption of the particles to the tip surface.

Figure 2-9: Schematic of a Conductive Probe Atomic Force Microscopy system

2.4.3: Scanning Electron Microscopy

Scanning Electron Microcopy uses a focused electron beam to raster scan the surface of the specimen. The interaction of the electron beam with the specimen causes both elastic and inelastic scattering of electrons. Elastically scattered electrons with a scattering angle of more than 90^{o} are known as backscattered electrons. Inelastic scattering is caused by a substantial transfer of energy from the incident electrons to the atoms of specimen. Incident electrons ionizing the sample atoms lead to secondary electrons (SE) and also generate Auger electrons, x-rays, and produce cathodoluminescence. Secondary electrons emitted due to inelastic scattering have low energy and are usually collected in the proximity of the sample using a positively biased detector. Secondary electrons are widely used to obtain topographic and morphological information from the sample. SE signal can resolve structures less than 10 nm, depending on the material. The incident electron beam of the SEM is focused using a magnetic lens and is raster scanned across the sample. Organic samples emit low secondary and back scattered electrons due to their composition of low atomic number elements. Organic samples act as insulating materials resulting in a charging phenomenon. A thin (<5 nm) layer of conductive gold or platinum can be

sputter-coated on non-conducting and organic samples to create the conductive surface necessary for characterization using SEM[64].

CHAPTER 3: MOTIVATION AND RESEARCH GOALS

In this work, we investigate—1) the electronic characteristics of an essentially new class materials as well as, 2) new techniques of thin-film deposition for hybrid electronic materials (HEMs). Item 1 is based upon a form of nanomaterial, fairly recently introduced into the literature by Professor Isiah M. Warner (LSU Dept. of Chemistry)[65]. Known as GUMBOS, or a **G**roup of **U**niform **M**aterials **B**ased on **O**rganic **S**alts, these materials have already exhibited potential "device-useful" properties such as fluorescence and magnetism [66-68]. GUMBOS piqued our interest as a potential component of next-generation HEMs intended for use in nanoelectronic devices, and to the best of our knowledge, this work represents a first-time investigation into their electrical properties. Item 2 above is based upon our innovations in techniques and equipment that we have newly designed to deposit thin-films of HEMs involving new materials such as GUMBOS as well as the more extensively studied carbon nanotubes (CNTs). Note that for the thin-film aspect of our work, we included CNTs which, albeit having more well-known material properties, do still present challenging problems in term of their deposition and integration into device technology. By working to understand the physical characteristics and fundamental electronic phenomena of a unique component of HEMs (i.e.-GUMBOS), while researching and developing the means by which to successfully synthesize and deposit HEM thin-films (i.e.-GUMBOS/CNTs), our research contributes to the scientific understanding of new materials while addressing the engineering innovations needed for their application to next-generation nanoscale device technology.

CHAPTER 4: NANOGUMBOS: CHARACTERIZATION AND THIN-FILM DEPOSITION

4.1: Introduction

The HEMs of interest in this work have originated from a well-known category of classification of substances known as ionic liquids (ILs). Ionic liquids are compounds whose melting point is less than or equal to 100 ^{o}C. They consist of free anions and cations in the liquid form. Although these compounds have been a part of the chemistry community since 1914, recent increase in interest in ILs is due to their use in solar cells[69, 70] as green solvents[71, 72], biomedical imaging[73] and fluorescence[74]. Ionic liquids can be carefully tuned for the required application by selecting and synthesizing particular combinations of anions and cations. Inorganic ionic compounds like table salt have small ions compared to typical ILs which have large and asymmetric ions that are both organic and inorganic. The asymmetry in the anion and cation sizes is one of the factors that affect their melting point. These relatively large ions are extremely tunable, thus making these materials highly functionalizable. The latter allows for the potential realization of a range of physical and chemical properties such as conductivity, fluorescence, and chirality. Figure 4-1 shows commonly used anions and cations of well-known ILs. There are several potential sites that can be functionalized to obtain the desired properties.

4.2: Group of Uniform Materials Based on Organic Salts (GUMBOS)

One of the challenges in the use of conventional organic materials in consumer electronics is their limited thermal stability. Ionic liquids whose melting points exceed room temperature (25 ^{o}C) are called frozen ionic liquids (FILs)[76]. Although much less extensively

studied than ILs, FILs have been used as solvents for polar and non-polar species[75]. Rutten, *et al.*(2007) used FILs as substrates for rewriting imaging[73]. However, in the overall scheme of IL research, FILs have generally taken a "backseat" in terms of detailed scientific investigation and fruitful engineering applications.

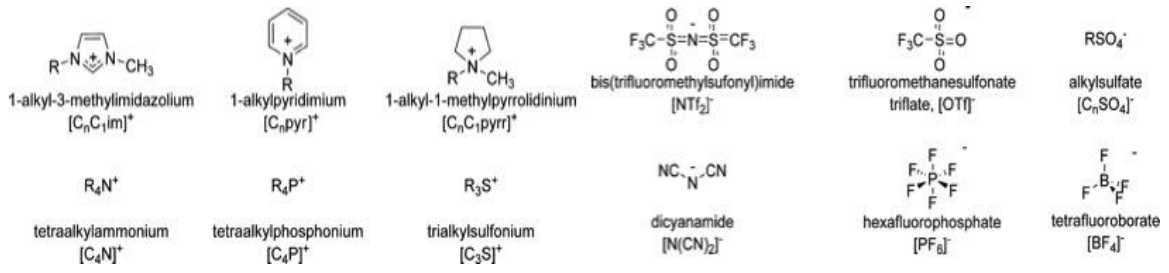

Figure 4-1: Commonly used anions and cations of Ionic Liquids (Reprinted with permission from [75]. Copyright (2011) American Chemical Society)

Thus, the synthesis of a **G**roup of **U**niform **M**aterials **B**ased on **O**rganic **S**alts (GUMBOS), by the Warner Group, has come into the fore as a major breakthrough in IL and particularly FIL research[77-83]. GUMBOS are FILs whose melting points are in the range of 25 to 250 ^{o}C. The precursor to the materials which came to be known as GUMBOS was first reported in a 2008 NanoLetters article, also from the Warner Group, which described melt-quench-emulsion as the method of micro and nanoparticle synthesis [65]. GUMBOS can be tuned to exhibit the wide range of physical and chemical properties for which ILs are known. Moreover, through functionalization of selected anions and cations for specific applications, GUMBOS have exhibited characteristics such as fluorescence, magnetism, and even anti-microbial effects [80]. For our interests, GUMBOS have high ionic conductivity and high thermal stability which, in turn, bode well for potential HEMs device applications.

4.2.1: Synthesis of GUMBOS: General Techniques

Although the scientific focus of our work has been primarily upon the characterization of GUMBOS and nanoGUMBOS for their potential amenability to next-generation nano-devices, we have been likewise motivated, from an engineering (and possibly long-term commercial) perspective, by the facile and relatively economical methods of preparation of these materials. Thus, in the way of background information, a brief description of some of the primary techniques for synthesizing these materials is now in order.

4.2.1.1: Micro-emulsion quench approach

This method of preparation was originally reported by the previously referenced 2008 NanoLetters by Tesfai *et al*. It uses an oil-in-water micro-emulsion approach for the creation of micro and nanoparticles. The IL 1-butyl-2,3-dimethylimidazolium hexafluorophosphate ([bm2Im][PF6]) has a melting point of 42 ^{o}C. This [bm_2Im][PF_6] is rinsed in de-ionized water and heated to 70 ^{o}C in a sealed vial with ultrapure water to melt the IL. The dispersion of the IL along with the DI water can be seen in Figure 4-2. The solution is uniformly mixed using a homogenizer, while maintaining the temperature at 70 ^{o}C for 10 minutes. Once a uniform mixture as desired is obtained, the resulting solution is sonicated for 10 minutes. The mixture is then rapidly cooled by placing it in an ice bath. This last step allows the temperature to drop drastically and thus form particles. The diameter of the nanoparticles was reported to be in the range of 60 to 120 nm. The simplicity of synthesis shows great potential for scalability.

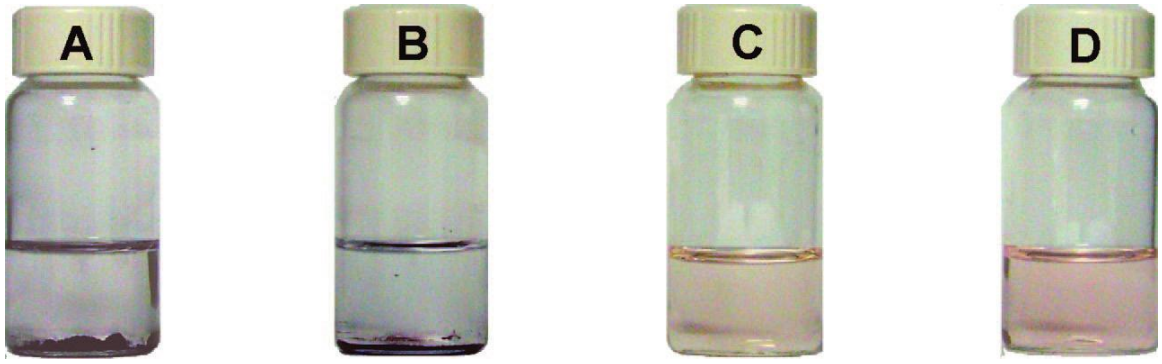

Figure 4-2: (as quoted from [65]) Micro quench emulsion method (A) Solid [bm2Im][PF6] in water at room temperature; (B) molten-state [bm_2Im][PF_6] phase separated from water at 70 ^oC; (C) o/w emulsion containing [bm2Im][PF6] as the inner phase; (D) [bm_2Im][PF_6] nanoparticle crop suspended in water at room temperature. In these images, [bm2Im][PF6] was stained with a water-insoluble dye (Nile Red) for visualization purposes. (Reprinted with permission from [65]. Copyright (2008) American Chemical Society)

4.2.1.2: Micro-emulsion quench with emulsifying agent

In this method, 1-butyl-2,3-dimethylimidazolium hexafluorophosphate [bm_2Im][PF_6] is rinsed in de-ionized water. Brij 35, an emulsifying agent, is added to ultrapure de-ionized water making it 1% Brij 35 solution. The solution is heated to 70 ^oC and [bm_2Im][PF_6] is added to the heated Brij 35 solution drop by drop while homogenizing. This is similar to the method (without emulsifying agent) above. The resulting solution is sonicated for 10 minutes to generate a uniform mixture. Following this, a rapid chilling is done by placing the solution in an ice bath, thereby decreasing the temperature far below the melting point. Here again, nanoparticles are formed. These nanoparticles are reported as having average sizes from 38 to 52 nm[65]. This result illustrates how the addition of the emulsifying agent has stabilized the solution resulting in even smaller nanoparticles. Detailed synthesis steps for the above two methods are reported elsewhere.[65]

4.2.1.3: Reverse micellar templating method

The reverse micellar templating method uses two precursor salts for an ion-exchange reaction. Two separate water-in-oil microemulsions are prepared using the precursor salts. Combining both micro emulsions in a 1:1 ratio due to diffusion followed by an ion-exchange reaction results in the formation of nanoGUMBOS. Tesfai, A., *et al*. (2009) synthesized magnetic and non-magnetic nanoparticles using this method [68]. The series of steps of the reaction are illustrated in the Figure 4-3. The sizes of the resulting particles can be controlled by the concentration of the solution.

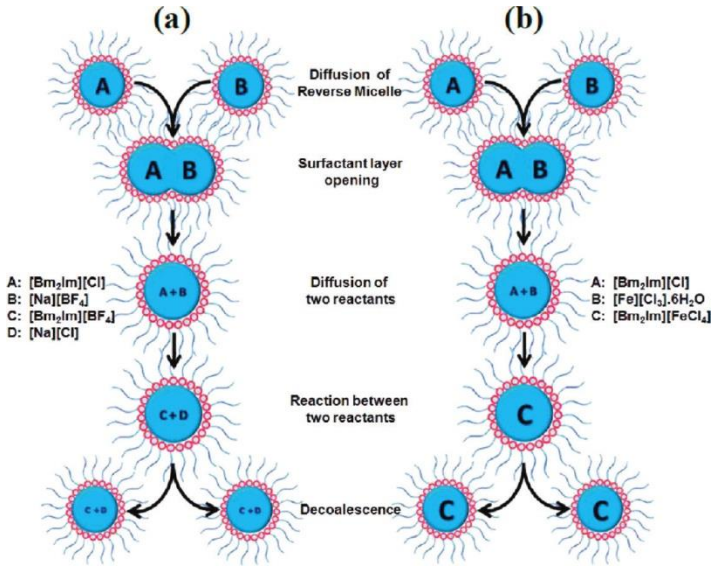

Figure 4-3: Basic processes for nanoparticle formation within reverse micelles. Individual reverse micelles are shown without free surfactants: (a) $[Bm_2Im][BF_4]$ nanoGUMBOS; (b)$[Bm_2Im][FeCl_4]$ magnetic GUMBOS particles. (Reprinted with permission from[68] . Copyright (2011) Royal Society of Chemistry)

4.2.2: Synthesis of nanoGUMBOS: Specific Species

NanoGUMBOS are known as "designer nanoparticles" since modifications to the cation-anion combinations of which they are comprised result in the manifestation of a host of interesting physical (i.e.-melting point, viscosity) and chemical (i.e.-fluorescence, antimicrobial

effects) properties[84]. In this work we have investigated several GUMBOS based candidates for their electrical characteristics. As an effectively a new class of materials with a wide range of potential applications, our research has sought to determine electro-optical characteristics of these materials that may be amenable to nanoscale electronics. This chapter describes the synthesis of various nanoGUMBOS candidates for electrical characterization.

4.2.2.1: Rhodamine 6G Tetraphenylborate ([R6G][TPB])

Detailed description of [R6G][TPB] synthesis can be obtained from [85]. In brief, rhodamine 6G Tetraphenylborate ([R6G][TPB]) is prepared by anion exchange reaction starting with two precursor salts, rhodamine 6G chloride ([R6G][Cl]) and sodium tetraphenylborate ([Na][TPB]). The aforementioned are used for the metathesis reaction in a biphasic mixture of water and dichloromethane (DCM). This reaction results in the formation of [R6G][TPB] GUMBOS, which are rinsed several times with DI water. Repeated rinsing removes the NaCl by-product as [R6G][TPB] is insoluble in water. The DCM solvent is dried to obtain the dry [R6G][TPB]. Figure 4-4 shows the chemical structure of the [R6G][TPB].

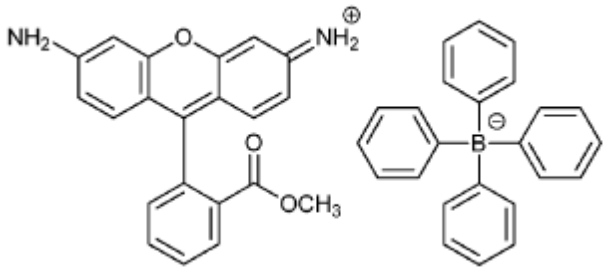

Figure 4-4: Chemical structure of [R6G][TPB] (Reprinted with permission from [85]. Copyright (2011) Royal Society of Chemistry)

(a) [R6G][TPB] nanoparticles

Nanoparticles of [R6G][TPB] are prepared by using the melt-quench-emulsion method. In this case, 100 µL of 1 mM [R6G][TPB] ethanol solution is added to 5 mL of DI water. The resulting solution is sonicated for 5 minutes. Filtration of the water and ethanol was performed using 0.45 µm nylon membrane filters prior to preparation of the nanoGUMBOS. The suspended nanoGUMBOS in DI water were then aged for 1 hour in the dark.

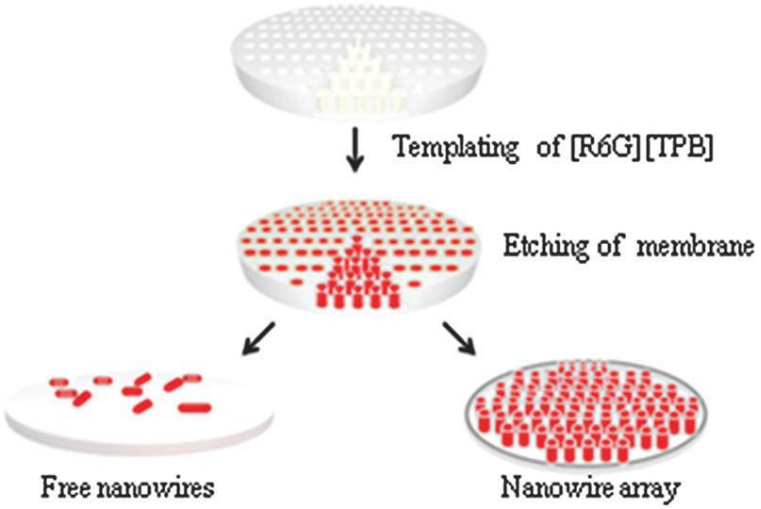

Figure 4-5: Fabrication of [R6G][TPB] nanowires and nanoarrays by AAO templating. (Reprinted with permission from [85]. Copyright (2011) Royal Society of Chemistry)

(b) [R6G][TPB] nanowires

A detailed description of the preparation of [R6G][TPB] nanowires can be obtained from [85]. A nano-porous anodic aluminum oxide (AAO) template was used to synthesize nanowires of [R6G][TPB]. As illustrated in Figure 4-5, an anodic template is submerged in a saturated solution of [R6G][TPB] in acetone and heated to 60^{o}C. This is done to evaporate the acetone and to fill up the nanopores with [R6G][TPB]. The anodic template itself is dissolved using a 1.0 M phosphoric acid solution. What remains are the [R6G][TPB] 1D nanowires. These nanowires are rinsed in DI water several times and dried to obtain nanowire arrays. Figure 4-5 shows the

series of steps needed to form the 1D structures. Electrical characteristics of [R6G][TPB] nanowires are discussed in the results section 4.4.2:.

4.2.2.2: Pseudoisocyanine bis(pentafluoroethanesulfonyl)imide [PIC][BETI]

A detailed description of [PIC][BETI] synthesis is provided in[86]. Pseudoisocyanine bis(pentafluoroethanesulfonyl)imide [PIC][BETI] is prepared by an anion exchange method. Precursor salts, pseudoisocyanine (PIC) iodide and lithium bis(pentafluoroethanesulfonyl)imide (LiBETI), were dissolved in a biphasic solution of methylene chloride and water (2:1, v/v) and stirred for a day at room temperature. The resultant solution is washed thoroughly using DI water to remove the LiI by-product. Methyl chloride is removed by vacuum drying at 40 ^{o}C to thereafter obtain [PIC][BETI] by freeze-drying. Figure 4-6 shows the flow of the reaction and the chemical structure of [PIC][BETI]. The melting point of [PIC][BETI] is determined to be in the range of 169-171 ^{o}C. NanoGUMBOS of [PIC][BET] are prepared by using an additive-free reprecipitation method as discussed in [66, 87]. A 150 µL of 1 mM [PIC][BETI] methanol solution is added to the 5 mL of DI water. This solution is sonicated for 5 minutes, obtaining nanoGUMBOS of [PIC][BETI]. Optical characterization is discussed elsewhere [86]. Figure 4-7 shows the TEM and SEM micrographs of [PIC][BETI] nanoGUMBOS. Rod-like structures with an average length of 0.8-2.2 µm and diameter of 60-100 nm are observed.

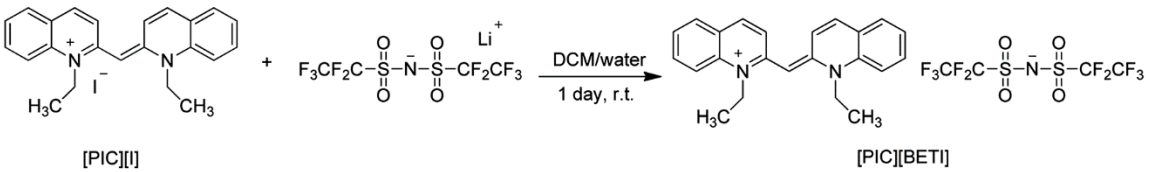

Figure 4-6: Synthesis of [PIC][BETI] (Reprinted with permission from[86]. Copyright (2012) Royal Society of Chemistry)

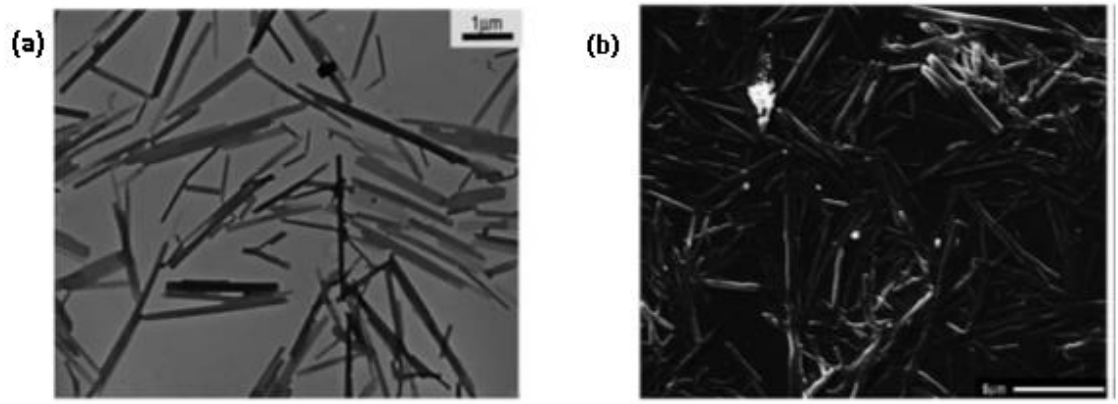

Figure 4-7: a) TEM and b) SEM micrographs of the [PIC][BETI] nanoGUMBOS (Reprinted with permission from[86]. Copyright (2012) Royal Society of Chemistry)

4.2.2.3: Pseudoisocyanine bis(trifluoromethanesulfonyl)imide [PIC][NTf_2]

A detailed description of [PIC][NTf_2] synthesis is provided in[86]. Pseudoisocyanine bis(trifluoromethanesulfonyl)imide [PIC][NTf_2] is prepared by an anion exchange method. Precursor salts, pseudoisocyanine (PIC) iodide and lithium bis(trifluoromethanesulfonyl)imide ($LiNTf_2$) were dissolved in a biphasic solution of methylene chloride and water (2:1, v/v) and stirred for one day at room temperature. The resulting solution is washed thoroughly using DI water to remove the LiI byproduct. Methyl chloride is removed by vacuum drying at 40 ^{o}C and then used to obtain [PIC][NTf_2] by freeze drying. Figure 4-8 shows the flow of the reaction and the chemical structure of the [PIC][NTf_2]. A melting point of [PIC][NTf_2] is determined to be in the range of 243-248 ^{o}C, notably quite high for an ionic liquid-based material. NanoGUMBOS of [PIC][NTf_2] are prepared by using an additive-free reprecipitation method discussed in [66, 87]. Next, 150 μL of 1 mM [PIC][NTf_2] methanol solution is added to the 5 mL of DI water. The resulting solution is sonicated for 5 minutes, obtaining nanoGUMBOS of [PIC][NTf_2]. Optical characterization is discussed elsewhere [86]. Figure 4-9 shows the TEM

and SEM micrographs of the [PIC][NTf_2] nanoGUMBOS. Interestingly, diamond shaped structures are observed with an average length of 0.8-2.2 µm and diameter of 60-100 nm. The diamond shape was determined to be due to a head-to-tail type of molecular orientation stacking within the [PIC][NTf_2].

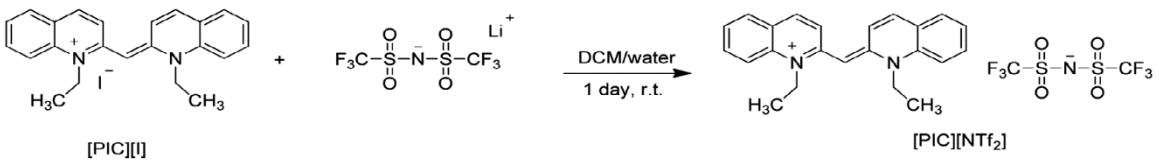

Figure 4-8: Synthesis of [PIC][NTf_2] (Reprinted with permission from[86]. Copyright (2012) Royal Society of Chemistry)

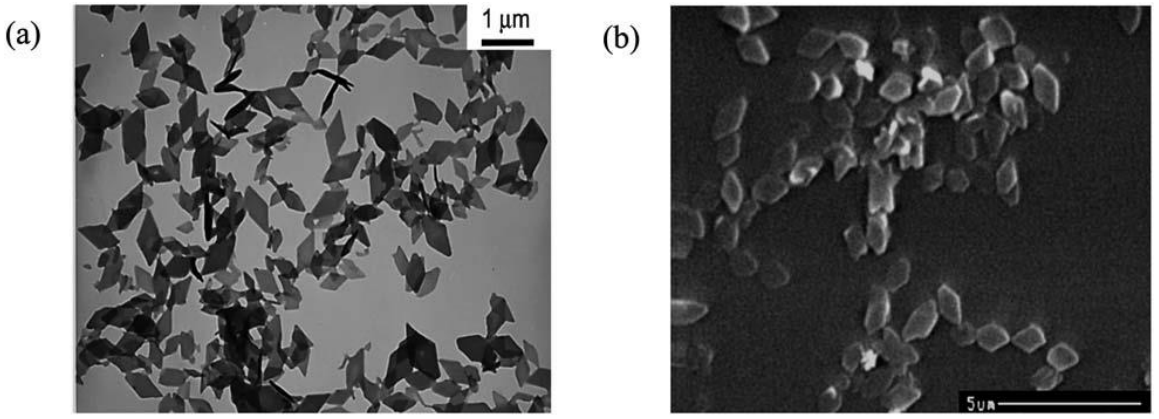

Figure 4-9: a) TEM and b) SEM micrographs of the [PIC][NTf_2] nanoGUMBOS (Reprinted with permission from[86]. Copyright (2012) Royal Society of Chemistry)

4.2.2.4: Thiacarbocyanine (TC) nanoGUMBOS

Thiacarbocyanines, a family of dyes, has been of great interest due to their aggregates and the structures which they form. The presence of the [BETI−] anion imparts hydrophobicity to the GUMBOS, creating a variety of ionically self-assembled structures. GUMBOS of TC dyes are prepared by using thiacarbocyanine (TC) dyes 3,3-diethylthiacyanine iodide ([TC0][I]), 3,3-diethylthiacarbocyanine iodide ([TC1][I]), 3,3-diethylthiadicarbocyanine iodide ([TC2][I])

and lithium bis(pentafluoroethane)-sulfonimide (LiBETI) salts at a molar ratio of 1 to 1.1. The reaction was performed in a biphasic mixture of water and dichloromethane (DCM) (1:5, v/v) under stirring for 24 hours. The remaining solution is washed thoroughly using DI water to remove the LiI byproduct. DCM is removed by vacuum drying at 40 ^{o}C to obtain TC GUMBOS by freeze-drying. The chemical structure of TC GUMBOS is shown in Figure 4-10.

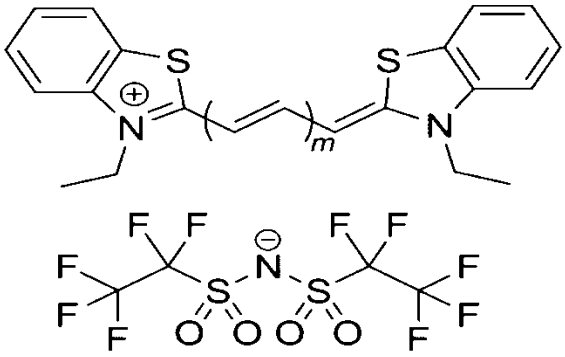

m = 0 [TCO][BETI]
m = 1 [TC1][BETI]
m = 2 [TC2][BETI]

Figure 4-10: Chemical structure of TC GUMBOS (Reprinted with permission from [88]. Copyright (2012) American Chemical Society)

TC nanoGUMBOS are prepared by using the additive-free reprecipitation method discussed in detail elsewhere [66, 87]. Here 100 µL of 0.1 mM TC GUMBOS ethanol solution is added to the 5 mL of DI water. The resulting solution is sonicated for 5 minutes and allowed to equilibrate for 10 minutes, obtaining nanoGUMBOS of TC GUMBOS. SEM images (Figure 4-11) of [TC0][BETI], [TC1][BETI], [TC2][BETI] nanoGUMBOS show that each have unique morphology and size. . Detailed synthesis and optical characterization is discussed elsewhere [88].

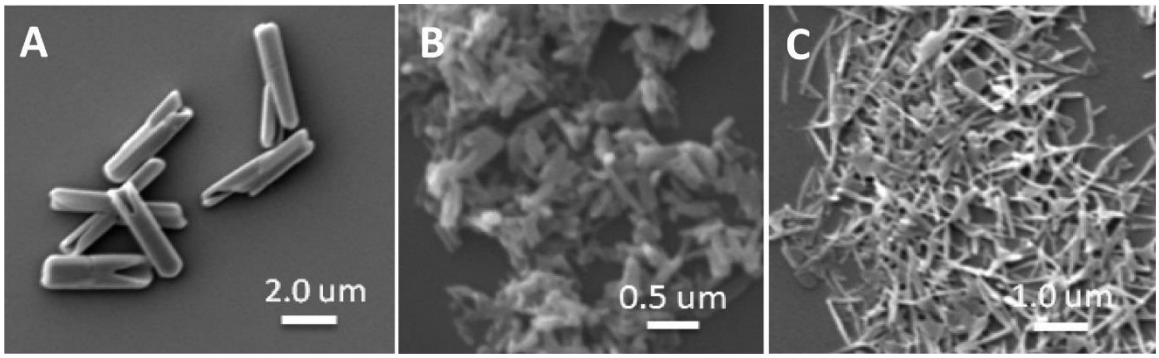

Figure 4-11: SEM micrographs of (A) [TC0][BETI], (B) [TC1][BETI], and (C) [TC2][BETI] aggregates (Reprinted with permission from [88]. Copyright (2012) American Chemical Society)

4.3: Experimental setup

4.3.1: Substrate preparation

Glass slides (Corning plain microscope slides, thickness ~1 mm) were cleaned with warm piranha solution (H_2SO_4:H_2O_2=1:1) for about 30 minutes to remove any organic impurities. A thin layer of gold (thickness ~200 nm) was deposited onto the glass by thermal evaporation. The gold coated glass slides were further cleaved into smaller pieces (1-1.5 x 1-1.5 cm^2) to serve as substrates for CP-AFM sample characterization.

4.3.2: Atomic Force Microscopy (AFM) imaging

A NanoR model atomic force microscope (AFM) from Pacific Nanotechnology (now Agilent) with a conductive tip is used for electrical characterization. The tip (DPE 14 /no Al), purchased from MikroMasch, is made of silicon with a 30 nm platinum (Pt) coating. The radius is less than 40 nm and height is ~20-25 µm, cone angle less than 40^o with resonant frequency of approximately 160 kHz and force constant of 5.7 N/m. The conducting probe is mounted on a rectangular 3.4 x 1.6 x 0.4 mm silicon chip.

4.3.3: Conductive Probe Atomic Force Microscopy (CP-AFM)

The AFM was operated in *contact mode* to obtain current-voltage (I-V) characteristics, where the conductive tip is used as one of the electrodes with the other being a gold substrate (section 4.3.1:), thereby forming a metal (Pt)-particle-metal (Au) junction. Prior to I-V measurements, AFM images were obtained by surface scanning in contact mode. The CP-AFM schematic is shown in Figure 2-9. The test site for CP-AFM is determined using AFM imaging. Applying a constant bias of 0.25 V, the tip is lowered in small increments to detect any signs of change in current to detect the nanoparticles. Using the SCS, voltage is swept in 0.05 V steps while simultaneously measuring the current.

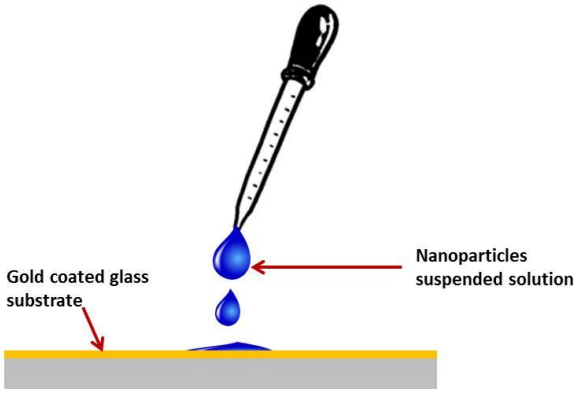

Figure 4-12: Schematic of the dropcasting of nanoparticles suspended in solution on the gold coated glass substrate

4.3.4: Sample preparation of [R6G][TPB] nanoparticles

The [R6G][TPB] nanoparticles were deposited onto the gold coated glass substrates (section 4.3.1:) by the dropcasting. A schematic of the dropcasting process in shown in Figure 4-12 . The [R6G][TPB] nanoparticle solution was kept in an ultrasonic bath for 15 minutes prior to the deposition process to minimize aggregation of the particles in the solution. Approximately 10 µL of [R6G][TPB] nanoGUMBOS in aqueous solution was dispensed onto the substrates.

The dispensed droplet was allowed to spread out evenly on the surface and dried in ambient air for 24 hours before further characterization experiments.

4.3.5: Test structure for characterization of [R6G][TPB] nanowires

[R6G]TPB nanowires were characterized using a gold (Au) inter-digitated comb or "finger" microstructure as shown in Figure 4-13. The [R6G][TPB] nanowires were dropcast across the microfabricated finger electrodes. This gold interdigitated structure served as a device

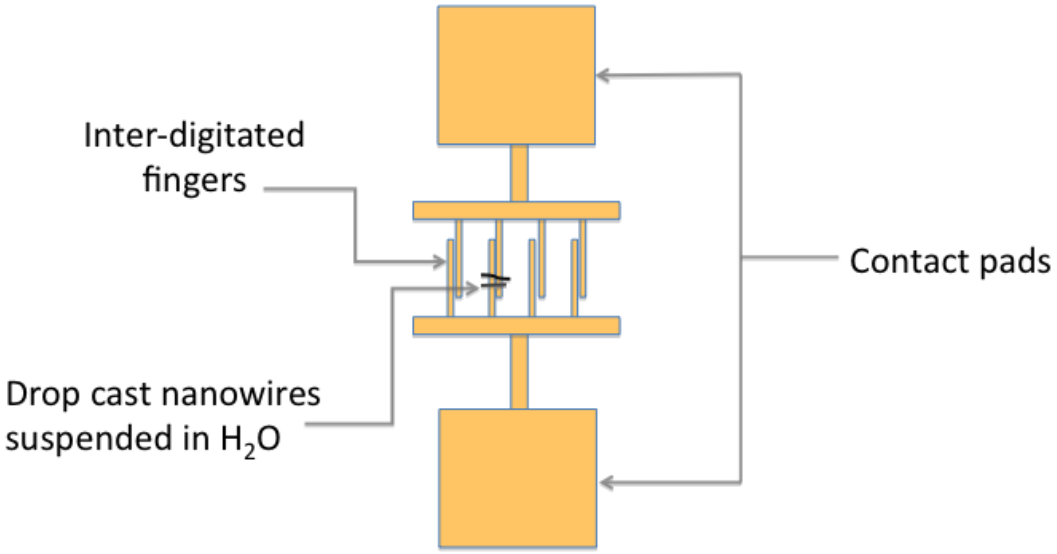

Figure 4-13: Schematic of nanowires dropcasted on interdigitated structure

prototype through which the electronic responses of the nanowires were measured. All of the measurements were done using a Semiconductor Characterization System (Keithley 4200 SCS) in a custom built vacuum chamber. The schematic of the experimental setup is shown in Figure 4-14(a). The vacuum chamber is pumped down to approximately 0.1 torr, then purged with dry nitrogen to maintain an inert ambient. The bottom plate of the chamber is designed for electrical connections from which measurements may be recorded (Figure 4-14 (b)).

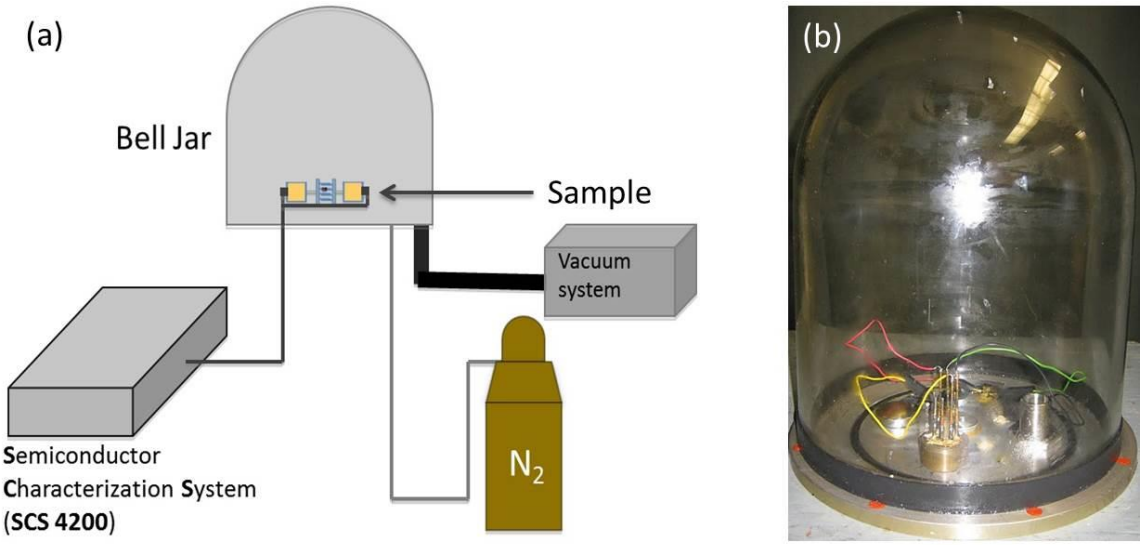

Figure 4-14: (a) Schematic of the Isolation chamber with electrical characterization system (b) Bell jar vacuum chamber with electrical connections

Gold interdigitated electrodes are fabricated using photolithography. A photolithographic mask was designed with interdigitated electrode spacing of 10 µm. The interdigitated structure was chosen to give flexibility and robustness in electronic characterization. The following procedure was followed for development of the interdigitated structure using optical lithography: i) mask design and printing, ii) spin coating of photoresist, iii) exposing and developing, iv) gold deposition, and v) photoresist liftoff.

4.3.5.1: Mask design and printing

The photolithographic mask was designed using AutoCAD in the LSU Division of Electrical and Computer Engineering's Electronic Material Device Laboratory (EMDL) and was printed at the University of Illinois Urbana-Champaign. Figure 4-15(a) shows the schematic and (b) actual mask image.

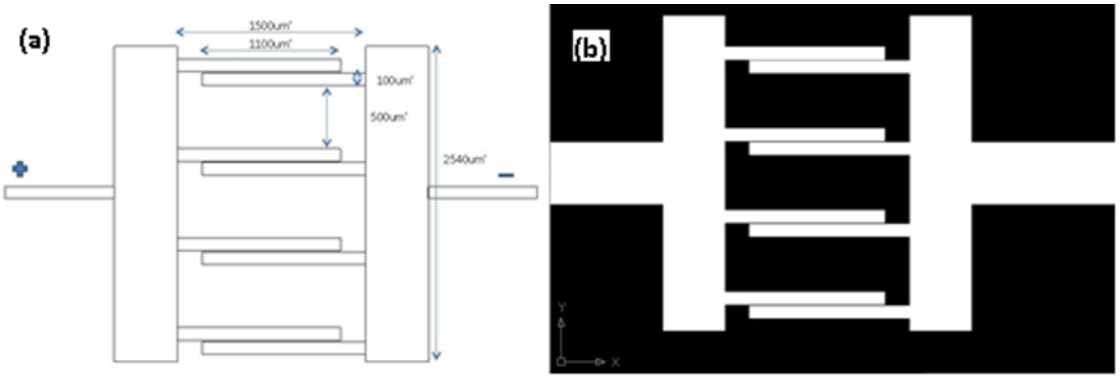

Figure 4-15: a) Schematic b) actual mask of the interdigitated structure with inter-finger distance of 10µm.

4.3.5.2: Spin coating of photoresist

Shipley 1813 positive photoresist was used for developing the mask template. Glass substrates were cleaned and heated for 1 minute on a hot plate of 100 ^{o}C to remove moisture. A thin layer of Hexamethyldisilazane (HMDS) is used to coat the glass as it promotes adhesion of the photoresist. The substrate was then spin coated with Shipley 1813 with the spin curve shown in Figure 4-16. This sequence was used to achieve a target thickness of 1.4 µm. This treated substrate was pre-baked at a constant 100 ^{o}C temperature in an Ultra Clean 100™ oven.

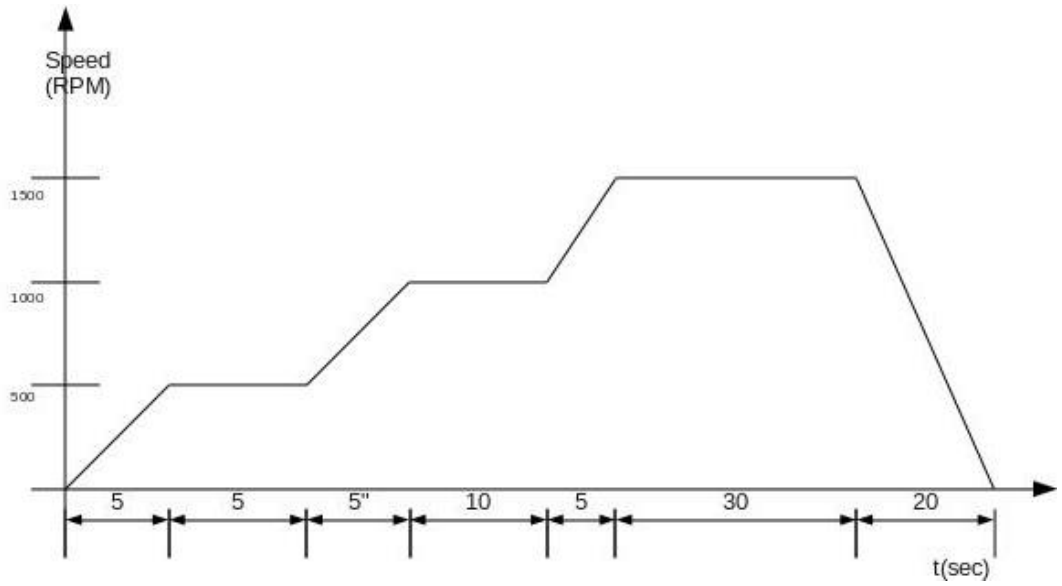

Figure 4-16: Spin curve for photoresist Shipley 1813

4.3.5.3: Exposure and development of photoresist

A Quintel 4000 ultraviolet (UV) mask aligner was used for a predetermined time (for Shipley 1813) to obtain uniform exposure based upon a lamp power of 150 mW per square inch of substrate. The substrate was agitated in MF 354 developer for 30-45 seconds and then with DI water to develop the resist. This was followed by a post-bake for 1 minute at 100 ^{o}C to remove moisture and to strengthen the photoresist structure.

4.3.5.4: Thermal Evaporation of gold

Gold (Au) of 99.99% purity from Sigma-Aldrich in the form of pellets was used as obtained. A 0.1 µm thick Au layer was evaporated onto the lithographic structure using an NRC 703™ Thermal Evaporator.

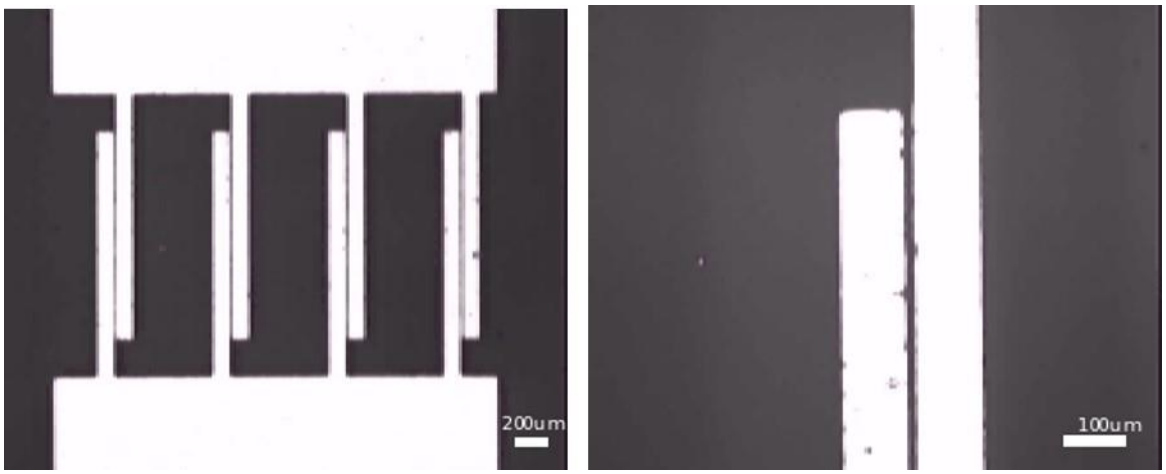

Figure 4-17: a) Optical microscope image of gold interdigitated structure, b) A pair of fingers of the interdigitated structure

4.3.5.5: Photoresist stripping and liftoff

The Au evaporated structure was immersed into an acetone bath. The bath was agitated by an ultra-sonicator for approximately 45 seconds, allowing the photoresist to dissolve. The

resulting structure was agitated in methanol and DI water for 30 seconds each to obtain the desired interdigitated structure as shown in the Figure 4-17.

4.3.6: Sample preparation of [PIC][BETI] and [PIC][NTf_2]

[PIC][BETI] and [PIC][NTf_2] are characterized using CP-AFM. These nanomaterials are dropcast on the gold coated glass substrates and allowed to dry at room temperature. Dried samples are used to obtain AFM images, after which CP-AFM was conducted. The same CP-AFM settings and sample preparation as discussed for [R6G][TPB] nanoparticles (section 4.3.4:) are used for both [PIC][BETI] and [PIC][NTf_2] nanostructures.

4.3.7: Sample preparation of [TC2][BETI] nanoGUMBOS for vapor sensing

When thiacarbocyanine (TC) GUMBOS solution is dropcast onto a substrate, as the solvent evaporates the nanowires therein self-assemble into nanostructures of various dimensions. This is due to the [BETI-] anion as it induces hydrophobicity and high surface energy causing the material to form rod-like structures. Two milligrams of the dry form of [TC2][BETI] GUMBOS was dissolved in 5 mL of ethanol. This preparation was sonicated for 10 minutes to obtain a uniform solution.

4.3.8: Test structure for characterization of [TC2][BETI] nanoGUMBOS for vapor sensing

Various forms of thiacarbocyanines are known for their chemical sensing properties[89, 90]. In this work we have investigated [TC2][BETI] nanowires for their vapor sensing abilities. To do so we used two primary methods—1) Direct analyte injection (Method 1), and 2) Carrier gas (Method 2). Each method involves a custom designed interdigitated ("fingers") sample mount with contact pads (see section 4.3.5:) onto which [TC2][BETI] nanowires have been

dropcast or electrosprayed. The finger-contact pad combination provides the necessary electrical connection between the nanowires and the external electronics of the experimental setup. This mount is housed within a 2.3 liter glass chamber in which the gas may be contained.

4.3.8.1: Direct analyte injection test structure (Method 1)

[TC2][BETI] nanowires were dropcast onto the interdigitated structure to form a nanowire sensor or test structure. (The interdigitated structure here is the same as that which was developed for the [R6G][TPB] nanowires; see section 4.3.5: In this method, the analyte is injected into the glass chamber directly and allowed to evaporate while the I-V response of the nanowire sensor is recorded. Selected inlets and outlets of the glass housing, as indicated in Figures 4-16 and 4-17, are used to purge the chamber with dry nitrogen as well as to provide a pathway for the electrical connections between the test structure and an external Semiconductor Characterization System (Keithley SCS 4200, not shown).

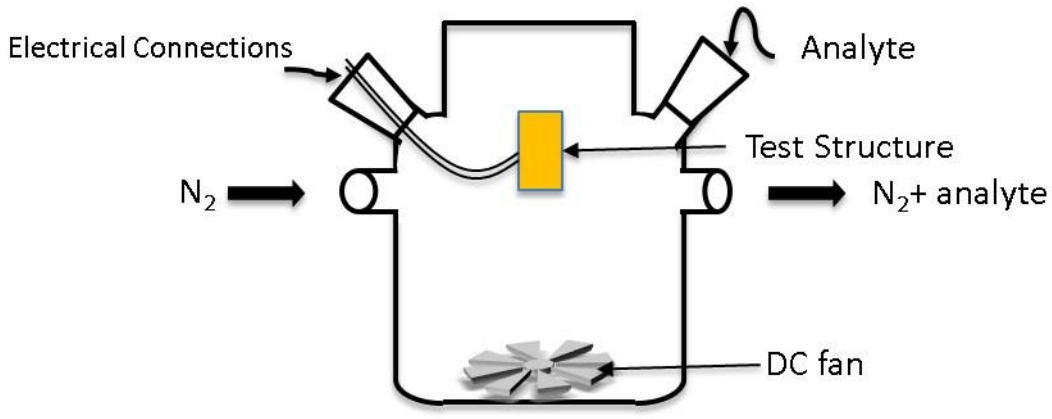

Figure 4-18: Schematic of the direct injection method

Initially the chamber is purged with dry nitrogen for 10 minutes to create an inert environment. Voltage across the electrodes of the *test structure* is swept from -20 V to +20 V

using the SCS and current is recorded without any analyte in the chamber to obtain a reference value for the sensor. Once reference values are obtained, a known amount of analyte is injected into the chamber via a micro needle inserted through the septum as shown in the aforementioned figures. In general, when a VOC (volatile organic chemical) is evaporated, depending on its density and molecular weight, it exerts vapor pressure.

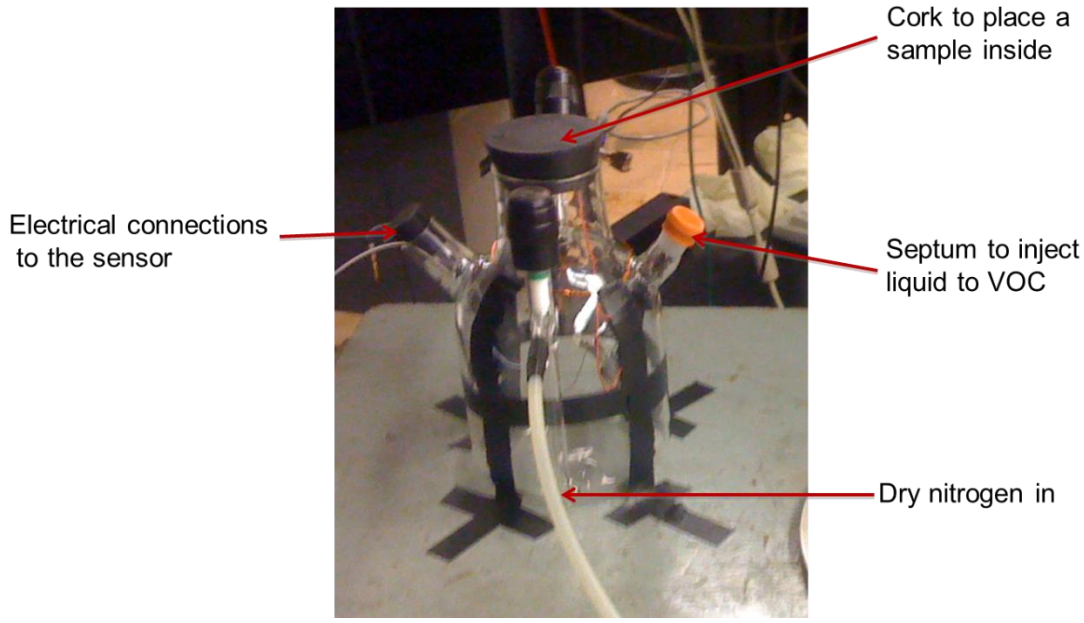

Figure 4-19: Direct injection vapor sensing experimental setup

Thus, the concentration of the analyte inside a chamber, i.e.- C_{ppm} (concentration in parts per million), varies from analyte to analyte. In order to compare the sensing results of the nanowires due to various analytes, the C_{ppm} needs to be constant. To keep the C_{ppm} of all the VOCs inside the camber constant, the volume of liquid injected is calculated using the equation shown[91]

$$C_{ppm} = \frac{10 C_o p V_{vol} R T}{M P_o V_o} \tag{4-1}$$

where C_{ppm} is the concentration of VOC in parts per million inside the chamber once evaporated. Also,

C_o is the initial concentration of the liquid (100)
p is density of the VOC
R, Universal Gas Constant (0.08205746 Latm $K^{-1}mol^{-1}$)
T, Room temperature 300^{o}K
M, Molecular Weight of the VOC
P_o, Pressure inside the chamber (1 atm)
V_o, Volume of the chamber (2.3 L).

C_{ppm} for aniline, dimethylamine, nitromethane, cyclohexane, trimethylamine are calculated with the V_{vol} of 1µL. The obtained C_{ppm} values are scaled down using C_{ppm}=100 to obtain V_{vol} (µL) of the analyte. The caluclated V_{vol} values for the different analytes are listed in Table 4-1 below.

Table 4-1: Table showing the calculated volume of VOC to be injected into the chamber

Analyte	**Density (p)**	**Molecular weight(M)**	**V_{vol} (µL)**
Aniline ($C_6H_5NH_2$)	1.0217	93.13	0.8
Dimethylamine [$(CH_3)_2NH$]	0.68	45.08	0.6
Nitromethane (CH_3NO_2)	1.127	61.04	0.5
Cyclohexane [C_6H_{12}]	0.779	84.16	1.0
Trimethylamine [$(CH_3)_3N$]	0.63	59.11	0.8

To assist in the evaporation of the injected analyte, a filter paper and a small DC fan is placed at the bottom of the chamber as shown in the schematic Figure 4-18. Most of the analytes used evaporate in approximately 2 minutes; however, the fan is allowed to run for 4 minutes to make sure that the vapor will mix uniformly in the chamber. Using the SCS voltage is swept from -20 to +20 V across the test structure as current measurements are recorded simultaneously.

4.3.8.2: Carrier gas injection experimental setup and test structure (Method 2)

(a) Carrier gas experimental setup

A schematic of the carrier gas setup used for vapor sensing is shown in Figure 4-20. This method uses the same glass chamber used in the direct gas method (Figure 4-18). However, instead of injection of analyte directly into the chamber, nitrogen (carrier gas) is used to carry the analyte into the chamber. Dry nitrogen is used as a carrier gas, for purging, and to maintain an inert environment in the 2.3 liter glass chamber. The flow rate of the dry nitrogen is controlled using a mass flow controller (MFC) which is calibrated for flow control to as low as 100 mL/min. The MFC flow rate is monitored and fine-tuned by an external controller. To start the process of detecting VOCs, the chamber is purged with dry nitrogen before any measurements. Once purged, inlet and outlet ports are closed to maintain the inert environment. A constant voltage is applied and current is measured using the SCS for reference before the introducing the analyte. A controlled amount of analyte carried by carrier gas (N_2) is introduced while a constant voltage is applied. During the process, change in the current is measured using the SCS.

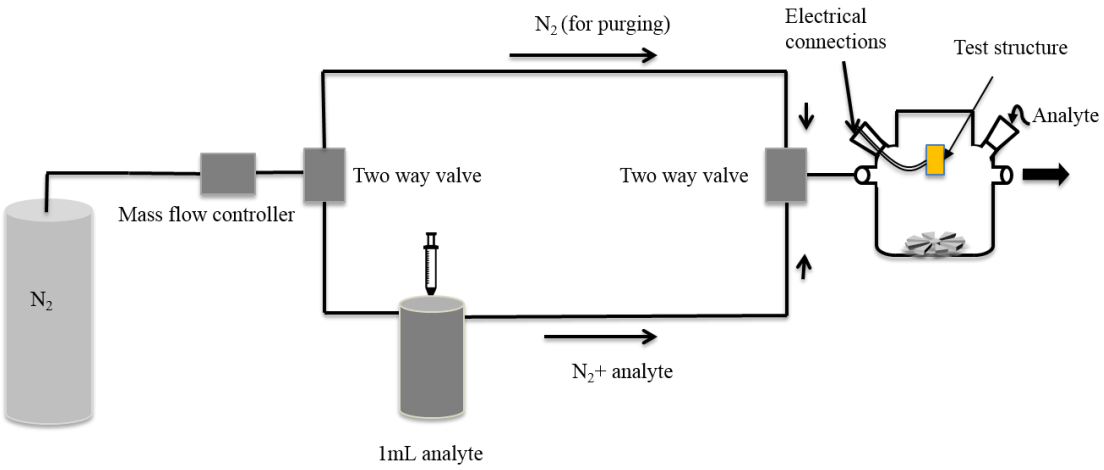

Figure 4-20: Schematic of the vapor sensing using carrier gas method

(b) Carrier gas test structure

For carrier gas method [TC2][BETI] nanowires are deposited on the interdigitated structure using electrospraying to create uniform coverage. Electrospraying was discussed in detail in section 2.3.1:. Electrospraying of [TC2][BETI] solution generates fine droplets when deposited onto the interdigitated structure, and upon the evaporation of solvent (ethanol), [TC2][BETI] self-assembles into nanowires.

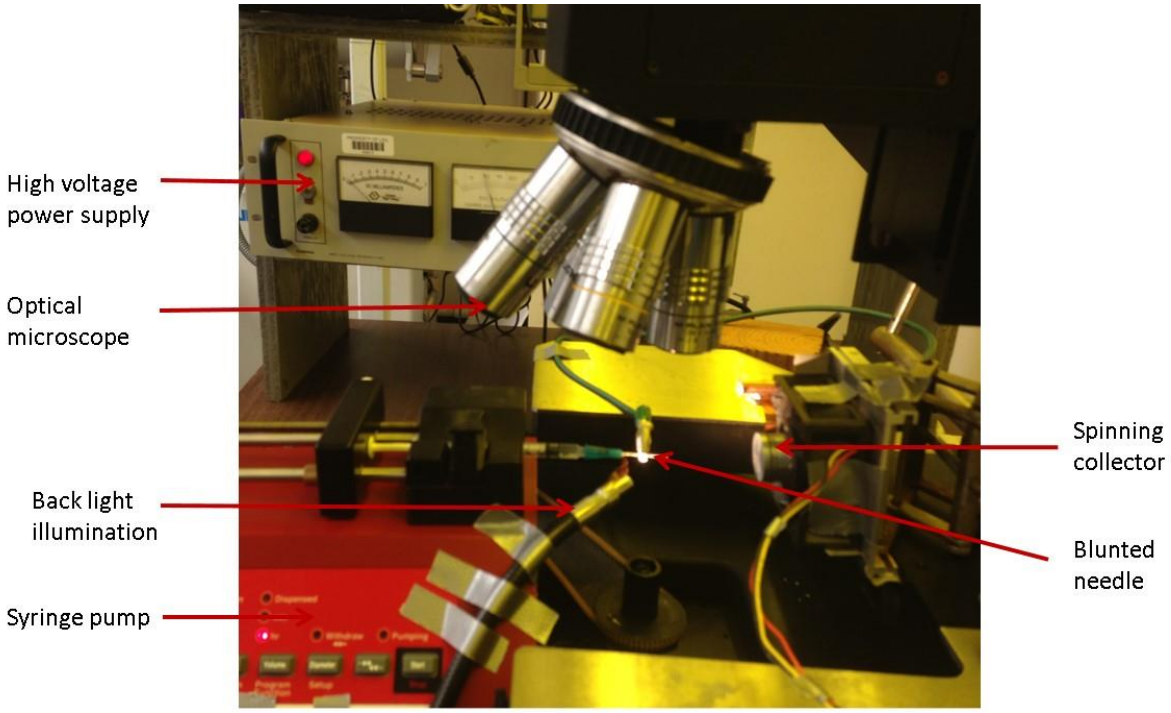

Figure 4-21: Needle electrospraying setup

Figure 4-21 is a photograph of our electrospraying setup. A syringe pump (NE-300, New Era Pumping systems) is used for flow control of the solution down to as low as 1 µL/hr for BD-1 mL syringe and 1257 mL/hr for BD-60 mL syringe. A DC power supply with range of 0 to 30 kV (Gamma High Voltage) is used. A needle of BD 25G was blunted using sand paper to obtain a uniform electric field. The syringe has an internal diameter of 4.699 mm (BD syringe). A DC high voltage is applied to the needle while the collector is connected to ground.

The collector is spun at a constant speed by placing it on a DC motor for the purpose of obtaining a uniform deposition. An optical microscope is focused on the tip of the needle to monitor and record the electrospraying. High intensity back light is shone as pictured on the end of the blunted needle to illuminate the spray droplets. Piranha cleaned 1 x 1 cm substrates are glued to the collector using conductive double-sided tape. The distance between needle and the substrate and applied potential are varied to obtain a cone jet mode for [TC2][BETI] GUMBOS. A successful electrospray is achieved for a distance of 3 cm, with voltage range of 4.5 kV to 7 kV. Voltages above 7 kV are avoided due to electric arc generation breakdown from needle to ground. Figure 4-22 shows scanning electron microscope (SEM) micrographs of [TC2][BETI] nanowires deposited by needle electrospraying on glass. In preparation for SEM imaging, the samples were sputter coated with 5 nm of platinum. A reasonably full coverage of the glass substrate by nanowires is observed. Nanowire thickness varied from 200 to 400 nm with an average length of 5 μm. The nanowire network is a highly porous structure with a high surface area.

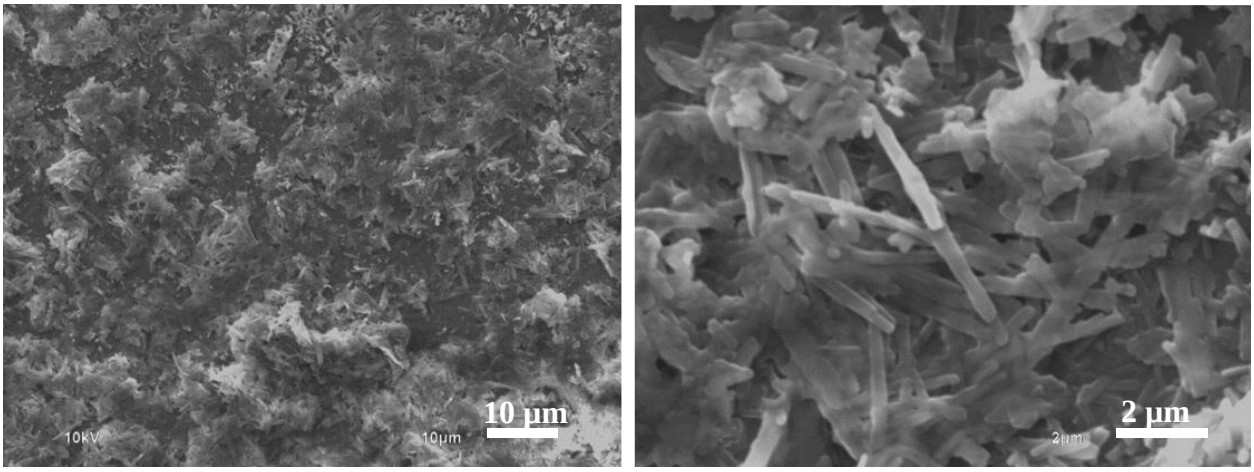

Figure 4-22: SEM images of the [TC2][BETI] nanowires deposited with electrospraying for carrier gas method

4.4: Results and Discussion

4.4.1: [R6G][TPB] nanoparticles: Imaging and I-V Characterization

Figure 4-23 shows the AFM topographic image of the [R6G][TPB] nanoparticles dropcasted onto the gold substrate. These images are obtained prior to CP-AFM experiments. Topographic AFM indicates aggregation of nanoparticles on the gold substrate. Aggregation of the nanoparticles is due both their high surface energy and dropcasting (method of deposition). Below the topographic image of Figure 4-23 is a line scan that represents the diameter of the deposited (aggregated) nanoparticles of [R6G][TPB]. Sizes of the nanoparticles obtained from the line varied from 200-500 nm due to their aggregation.

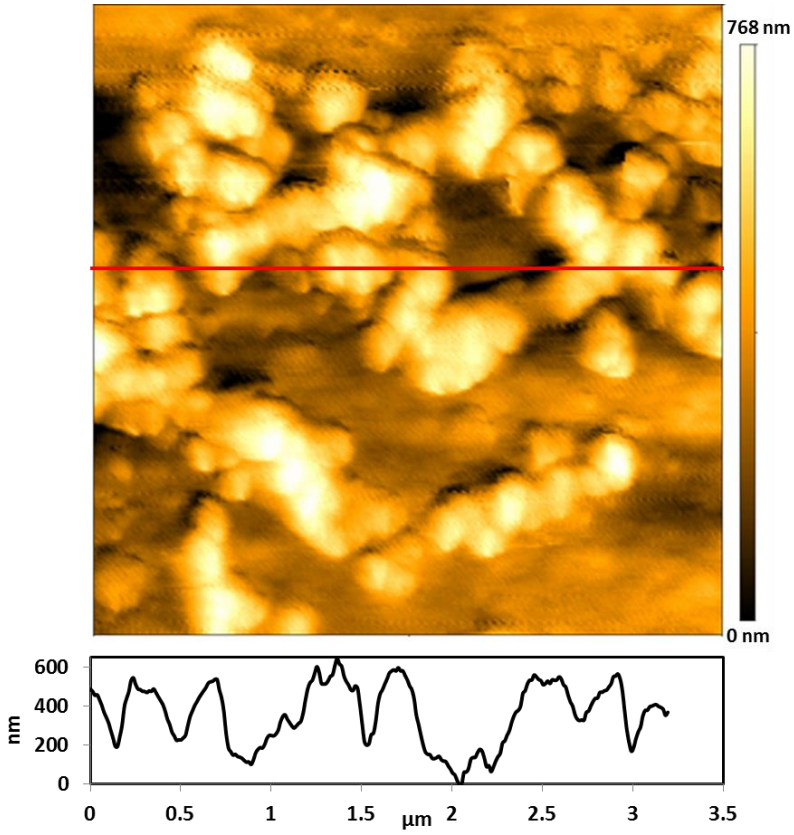

Figure 4-23: Atomic Force Microscopy (AFM) images of [R6G][TPB] nanoGUMBOS, topographic image of the dropcasted [R6G][TPB] nanoparticles on gold surface

As AFM images indicated aggregation of the [R6G][TPB] nanoparticles, CP-AFM measurements were used to investigate the electrical responses of the particles for this morphology. Using a Pt coated conductive AFM tip as one electrode and the Au substrate of the sample as the other (see section 2.4.2:), a metal-nanoparticle-metal junction was formed. Figure 4-24 shows the I-V characteristics of the [R6G][TPB] nanoparticles where each colored trace represents a different test site on the sample. A fairly linear I-V characteristic is evident for each site to which the conductive probe was applied. The current response of the nanoparticles through the Pt-[R6G][TPB]-Au junction was in the range of 10^{-7} to 10^{-6} A for a corresponding voltage sweep from 0 to 1 V.

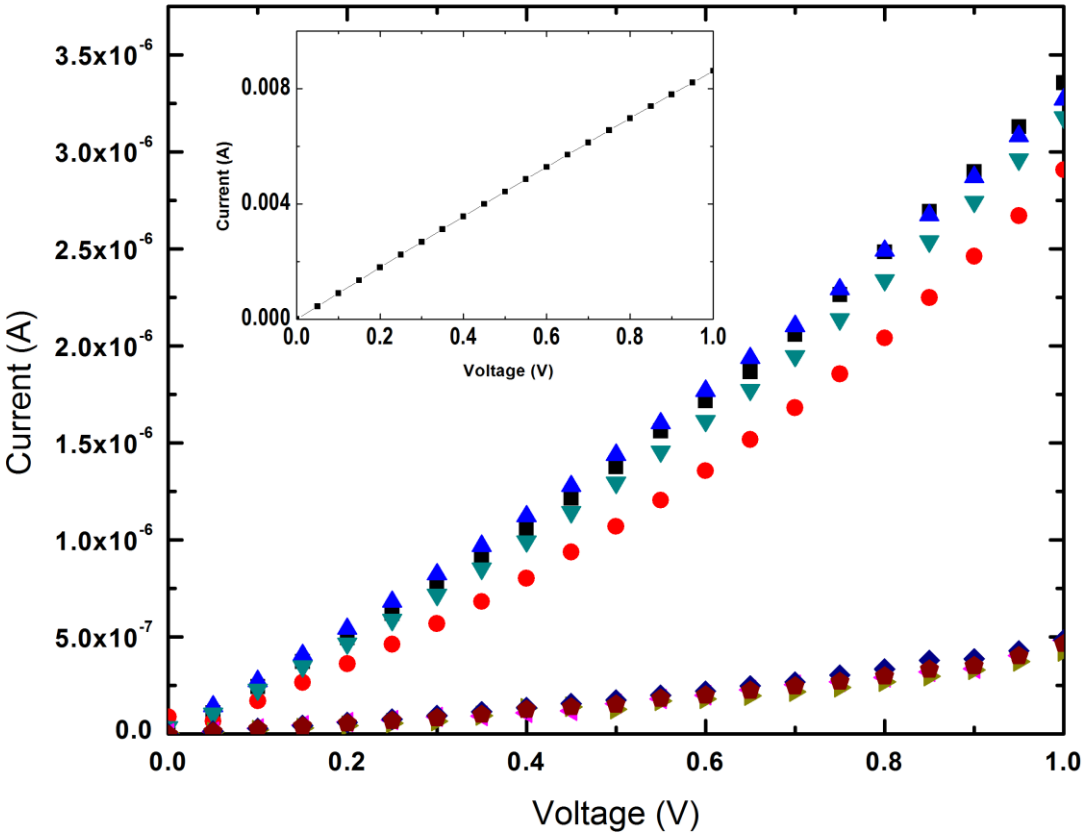

Figure 4-24: I-V characteristics of [R6G][TPB] nanoparticles with CP-AFM. Each colored trace is representative of the I-V characteristics for various test sites along the sample (Reprinted with permission from Springer [93]).

The current response for this kind of junction has been investigated and reported as being due to a combination of several factors such as the injection of carriers at the junction barrier, metal-semiconductor-metal junction, and particle aggregation[92]. As a fundamental function, the nanoparticles do conduct, albeit with resistance calculated from the curve in the range of 0.3 MΩ to 3 MΩ. The inset graph in Figure 4-24 shows I-V characteristics of the platinum coated tip directly in contact with the gold surface (short-circuit) for reference with current limited to 1 mA to avoid excessive heating of tip-substrate junction. The short circuit characteristic is linear with very high current on the order of 10^{-3} A as expected due to the radius of the tip (< 40 nm) and the thickness of the Au (100 nm).

4.4.2: [R6G][TPB] nanowires: Imaging and I-V Characterization

Synthesis of [R6G][TPB] nanowires using an anodic aluminum oxide template method is discussed in section 4.2.2.1:. An approximately 10 μL aqueous solution of [R6G][TPB] nanowires was dispensed and dried on Au-coated glass substrates for AFM imaging. The AFM images and height profiles of the dropcasted [R6G][TPB] solution of nanowires are shown in Figure 4-25. Dropcasting of nanowires results in a degree of aggregation which leads to discontinuity in the surface coverage, random orientation, and the stacked nature of the nanowire ensembles. The aggregation of functional nanomaterials and structures in dropcasted samples has been a challenging issue in materials research which can lead to a fairly wide distribution of their measured dimensions[94]. The acquired images from our scans revealed the presence of cylindrical wires with thicknesses ranging from approximately 200 nm to 400 nm. These values do correspond to the pore size variations of the anodic templates in which the nanowires were grown. The length of the nanowires varied from 1 μm to 3 μm. The red line across each AFM scan in Figure 4-18 corresponds to the height profiles shown below the images of the samples.

Current-Voltage characteristics of the [R6G][TPB] nanowires are obtained by dropcasting them onto the gold interdigitated structure. Detailed fabrication of this structure is discussed in section 4.3.5:. Ten microliters of DI water suspended nanowires are dropcast onto the inter-digitated structure and allowed to dry in a 0.1 torr vacuum for 30 minutes. Figure 4-26 depicts an array of I-V curves acquired from the Au-[R6G][TPB]-Au junction for a series of electrical measurements.

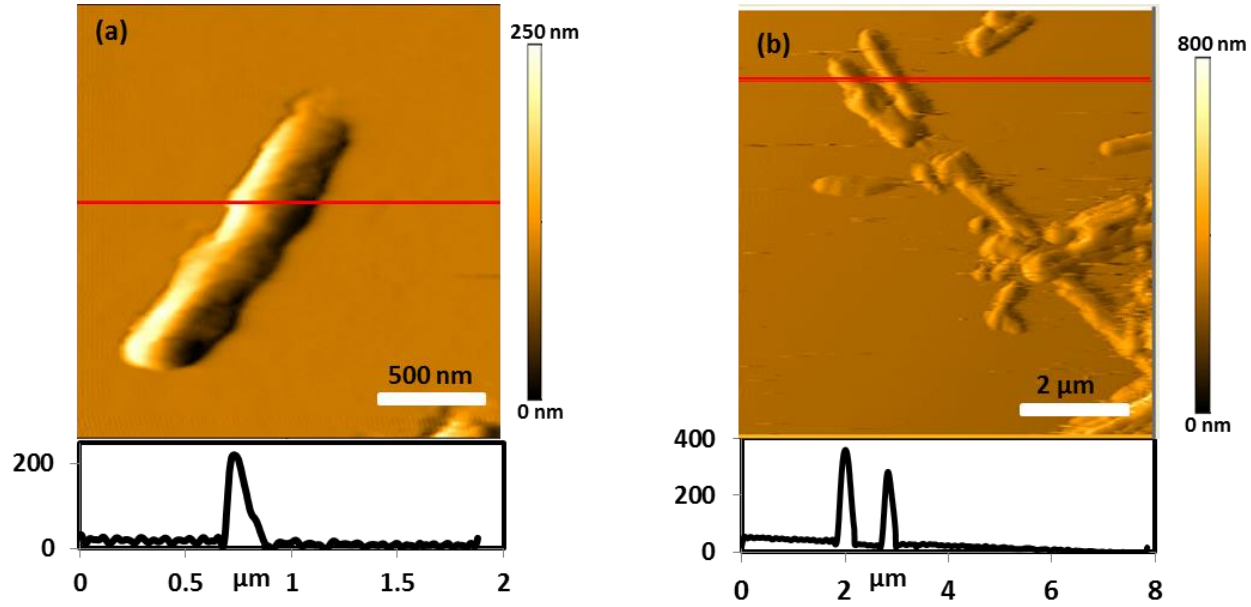

Figure 4-25: a) Atomic force microscopy images of the [R6G][TPB] nanowires, b) Red line represents the height profile line scan (shown below the topographic images) of the nanowires.

The current measurements through the junction varied from 0.8 µA to 1.8 µA for voltage sweeps from 0 to 1 V. The threshold voltage for molecule stability for a reproducible I-V response was around 1 V, beyond which irreversible breakdown of the R6G molecular structure followed. A low leakage current through the substrate, on the order of 10^{-11} A (as shown in the inset of Figure 4-26), was obtained from the underlying interdigitated Au comb devoid of dropcasted nanowires. The charge transfer model across two-electrode metal-molecule-metal junctions (or donor-molecular bridge-acceptor geometry) has been reported to be a sensitive function of the nanowire

diameter, contact area of the active elements (i.e.-the number of molecules participating in the electron transfer), through bond (TB) tunneling, and the nature of electronic coupling between the metal electrodes and the molecule[94]. Further studies in this direction have shown that there is a strong correlation between the current flow or electron transfer and the molecular structure of the incorporated molecule. The precise control of energy gap (ΔE) between the energy states (HOMO-LUMO) of the molecular bridge and the energy level of the donor-acceptor metal units have been identified as relevant factors in determining the electron transfer rate[94-96].

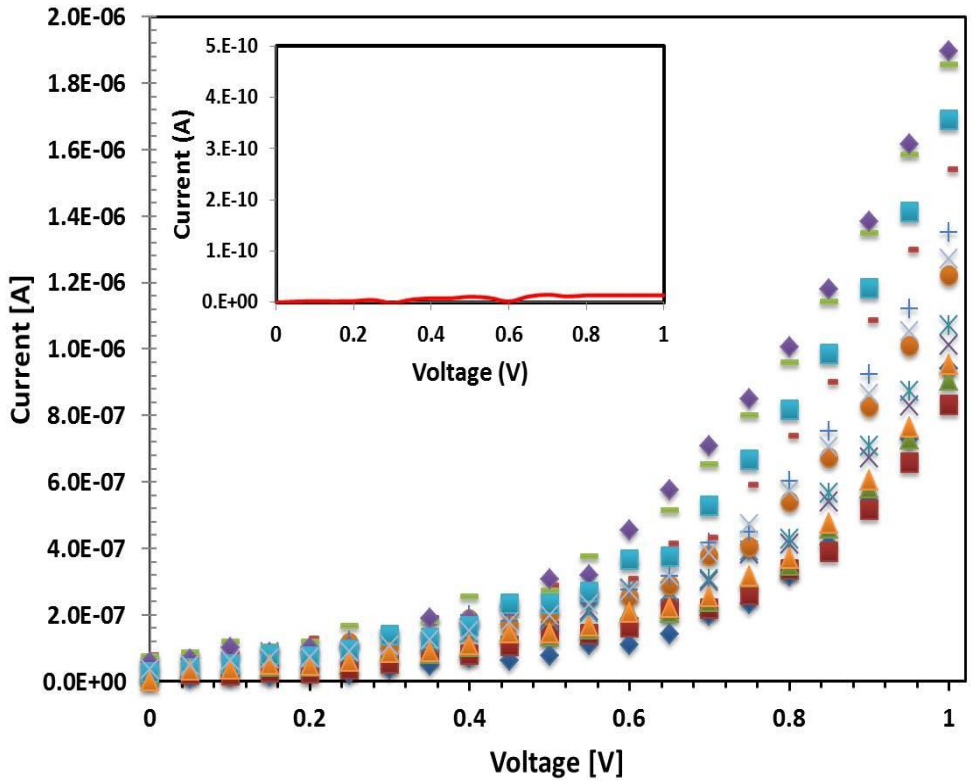

Figure 4-26: Current voltage characteristics of [R6G][TPB] nanowires swept from 0 to 1V. Each trace shows data acquired from each of several [R6G][TPB] nanowire samples. Inset showing leakage current on the order of 10^{-11}A through the Au on glass substrate devoid of nanowires.

The current variation from sample to sample in our measurements could be primarily due to the nature of the aggregation and the surface alignment of the [R6G][TPB] nanowires across the interdigitated electrodes.

4.4.3: [PIC][BETI] and [PIC][NTf_2] nanoGUMBOS: Imaging and I-V Characterization

The [PIC][NTf_2] and [PIC][BETI] nanoGUMBOS were dropcast onto gold coated glass substrates and dried under ambient conditions. Conductive probe AFM (CP-AFM) measurements of [PIC][NTf_2] and [PIC][BETI] are made in the same AFM setting, including the kind of tip (DPE 14/no Al), as was used for [R6G][TPB] nanoparticles. The voltage was swept from -1 V to +1 V, and the electrical response was recorded using the SCS. Prior to the I-V measurements, AFM images of the GUMBOS and nanoGUMBOS were also obtained by scanning (Pacific Nanotechnology, Model: P-MCU-SICT-O tip) in contact mode to study their respective morphologies. The raster scan by AFM was performed at a constant frequency of 1 Hz. Figure 4-27 shows the AFM images of [PIC][BETI] and [PIC][NTf_2] nanowires.

Diamond-shaped structure formations were observed with [PIC][NTf_2] nanoGUMBOS with approximate lengths and widths[1] of 1 μm and 600 nm, respectively. This self-assembled diamond shaped structure is attributed to repeated head-to-tail molecular stacking. [PIC][BETI] forms rod like structures due to parallel stacking instead of head-to tail stacking. The [PIC][BETI] nanoform has an average length and width of 2 μm and 200 nm, respectively, as shown in Figure 4-27(b).

[1] In this context width (or height) is defined as the dimention from the substrate to the top of the nanowire.

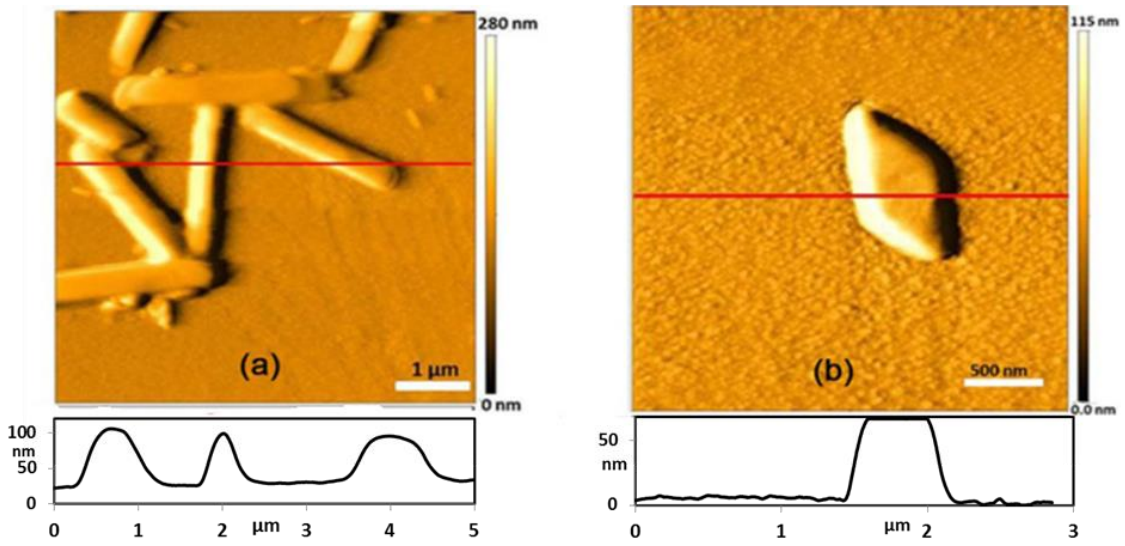

Figure 4-27: Atomic Force Microscopy images of (a) [PIC][NTf_2] and (b) [PIC][BETI] nanoGUMBOS on gold substrate (Reprinted with permission from Springer[97]).

Figure 4-28 depicts the family of I-V plots on a logarithmic scale as obtained for nanoGUMBOS via CP-AFM at different locations on the dropcasted samples. The CP-AFM results are generally dominated by varying distributions of particle sizes and their aggregates or ensembles at different locations. The I-V data measured for both [PIC][NTf_2] and [PIC][BETI] nanoGUMBOS show similar magnitude for current values ranging from 10^{-10} A to 10^{-8} A. The curves also represent an approximately symmetric behavior for the applied sweep between ±1 V. The observed electrical characteristics are in agreement with the literature [98-101]. The non-linearity in the I-V relationship obtained by the CP-AFM technique has been reported to be a sensitive function of a number of factors, e.g. the nature of aggregation of the nanomaterials, interaction at the AFM tip-nanoparticle-substrate interface, and the injection of charges (or flow of current due to electron tunneling) through the tip-nanoparticle junction barrier.

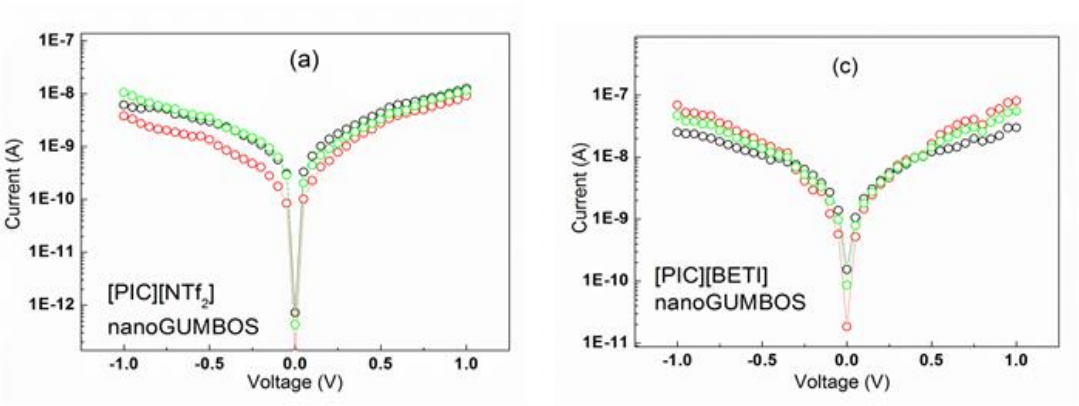

Figure 4-28: Log plot of Current-voltage (I-V) curves of [PIC][NTf_2] and [PIC][BETI] nanoGUMBOS obtained by conductive probe atomic force microscopy (CP-AFM) (Reprinted with permission from Springer [97]).

4.4.4: [TC2][BETI] nanoGUMBOS: Direct analyte injection method

The test structure developed for the direct gas method (see section 4.3.8.1:) is used for a dropcasted solution of [TC2][BETI]. Responses in the form of current to various vapors were recorded. Since different vapors have different vapor pressures, the precise volume of analyte to be injected into the given volume of the experimental chamber was calculated (Table 4-1). Figure 4-29 depicts the normalized current response of the nanowires (recorded from the test structure) due to different analytes. As all of the current-voltage (I-V) responses are symmetric, all of the compared values are taken at +20 V. The [TC2][BETI] nanowires, acting as a sensor, exhibited the maximum change in current due to aniline vapor. Various responses to other vapors such as diethylamine, triethylamine, nitromethane, and cyclohexane were observed as are also shown in Figure 4-28. These normalized current values are comparable to the values reported in the literature[102]. Figure 4-30 shows the sensor response to various concentrations of aniline injected into the chamber. The trend is close to linear in that as the volume of the aniline is increased, the current also increased.

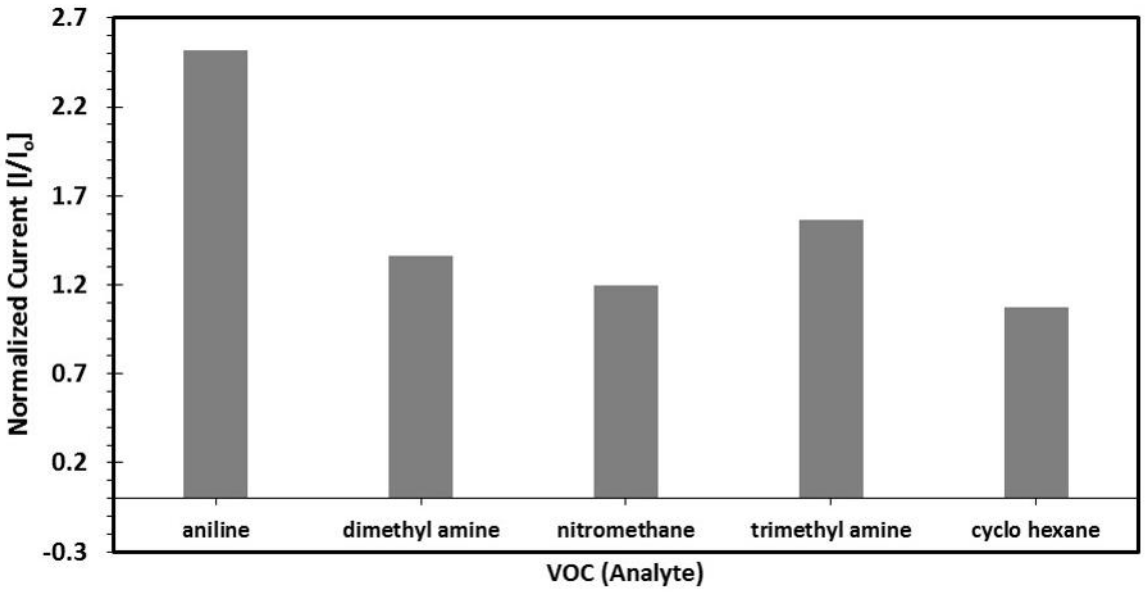

Figure 4-29: Normalized current response of test structure to various analytes

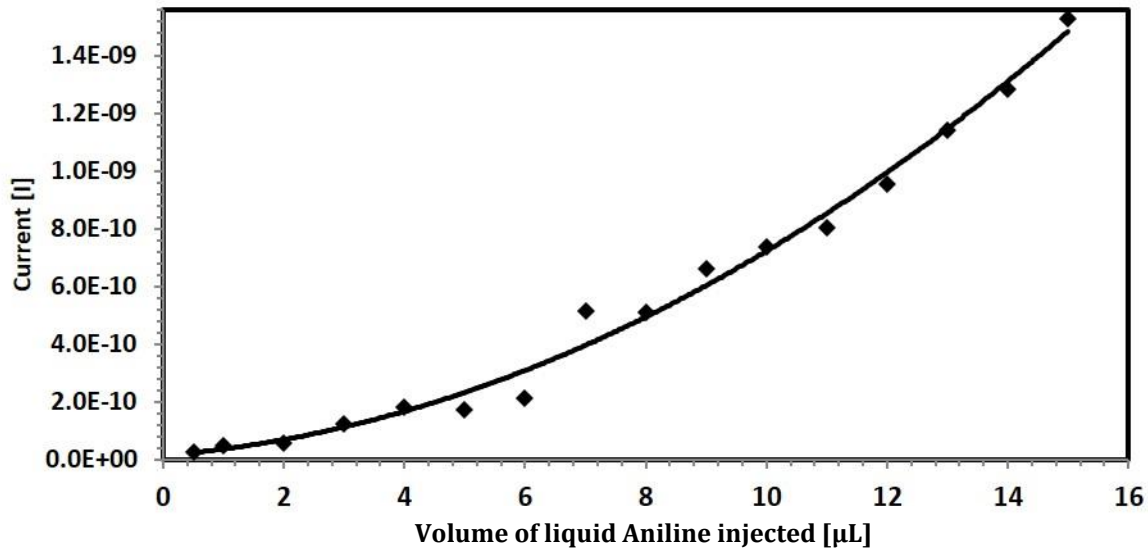

Figure 4-30: Response of [TC2][BETI] nanowires to an increasing volume of aniline injected into the gas containment chamber

4.4.5: [TC2][BETI] nanoGUMBOS: Carrier gas method

[TC2][BETI] nanowires were electrosprayed as a thin-film onto an interdigaited test structure as discussed in detail in section 4.3.8.2: (b). As is also described in 4.3.8.2: (b), this test structure was placed in an inert (N_2) environment of a 2.3 L glass gas containment chamber. An

analyte was conducted into the containment chamber by a carrier gas (N_2). The response of the nanowire sensor to the analyte was measured via changes in current. This response was recorded for different flow rates of the carrier gas. As the flow rate varies, a proportional amount of analyte is carried along with it. For different flow rates, different amounts of the VOC (aniline) were carried by the carrier gas. The graph in Figure 4-31 shows the effect of flowrate of injected anline (analyte) on the [TC2][BETI] nanowire sensor response time. In Figure 4-31, the y-axis represents the time (minutes) over which there is increase in the current through the sensor.

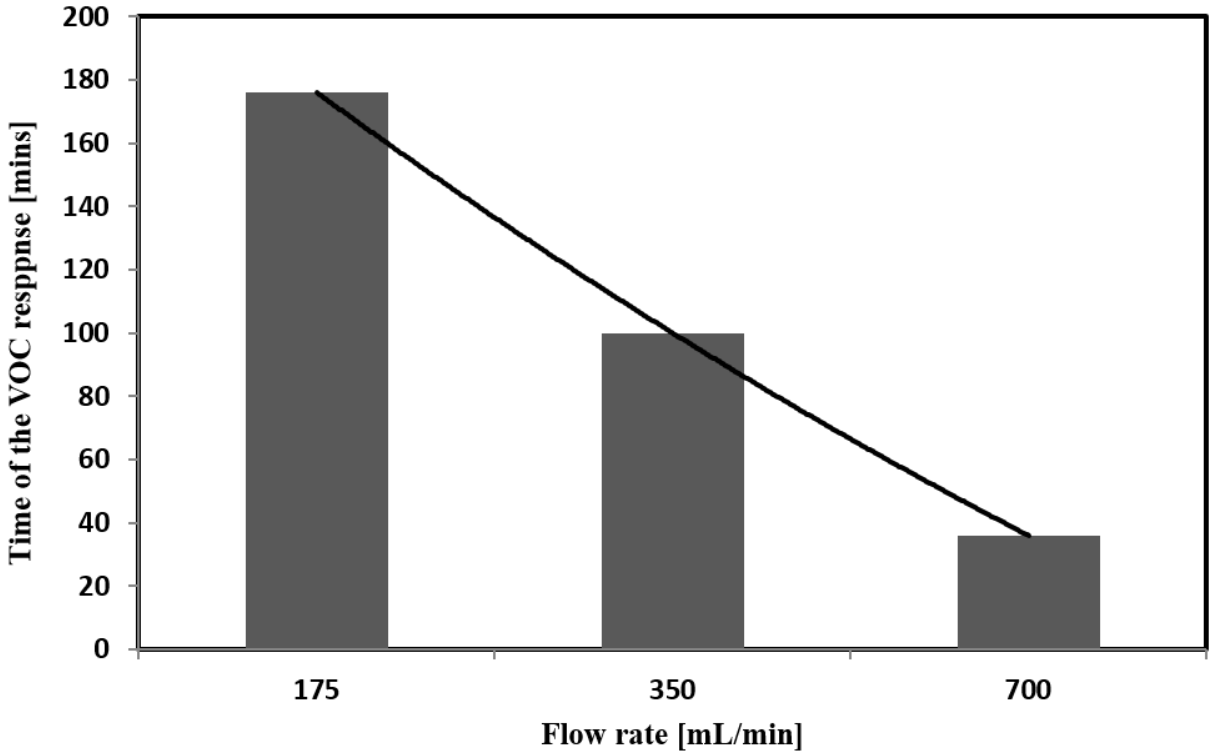

Figure 4-31: Carrier gas method used for detection of aniline vapors at different flow rates.

As seen in the Figure 4-31, for a 175 mL/min flowrate the [TC2][BETI] nanowire sensor responded for approximately 176 minutes and over time reached a peak value of 1.3 nA (average) for 107 minutes (Figure 4-32). As the volume of the analyte decreased, the current followed the aniline as expected. For a 350 mL/min flowrate, the nanowire sensor responded to

the analyte for approximately 100 minutes. In this case, over time the sensor reached a maximum current value of 1.2 nA—approximately the same current as in the 175 mL/min flowrate case—and remained saturated for approximately 51 minutes (Figure 4-32). For the 700 mL/min flow rate, nanowire sensor responded for approximately 36 minutes. However, it only reached maximum value of 0.65 nA (Figure 4-32), unlike in the 350 and 175 mL/min cases. We suspect the reason for the lower current may have been due to the faster removal of aniline vapor from the chamber under the higher flowrate of 700 mL/min.

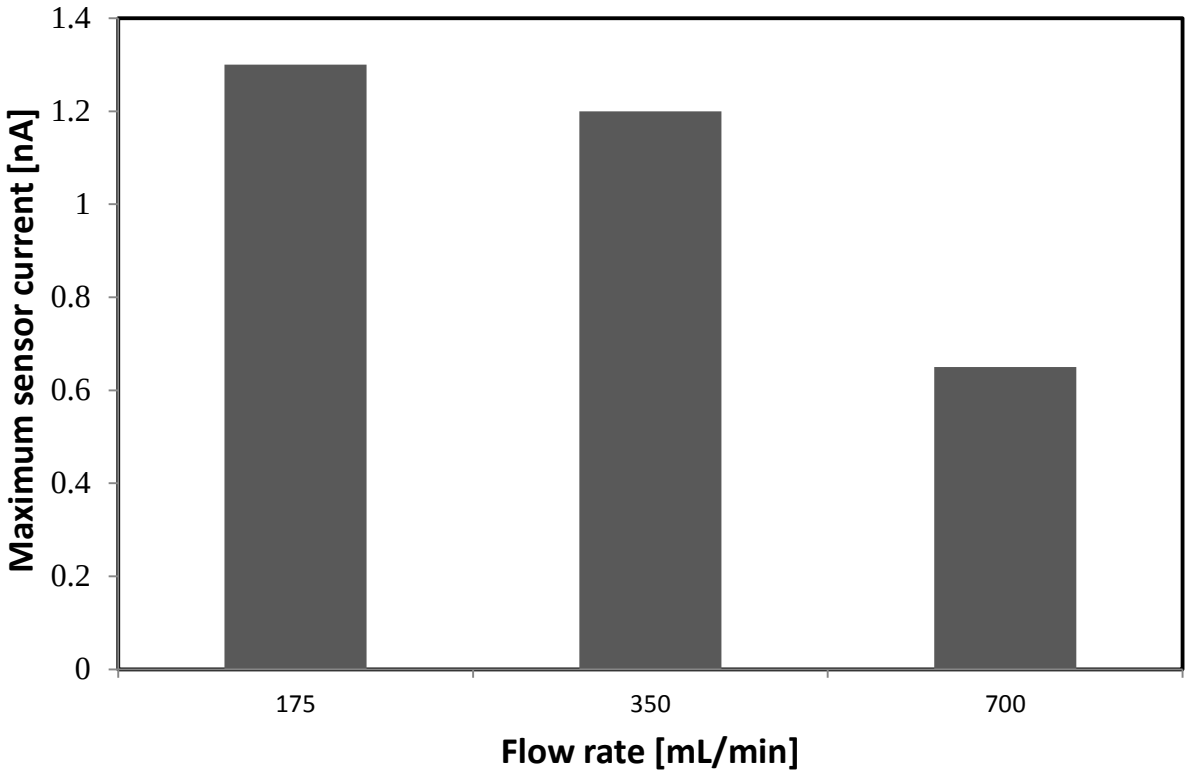

Figure 4-32: Maximum sensor currents for different aniline flow rates

These results illustrate the affinity of [TC2][BETI] nanowires for aniline vapors. However, the sensor response was proportional to the amount of the aniline and was completely reversible, indicating that sensing is due to the physical adsorption of the analyte onto the nanowires. With a decrease in the magnitude of current due to removal of adsorbed aniline

molecules on the nanowires, the [TC2][BETI] sensor returns to its initial state. Likewise, the sensitivity of the sensor was found to increase linearly with respect to the concentration of aniline vapor, as per our previous experiments. Constant current over a period of time for the 350 and 175 mL/min flow rates is indicative of the saturation level of [TC2][BETI] nanowires as aniline sensors in this set of experiments.

4.5: Conclusions

We have successfully characterized a new class of nanomaterials known as nanoGUMBOS. This work represents first time characterization of these materials to investigate their electrical properties. AFM surface scanning and height profiling of nanostructures was used for thickness and width measurements. Conductive probe AFM was used to measure I-V response of [R6G][TPB] nanoparticles, [PIC][BETI] and [PIC][NTf_2] nanostructures. The I-V response of [R6G][TPB] nanowires and [TC2][BETI] nanowires are investigated using interdigitated electrodes. Thin-films of [TC2][BETI] are developed using electrospray deposition. The vapor sensing characteristics of the film are investigated. These nanowires exhibited sensing capability with respect to various vapors and maximum response for aniline vapors. The nature of sensing is determined to be physical adsorption of analyte molecules on the nanowires using carrier gas method.

CHAPTER 5: STUDY OF ELECTROSPRAY ASSISTED ELECTROPHORETIC DEPOSITION OF CARBON NANOTUBES ON NON-CONDUCTIVE SUBSTRATES[2]

5.1: Introduction

The invention of helical microtubules of graphitic carbon by Iijima in 1991 has inspired substantial research into the application of single-walled and multi-walled carbon nanotubes (SWCNTs and MWCNTs) in field emission devices, chemical sensors, and thin film transistors (TFT) technology [103-105]. In recent years, carbon nanotube based thin films have been extensively investigated due to their high surface area per mass ratio, mesoporous structures, electrical conductivity and their high chemical stability [106]. Some of the potential applications in this direction include super-capacitors [107], batteries[108], microelectronics[109], gas[110] and analyte sensing[111], flexible displays[112], and for electrode material[113]. For the above applications, CNTs need to be deposited on a range of substrates, both conductive and non-conductive. The conventional direct growth models of CNTs, e.g. arc-discharge, laser ablation and chemical vapor deposition (CVD) [114-117], are generally characterized by high temperature processing (typically ~800–900 °C), the presence of unwanted metal catalysts, soot-like carbonaceous skeins in the final nanotube yield and the need for expensive vacuum systems. These growth parameters pose serious complications to the direct incorporation of CNTs in several applications viz. low temperature micro-electromechanical systems (MEMS), flexible and printable thin film transistor (TFT) technology [118] and molecular electronics. To mitigate these challenges, in recent years, numerous research initiatives have been undertaken in the development of facile, room temperature, economical CNT wet coating techniques from different stable suspensions such as the Langmuir-Blodgett (LB) method, self-assembly of

[2] This chapter in its current form is accepted for a journal article publication. Kanakamedala K , DeSoto J, Sarkar A, Daniels-Race T.," Study of Electrospray assisted Electrophoretic deposition of Carbon Nanotubes on Insulator Substrates". *Electronic Materials Letters*. It is reproduced by permission from Electronic Materials Letters (Appendix D)

functionalized CNTs on chemically modified substrates, dip coating, drop casting, spin coating, and more[119] . However, the non-reproducibility of most of these processes in regard to the deposition yield, non-uniformity of the deposits and limitations in multi-layer film growth with precise control over the thickness add to the bottlenecks of these methods.

With prevailing interests in search of a reliable and efficient solution-based deposition method, electrophoretic deposition (EPD) [120, 121]has emerged as a promising technique over the last decade. The benefits of EPD include an economical approach towards thin film fabrication due to its cost-effectiveness, the need for a relatively simple apparatus, reproducibility and precise control in the deposit thickness, high deposition rate and the ability to scale up to large product volumes and sizes.

5.1.1: Electrophoretic Deposition

The mechanism of EPD can be generally conceptualized by two steps[122, 123]. In the first step, known as electrophoresis, charged particles that have been dispersed in a liquid suspension migrate towards the electrode of opposite polarity due to the application of a direct or pulsed current electric field across the suspension. In the second step, referred to as the deposition step, the particles coagulate and adhere to the electrode surface, thereby assembling as a coherent deposit.

Conventionally, one of the pressing factors in EPD has been the requirement of an electrically conductive target substrate. For most EPD processes reported in the literature, the substrates have been metallic or carbon/graphite sheets. However, contrary to this common assumption, recent research findings outline the deposition of nanomaterials onto porous non-conducting alumina and NiO-YSZ surfaces which, prior to, had been deposited on carbon/graphite sheets [124-126]. Our research, on the other hand, has focused upon the

feasibility of EPD of CNT networks onto semi-conducting and insulator substrates used in transistor technology. In this direction, we have recently demonstrated EPD of CNTs on semiconductor (silicon) [127, 128] and insulator (glass) [129] substrates functionalized with self-assembling organosilane (3-aminopropyl-triethoxysilane or APTES) molecules. EPD of CNT films onto glass substrates was accomplished by drop-casting an initial thin layer of CNTs onto hydrophilic APTES treated glass substrates. The initial drop-casted layer of CNTs on the surface functionalized glass substrates served as the underlying conductive layer to assist in the migration of CNTs during the electrophoresis process. However, the inherent non-reliability of the initial CNT drop casting method in obtaining continuous CNT deposits on the APTES treated glass substrates was the limiting factor in the reproducibility of the sequential EPD process. Additionally, the incorporation of non-conducting APTES binder molecules in the deposition process flow adversely affected the conductivity of the final CNT deposits. The present communication reports significant progress in the fabrication of uniform CNT coatings on bare glass substrates, without organosilane surface treatment, by the sequential combination of electrospraying with the conventional EPD process. Electrospraying has been widely used as a technique for the deposition of various compatible nanomaterials dispersed in a solution.

5.1.2: Electrospray Deposition

Electrospraying is a simple, cost-effective process for liquid atomization by subjecting the liquid droplets from an orifice, e.g. syringe needle, to an intense electric force (on the order of kV) causing them to break down into smaller droplets [130]. The charged droplets continuously disintegrate into smaller charged droplets until the surface tension on the smaller droplets is greater than the applied electric field. Owing to the nature of the electrospraying technique, the charge distribution on the generated droplets results in inter-particle repulsion,

which forces them to spread out and create a very uniform film in the deposition of nanomaterials [45, 131-134]. The droplet size and the final spread can be precisely controlled by optimizing the applied voltage, flow rate, and the distance between the tip and the target [42].

The proposed electrospray-assisted EPD technique eliminates the use of organic self-assembling silane molecules from the deposition process flow, and it addresses the non-reliability of the CNT drop casting method for glass surfaces. As will be discussed, we have successfully used the electrospraying process to create a continuous thin film CNT deposition onto glass substrates which, in turn, further assisted in the reproducible growth of CNT films by the subsequent EPD process. Figure 5-1 represents the over-all fabrication strategy as proposed in this report. The relevant sections of this study reveal pertinent details with regard to preparation of the CNT suspension, electrospraying and the EPD experimental set-up. Furthermore, surface characterization of the deposited CNT films, including the effect of the initial electrosprayed CNT layer on the final film thickness, is discussed in relation to various deposition parameters. To the best of our knowledge, no prior work of such kind has been reported in the CNT deposition literature. Thus, the results of this study potentially pave the way to the integration of the electrospray-assisted EPD technique in a wide range of materials research and technology.

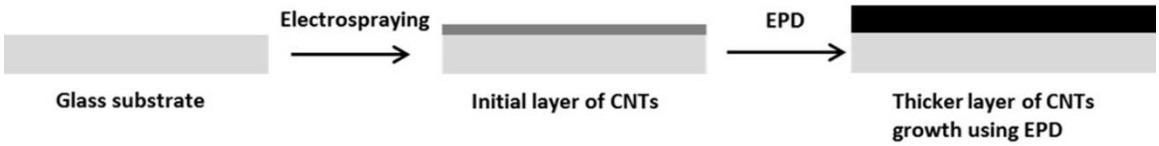

Figure 5-1: Schematic diagram of the electrospray-assisted electrophoretic deposition strategy

5.2: Experimental Procedure:

5.2.1: Acid-refluxing of the carbon nanotubes

A quantity in the amount of 100 mg of as-purchased multi-walled CNTs (purity: > 95%, dimension: 6–13 nm (OD) × 2.5–20 μm (length), CVD, Sigma Aldrich, St. Louis, MO, USA) was acid refluxed in 40 mL concentrated sulfuric (H_2SO_4) and nitric (HNO3) acid (volume ratio = 3:1, respectively). The CNT-acid solution was then heated at 120 °C for 30 minutes on a hot plate. The acid-heat treatment of the CNT solution produced a black slurry, which was cooled for 1 hour in a fume hood. The acid-refluxed solution was then carefully diluted with deionized (DI) water (18.2 MΩ-cm) and filtered through a Buchner funnel using medium retentive filter papers (pore size: ~11μm). The exact quantitative value of CNTs lost in the filtration process is difficult to measure but was estimated to be ~30%. The filter papers with the accumulated CNTs were further used for the preparation of electrospray and EPD solutions.

5.2.2: Preparation of electrospray and EPD CNT solution

The electrospray solution was prepared by submerging the filter paper containing acid-treated CNTs into 120 mL of ethanol (EtOH) and ultrasonicating for 2 hours to obtain a uniform dispersion. The concentration of the final CNT-EtOH solution was estimated to be ~ 0.58mg/mL. Following the same acid treatment and Buchner filtration process, the CNT solution for EPD was prepared by submerging the filter paper in 10mL of isopropyl alcohol (IPA). This mixture was then ultrasonicated for 1 hour to obtain a uniformly dispersed CNT solution (concentration: ~7mg/mL). Before each set of deposition experiments, the CNT-EtOH and CNT-IPA solution were ultrasonicated for 2 minutes to minimize agglomeration of the CNTs in the media.

5.2.3: Substrate preparation

For all of the deposition experiments, microscopy-grade non-conducting glass slides (2 cm x 1 cm) were used as the target substrates. The glass pieces were thoroughly treated with a warm piranha solution (H_2SO_4: H_20_2) for 30 minutes to remove any organic contamination. This treatment also rendered the surfaces of the glass samples sufficiently hydrophilic to aid in interfacial adhesion. The pieces were then allowed to cool, washed thoroughly with DI water, and finally dried in a nitrogen stream.

5.2.4: Deposition of initial CNT layer by electrospraying

A schematic of the electrospraying setup is shown in Figure 5-2.. The glass substrate was mounted onto a grounded aluminum target. A 10 mL syringe was filled with ethanol-CNT solution. A steel syringe needle (23G) was blunted to obtain a uniform electric field. A voltage of 8.5kV was applied between the steel needle tip and the ground electrode using a high voltage power supply (0-30 kV) from Gamma High Voltage Research, Inc. A constant liquid flow rate was maintained at 50 µL/min throughout the deposition process. The distance (d) between the syringe needle tip and target substrate was held constant at 5 cm. The deposition parameters were thus optimized to obtain a uniform Taylor Cone [130]. The ground electrode was spun at a constant velocity to ensure uniform deposition. After the electrospraying process, the deposited thin films were dried in a laminar flow system.

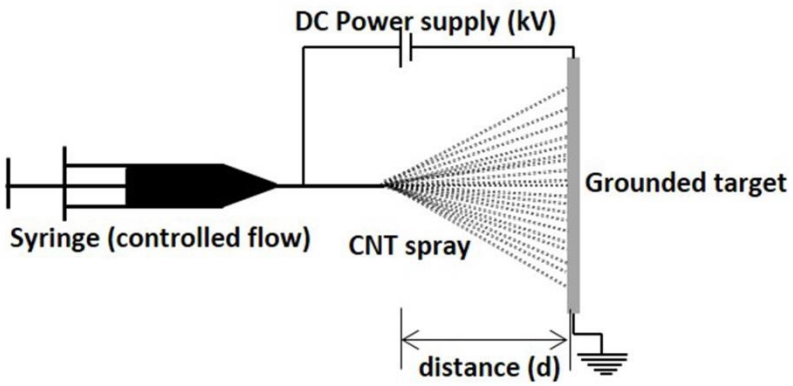

Figure 5-2: Schematic diagram of the electrospray deposition

5.2.5: Electrophoretic deposition of CNTs

In the EPD step, glass substrates with the initial electrosprayed layer of CNTs were utilized as the anode. A schematic diagram of the electrophoretic deposition process is shown in Figure 5-3. A copper sheet (2cm x 1cm) was used as the cathode. The inter-electrode distance is kept constant at 2.54 cm. After deposition, the samples were dried in a dry nitrogen environment before further analysis.

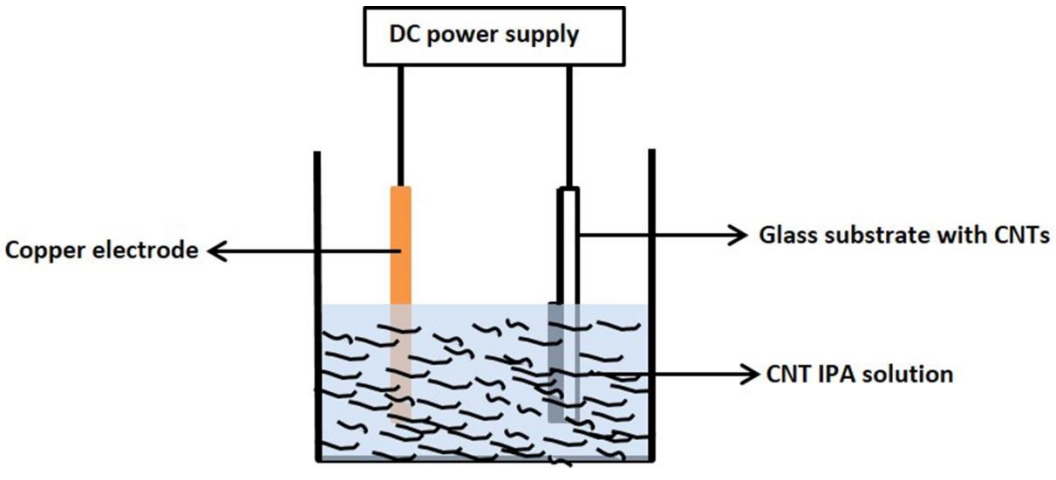

Figure 5-3: Schematic diagram of the electrophoretic deposition

5.3: Results and Discussion

The acid refluxing treatment imparts covalent surface functionalization of the as-purchased CNTs, thereby attaching carboxylic groups (–COOH-) on the surface of the tubes, which induces negative surface charges. The resultant electrostatic repulsion between the surface charges prevents inter-tubular agglomeration and ensures appreciable stability of the CNT-EtOH and CNT-IPA suspensions all throughout the deposition experiments. Additionally, dissolution of unwanted, residual metal growth catalysts, the formation of carbonaceous skeins in the nanotube powder, and shortening of the nanotubes were all also accomplished by the acid-heat treatment [135].

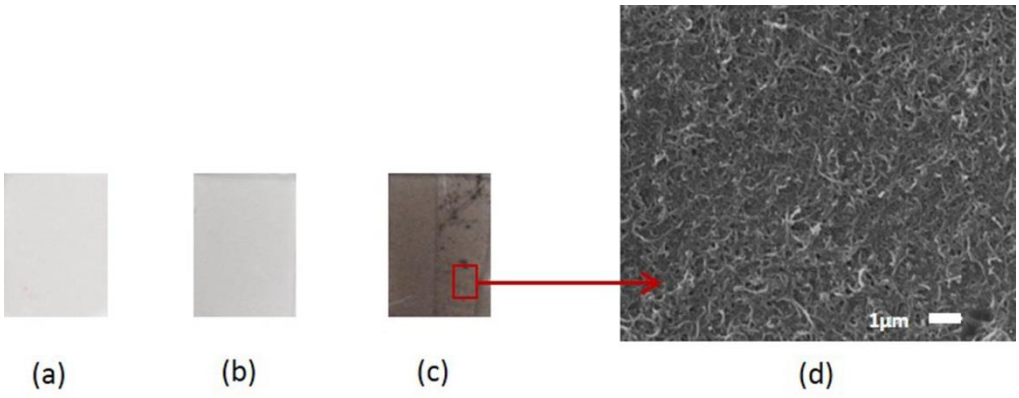

Figure 5-4: Electrospraying coating results on non-conducting glass substrates with an applied constant voltage of 8.5 kV and constant flow rate of 50 µL/min for (a) for 5 min showing poor CNT coating, (b) for 10 min showing improved coating, (c) for 20 min, and (d) SEM imaging with 20 min deposition duration showing high quality surface coating.

Figure 5-4 (a-c)[3] depicts the electrospray coating results with varying time duration on the bare glass substrates without any surface silane functionalization. It was observed that for spraying duration of 5 mins, the deposition was almost negligible, as shown in Figure 5-4 (a). Optical microscopic observation revealed formation of non-uniform and discontinuous CNT

[3] Figure 5-4 (a-c) were obtained by photographing the electrosprayed CNT-on-glass samples after 5, 10, and 20 minutes (respectively) using a digital camera.

deposits on the sample. The coating quality improved substantially as the spraying duration was increased to 10 mins, above which high quality, continuous CNT coated surfaces were observed. The optical image presented in Figure 5-4 (b) with deposition duration of 10 mins shows improvement in CNT surface coverage, and Figure 5-4 (c) with duration of 20 mins displays the superior nature of the CNT deposits. The SEM image in Figure 4 (d), with electrospraying deposition of 20 mins, indicates appreciable coverage and packing density without any microstructural voids or discontinuities in the CNT films. Quantitative film thickness measurements were also performed using a KLA-Tencor D-100 Alpha Step surface profiler. It was noted that for constant flow rate and inter-electrode E-field, the CNT film thickness showed a linearly increasing trend with increasing electrospraying deposition duration (in mins), as displayed in Figure 5-5.

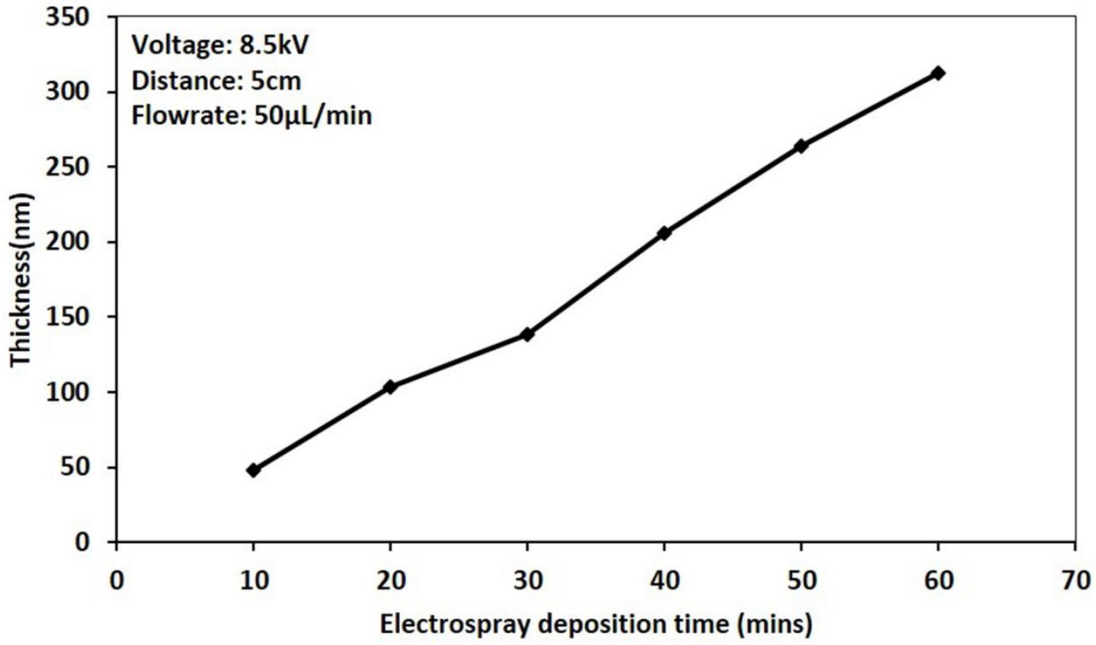

Figure 5-5: Thickness of CNT coating electrosprayed on glass substrates as a function of deposition time for an applied E-field of 8.5 kV and flow rate of 50 µL/min.

The uniformity and continuity of the underlying CNT coating was identified as an important parameter critical to the quality of the eventual CNT film growth by EPD. In order to investigate the effect, a series of EPD experiments was performed on different electrosprayed samples with varying spraying times. As depicted in Figure 5-6(a), the electrophoretic deposition (with an applied E-field = 60 V/cm, time duration = 3 mins) from CNT-IPA solution on the glass samples electrosprayed for 5 mins resulted in discontinuous and non-uniform film growth. This agrees with the results presented in Figure 5-4 (a), which showed almost negligible or discontinuous CNT deposits for spraying duration of 5 mins. As the continuity and the CNT coating quality improved underneath with increasing spraying duration of 10 mins and above, the EPD results showed significant improvement. Figure 5-6(b) and Figure 5-6 (c) show the superior nature of the final CNT yield and quality obtained on electrosprayed samples with spray duration of 10 mins and 20 mins, respectively. The SEM image (Figure 5-6(d)) of the sample in Figure 5-6(c) also revealed appreciable surface coverage and homogenous packing density in the CNT layer without any microstructural discontinuities. These results reiterate the critical role of the electrospraying step in the proposed fabrication strategy.

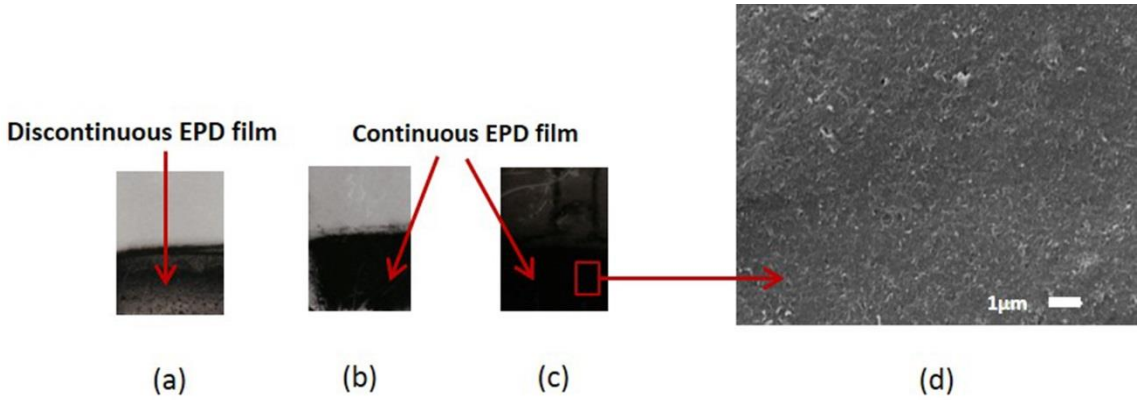

Figure 5-6: EPD (performed with E-field = 60 V/cm, deposition time = 3 min) results on electrosprayed samples (a) for 5 min showing poor CNT coverage, (b) for 10 min showing improved surface coverage, (c) for 20 min, and (d) SEM imaging with 20 min electrospraying time showing dense CNT packing without microstructural dis-continuity. The results substantiate the effect of underlying coating on the final CNT film growth.

To explore the effect of varying electrospraying duration on the final thickness of the CNT films, quantitative thickness measurements were performed using a KLA-Tencor D-100 Alpha Step surface profiler. It was observed that for constant electrospraying duration of 20 mins and constant EPD time for 3 mins, the film thickness increased as the applied inter-electrode E-field during EPD increased from 10 V/cm to 60 V/cm. This trend supports the traditional Hamaker equation [123] of electrophoresis that establishes a linear relationship between the weight of the particles (or the thickness of the films) deposited per unit area of electrode with the applied potential during the deposition step.

CNT films as thick as ~4.5 μm were fabricated using this technique, as presented in Figure 5-7(a). CNT film thickness with constant EPD parameters (inter-electrode E-field = 60 V/cm and deposition time = 3 mins) showed an initially increasing trend with increasing electrospraying duration and eventually became saturated for samples electrosprayed for 30 mins to 60 mins (Figure 5-7(b)). This observation is also supported by our resistivity measurements (as can be noted in Figure 5-8(b) of the next section), which showed saturated values for samples electrosprayed for 30 mins and above.

5.3.1: Resistivity measurements

It has been reported that multiple factors, e.g., the chirality of the nanotubes, defects introduced during the synthesis and post-synthesis deposition methods, degree of dispersion, presence of residual surfactant and CNT morphology influence the over-all sheet resistance values of the CNT films fabricated by different wet coating methods[136]. Resistivity measurements of the deposited CNT films in our experiments were performed by the four-point probe measurement technique. As has been pointed out in section 5.2:, electrospray deposition of

the CNTs results in a thin and uniform spread of CNTs across the substrate due to inter-particle repulsion arising from the charge distribution of the spray droplets.

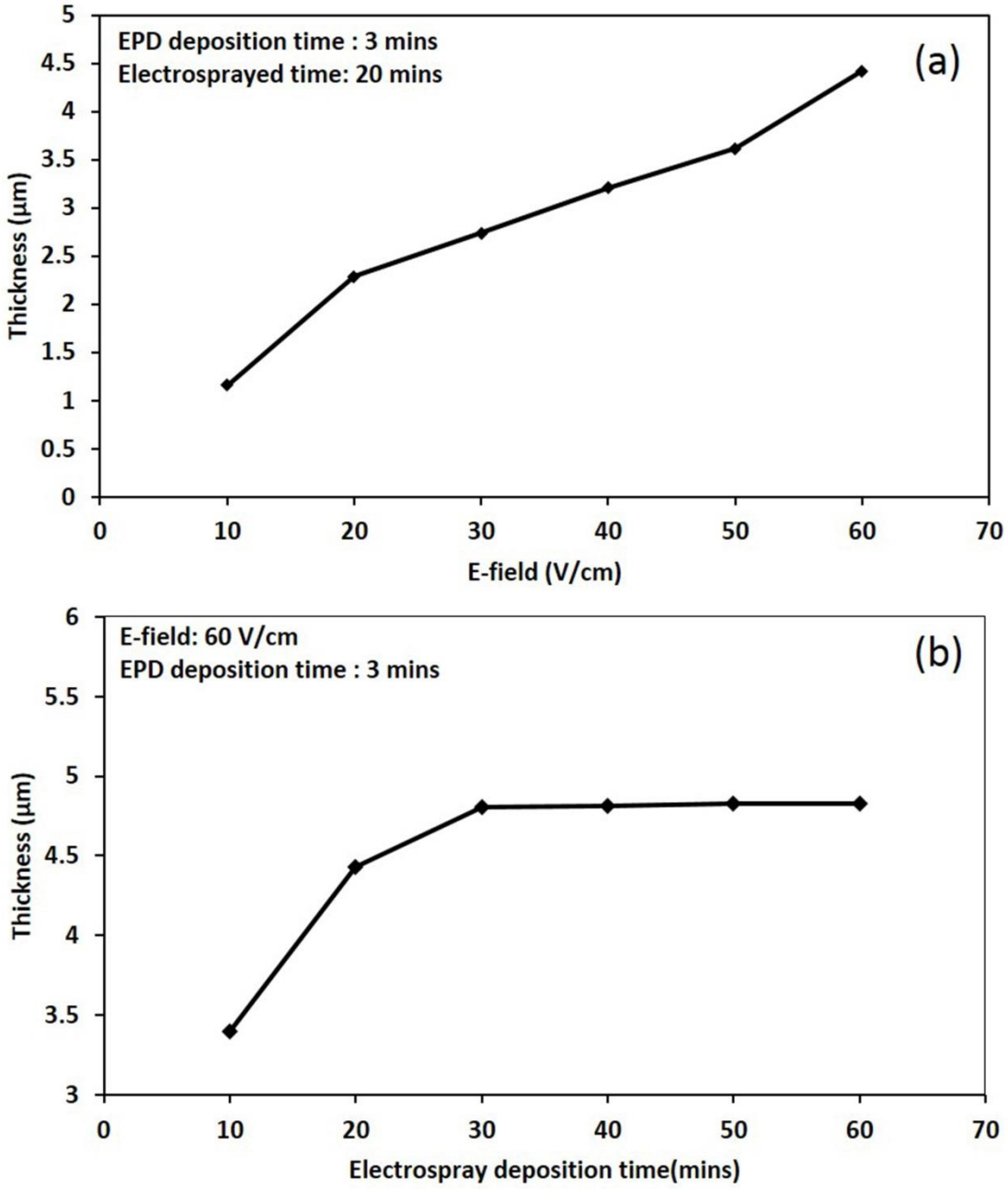

Figure 5-7: Thickness values of the CNT films (a) with varying E-field during EPD with constant deposition time of 3 min on samples electrosprayed for 20 min, and (b) varying electrospraying deposition time with constant EPD parameters (E-field= 60 V/cm and time= 3 min).

As has been pointed out in section 5.2:, electrospray deposition of the CNTs results in a thin and uniform spread of CNTs across the substrate due to inter-particle repulsion arising from the charge distribution of the spray droplets. With the gradual increase in electrospraying time, interconnections among the deposited CNTs increase, resulting in the growth of a continuous film on the glass surfaces. The number of interconnections obtained in the electrosprayed layer affects the conductivity of the CNT films which, in turn, directly affects the thickness and morphology of the eventual CNT film growth by the conventional EPD technique. Figure 5-8 (a) shows the variation in sheet resistance of the electrosprayed CNT films in relation to the duration of deposition (mins) with the applied E-field and inter-electrode distance held at constant values. As the thickness of the CNT films increased with the increase in the electrospraying deposition time (from 10 mins to 60 mins), the measured sheet resistance values (in Ω/□) of the films showed an initial decreasing trend with eventual saturation for deposition duration of 40 mins and above, as shown in Figure 5-8(a). As can be noted in the figure (Y-axis represented in log scale), the sheet resistance obtained after 10 mins of deposition, measured on the order of 100 MΩ/□, exponentially decreased to the order of 0.1MΩ/□ for 20 mins of deposition, before saturating at ~10kΩ/□ for higher deposition duration. The higher sheet resistance for 10 mins of deposition time can be attributed to fewer interconnections between the nanotubes resulting into a more porous morphology of the deposits. This porous nature is known to have an effect on the charge transport mechanisms of the thin films [137]. Figure 5-8 (b) represents the sheet resistance values of the final CNT films by EPD (performed at constant E-field: 60 V/cm and constant time duration of 3 mins in the CNT-IPA solution) in relation to the varying electrospraying duration (10 mins to 60 mins) of the underlying CNT coating. The resistance values in general exhibited similar trend with a high initial value (~4.7 kΩ/□). The porous

morphology of the highly resistive underlying electrosprayed CNT coating obtained after 10 mins of deposition is expected to contribute to this result. The effect of the electrospraying duration beyond 10 mins was observed to be less pronounced on the final resistivity of the CNT films by continuous EPD, as the sheet resistance values saturated to ~218Ω/□ from 20 mins to 60 mins.

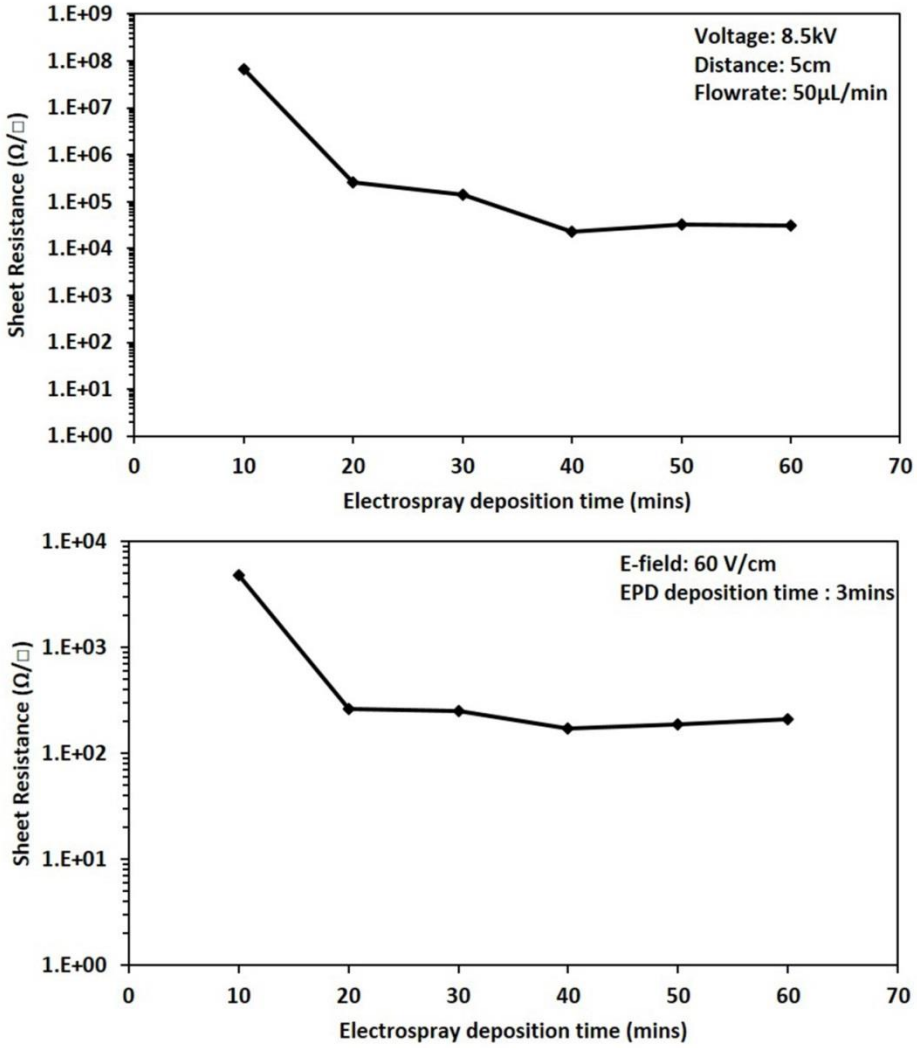

Figure 5-8: (a) Variation in sheet resistance of the electrosprayed CNT films as a function of deposition time from 10 min to 60 min, and (b) variation of sheet resistance values of the final CNT coating by EPD in relation to varying electrospraying deposition time from 10 min to 60 min (EPD was performed at a constant applied E-field of 60 V/cm with 3 min of deposition on the underlying CNT coating).

5.3.2: Comparison of Raman spectra of different CNT samples:

Raman spectroscopy of different CNT samples was studied using a Jobin Yvon Horiba Labram Raman spectrometer with a HeNe laser of incident wavelength 638.4 nm. The Raman spectra of as-received MWCNTs (>99.5% pure), acid refluxed CNTs dispersed in ethanol (CNT-EtOH), and acid refluxed CNTs dispersed in IPA (CNT-IPA) are shown in Figure 5-9 (a), (b), and (c), respectively. Figure 5-9 (d) represents the spectrum of the initial thin CNT films deposited by the electrospraying method only while Figure 5-9 (e) depicts the spectrum of the final CNT deposits obtained by the electrospray-assisted EPD process. All of the spectra have been plotted from 1000 cm^{-1} to 2800 cm^{-1} wavenumber as no significant radial breathing modes (RBMs) were observed, which also indicated the absence of SWCNTs in the CNT samples. The typical Raman bands of the CNT structure at ~1337 cm^{-1} (D-band), ~1572 cm^{-1} (G-band), ~1608 cm^{-1} (D'-band) and ~2648 cm^{-1} (G'-band) were observed for all of the analysed spectra.

Table 5-1: I_G/I_D ratio for Pristine CNTs, CNTs in EPD solution, Electrospray Solution

Sample	Pristine	EPD solution	Electrospray solution
I_G/I_D	0.65	0.50	0.43

Similar wavenumbers prove conclusively that the pre-deposition processing steps (acid refluxing treatment and ultrasonication) of the CNT powder and the subsequent deposition experiments did not induce any significant modification in the vibrational nature of CNTs. The D-band is indicative of the inherent structural disorder and defective nature of the CNT structure. As reported in the literature[138, 139], the intensity ratio of G-band (I_G) to the D-band (I_D) in the Raman spectra can be represented as an estimation of the degree of defects induced in the carbon network during CNT synthesis and post-synthesis deposition steps. The decrease in the value of

the I_G/I_D ratio from 0.65 in the pristine CNT samples to 0.43 in the CNT-EtOH electrospraying solution and from 0.65 to 0.5 in the CNT-IPA EPD solution (shown in Table 5-1) can be attributed to the increase in the structural defects of the CNTs due to the combined effect of the acid-refluxing treatment followed by the prolonged ultrasonication step in our dispersion experiments

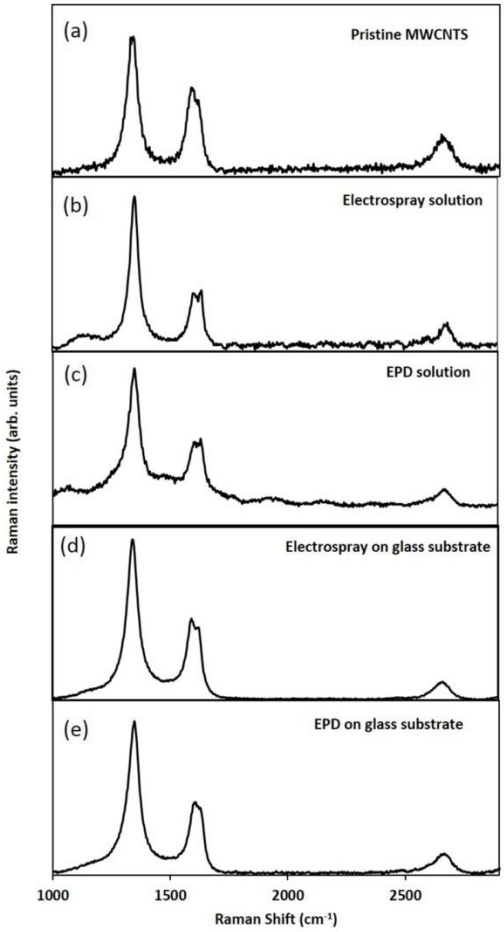

Figure 5-9: Raman spectra of (a) pristine MWCNTs, (b) acid refluxed and ultrasonicated CNT solution in ethanol, (c) ultrasonicated electrospray CNT-IPA for EPD, (d) electrosprayed CNT coating on glass substrate, and (e) final CNT coating obtained by EPD. All of the spectra displayed signature Raman peaks of MWCNTs at 1336 cm^{-1}, 1587 cm^{-1} and 2648 cm^{-1} wavenumber.

5.4: Conclusions

In this communication, a unique fabrication strategy of combining an electrospraying coating technique with electrophoretic deposition (EPD) has been successfully demonstrated to fabricate thick CNT films on non-conducting glass substrates. CNT film as thick as ~ 4.5 μm was fabricated on glass samples at an applied E-field of 60 V/cm for 3 mins on an initial electrosprayed CNT coating of ~ 100nm thickness. The quality and thickness of the final CNT deposit by EPD were observed to be dependent on the initial surface coverage by the electrosprayed CNT layer, on the applied E-field, and on the duration of deposition by the EPD process. These results represent significant progress with respect to our previous EPD research on semiconductor and insulator substrates in that this deposition model eliminates the need for polymer binder molecules and substitutes the drop-casting process by an electrospraying technique. The experimental results in this report are indicative of an innovative, economically viable, and reproducible fabrication strategy in the development of scalable and uniform CNT depositions on non-conductive substrates. With regard to potential future work in this direction, our research efforts will focus upon extending the proposed electrospray-assisted EPD technique to deposit CNTs onto SiO_2 and Si_3N_4 surfaces for thin film transistor technology without major variations in the deposition setup. Research endeavours are also underway for detailed investigation of surface properties of the final CNT films in relation to various process parameters, e.g. variation in the E-field, inter-electrode distance, and concentration of the solution during the electrospray process. A quantitative study in the estimation of adhesion strength between the deposited CNT films and the glass surface is also in progress.

CHAPTER 6: FARADAY ELECTROSPRAYING

6.1: Introduction

Needle electrospraying as discussed in this chapter is a viable and versatile tool for the deposition of thin films over a small area. However, there are several key challenges to this technique for large scale deposition. For large area deposition using needle electrospraying, a matrix of needles is required, which increases the chance of needles becoming clogged due to the creation of complex electric fields. To overcome the limitations of needle electrospraying several alternative methods have been proposed. Among these are porous and upward needleless electrospinning. Mainly for high production rates, higher rates of solution delivery via electrospraying are needed. For some perspective on this problem, the aforementioned methods will be discussed followed by an inventive solution as derived from our research.

6.1.1: Porous electrospinning method

This method was reported by Dosunmu, O. O, et al. (2006)[140]. The solution form of the material to be deposited is pumped through a porous cylindrical metal structure, to which a high voltage is applied, causing the liquid to spray in all directions. Fibers produced by this process are collected on the co-axial cylindrical structure. This method delivers a high solution rate compared to needle electrospraying. Although this method produces a large throughput of fibers, it also produces variation in the fiber diameter and has a high chance of hole clogging, both of which would lead to a decrease in the rate of production.

6.1.2: Multiple spikes electrospinning method

This method relies on a magnetic field for the generation of spikes on the free surface of a ferromagnetic liquid. Two layers of solution are required for the deposition. As shown in

Figure 6-1, the bottom layer is the ferromagnetic liquid which is subjected to a changing magnetic field and will become the source of "spikes" (peaks) on the free surface. A polymer solution is deposited and serves as the top layer. When a high electrostatic potential is applied to the free liquid surface, these spikes in the ferromagnetic liquid now act as jetting centers for the polymer solution. As several hundreds of spikes can be generated by the magnetic field, multiple jets emerge from the free surface, resulting in a higher deposition rate. A sawtooth collector is used to stabilize the jets. This method increases the production rate; however complications can develop as a result of the magnetic field. Solvents for the material to be deposited must be selected carefully so that they are not miscible with the underlying ferromagnetic liquid. A more detailed description of this method can be found in the literature [141].

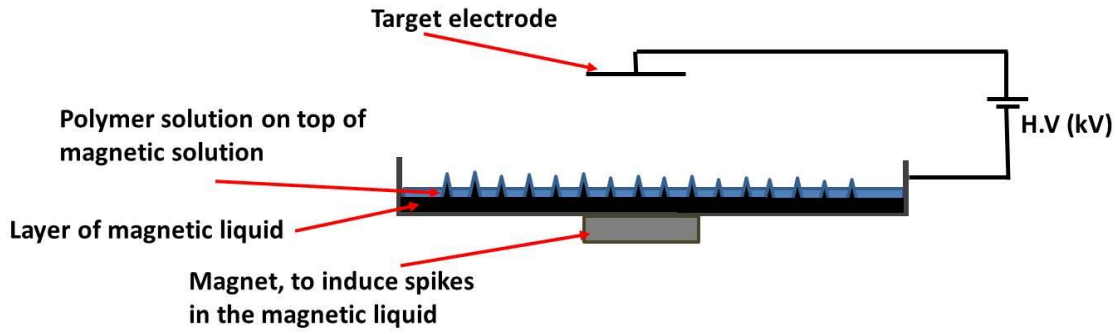

Figure 6-1: Schematic of the multiple spikes electrospraying method

6.2: Faraday Electrospraying

Sound waves are propagated by the compression and relaxation of the given medium. As they are mechanical waves, they cause mechanical disturbances in the medium through which they travel. Sound travels in three media (gases, liquids and solids) depending on the density of the medium. When sound energy is applied to liquid, depending on the density and viscosity of that liquid, mechanical disturbances are created. Figure 6-2 illustrates the effect of liquid in a small container subjected to sound waves. Wave-like motion on the surface of the liquid is

observed due to sound waves. When the container is conductive, the application of high voltage from the liquid surface to collector (as shown in the Figure 6-3) produces the electrospraying effect. The latter is due to the waves acting as high charge density centers at the crest of the liquid disturbances. Due to the Rayleigh Limit [54], the crest of the waves (due to high charge density) become the source of electrospraying from the solution.

Figure 6-2: Disturbances on the liquid surface due to sound waves.

6.2.1: Experimental setup

A schematic of the experimental setup is shown in Figure 6-4. An aluminum container of 3 cm radius is used for containing the liquid. A syringe pump is used to feed the container with the solution to be deposited. An audio speaker with frequency response of 95 to 4000 Hz, power rating 175 W RMS, and an input impedance of 8 ohms is used to excite the liquid. Various frequencies are applied through a function generator and power amplifier.

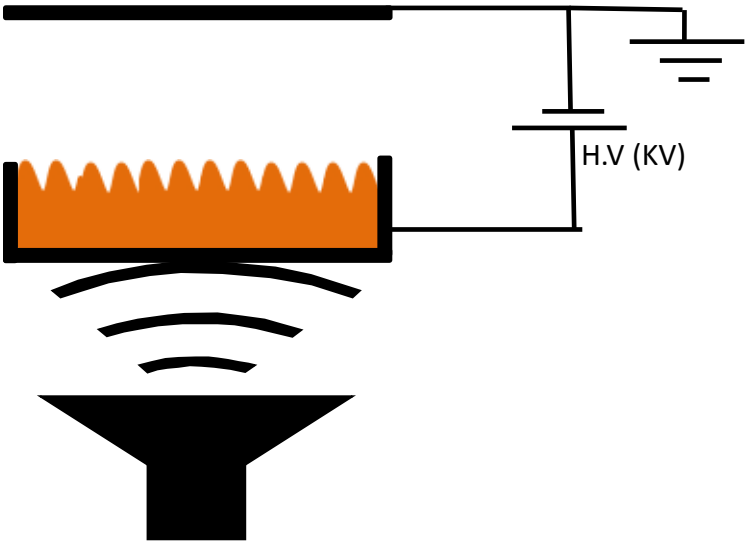

Figure 6-3: Application of high potential to the free surface of the liquid causing electrospraying.

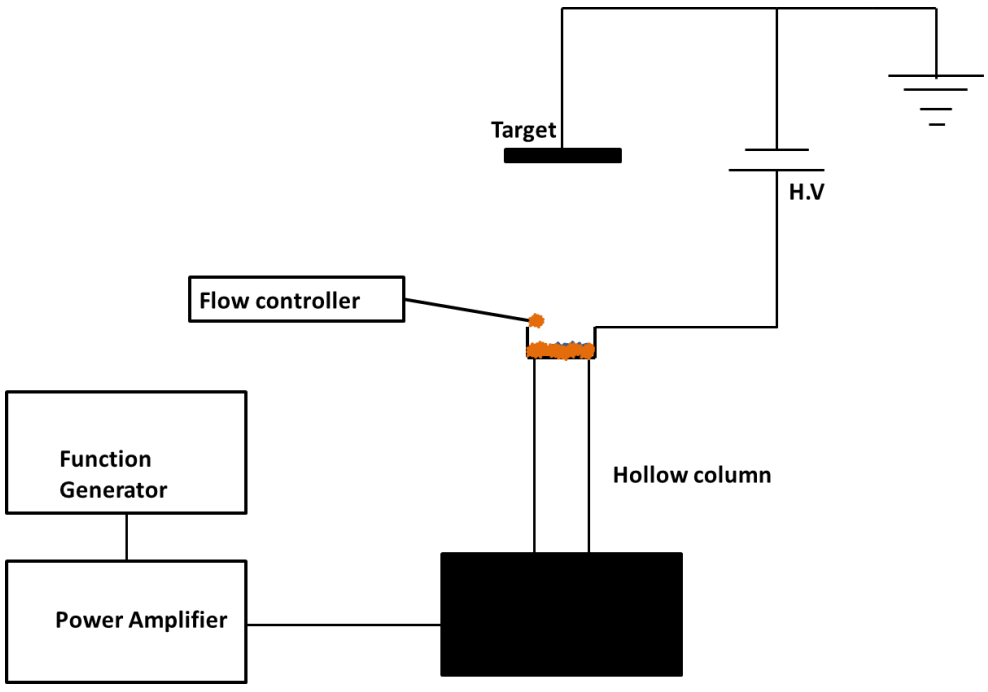

Figure 6-4: Schematic of electrospraying with sound waves setup

6.2.2: Results and Discussion

Disturbances on the surface of the liquid are observed depending on the frequency of excitation. The frequency of the audio speaker is varied from 10 Hz to 4 kHz. As the frequency applied to the contained solution is increased, the waves produced on the surface form patterns of increasing frequency as well. Figure 6-5 shows the liquid wave patterns generated for 1 mL of ethanol at 240 Hz frequency.

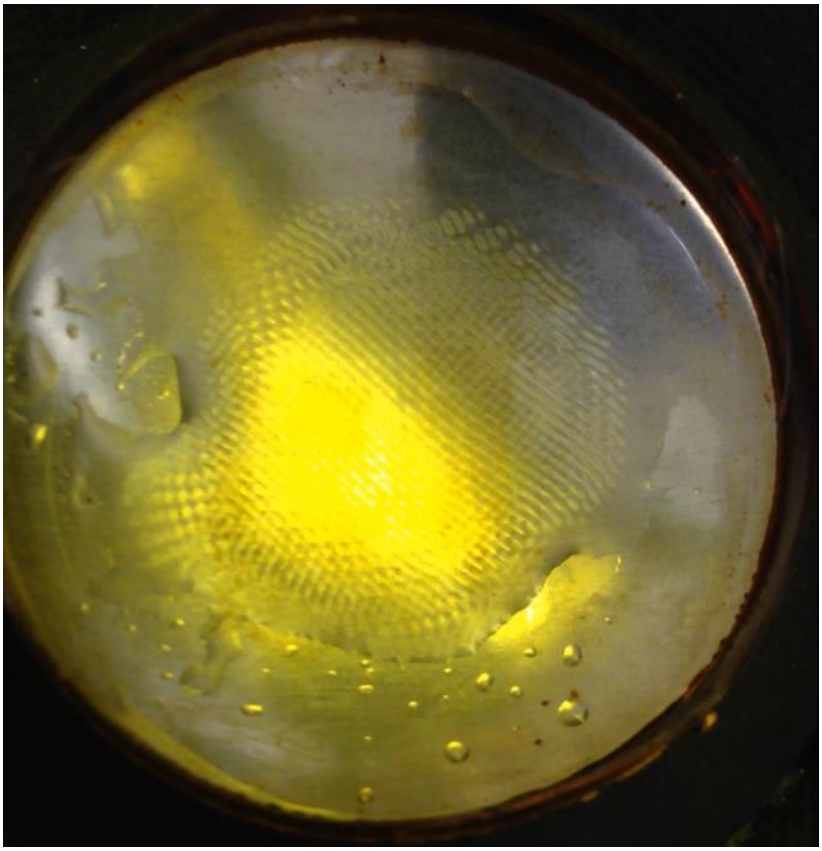

Figure 6-5: Liquid wave patterns on the free surface generated by the sound waves

When a high potential of 25 kV is applied to these liquid wave patterns, electrospraying of the liquid was observed. In our tests of this unique technique, ethanol was used as the solution. Figure 6-6 shows the electrospray of ethanol from the free surface.

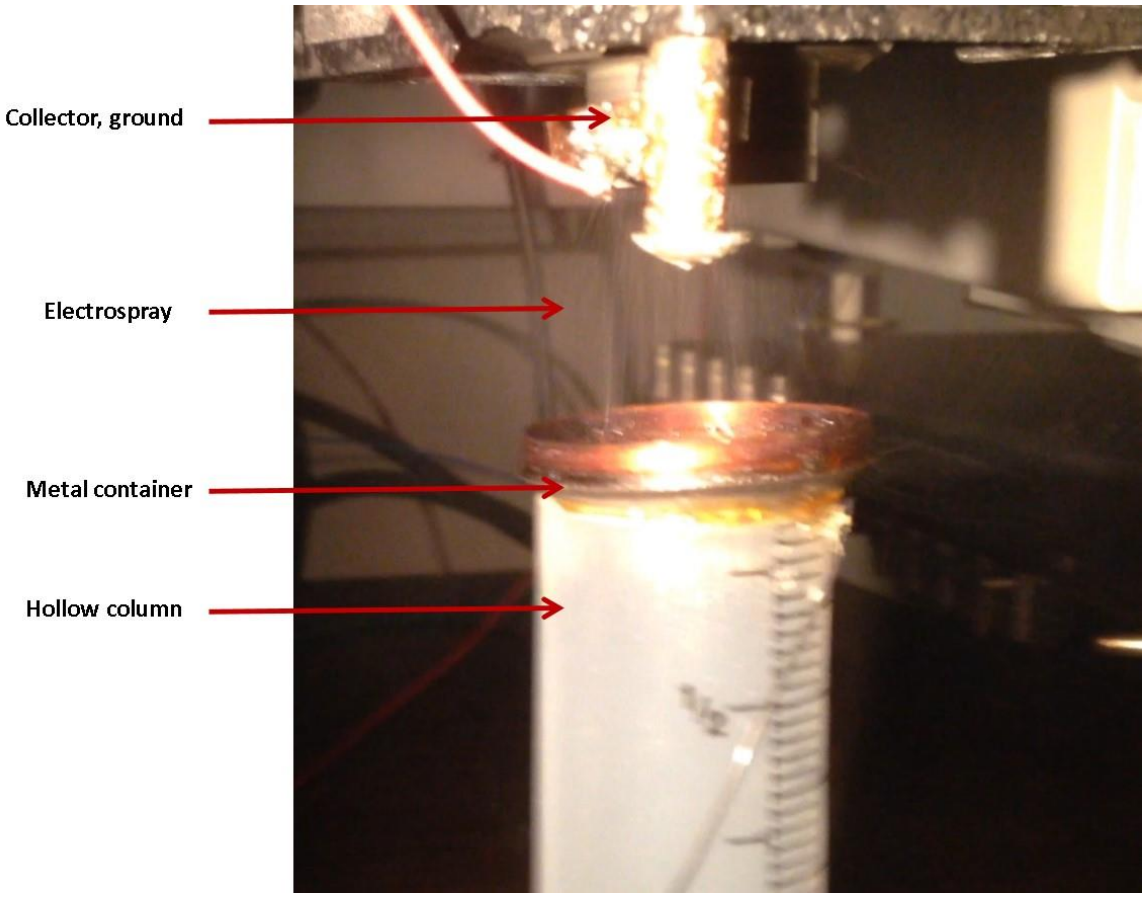

Figure 6-6: Electrospray of ethanol with Faraday waves

6.2.3: Conclusions

Initial results show that electrospraying with Faraday waves has the potential for high solution delivery. This method can also avoid the clogging observed in the needle electrospraying method and eliminates the solvent miscibility issues with the multiple spikes method.

CHAPTER 7: SUMMARY AND RECOMMENDATIONS FOR FUTURE WORK

7.1: Summary of results

NanoGUMBOS characterization

In this work, we have examined the electrical characteristics of several interesting nanoGUMBOS candidates that belong to a new class of materials. Interest in these materials stems from their extended range of thermal stability (compared to traditional ionic liquids) and their ease of synthesis into various nanoforms. Images of samples via Atomic Force Microscopy (AFM) were obtained for [R6G][TPB], [PIC][BETI], and [PIC][NTf_2] nanostructures to understand their morphology. Conductive probe atomic force microscopy (CP-AFM) was used to understand their electrical behavior. Nanowires of [R6G][TPB] and [TC2][BETI] were characterized using an interdigitated structure. [TC2][BETI] forms in-situ nanowires upon deposition onto substrates due to aggregation as the solvent evaporates. This phenomenon was used to deposit thin-films of [TC2][BETI] using electrospaying. [TC2][BETI] films showed uniform coverage of the substrate. Further, we have demonstrated that these [TC2][BETI] thin-films can be used as electronically responsive chemical sensors of various vapors.

Carbon Nanotubes thin-films deposition on non-conductive substrates

Carbon Nanotube (CNT) thin-films have been extensively investigated for various applications ranging from opto-electronics to biological applications. CNTs thin-films are deposited upon a variety of substrates including conductors, semi-conductors, and insulators. Of these, CNT deposition on insulators is both interesting and a challenging task. In this we work, we have developed a technique for the deposition of carbon nanotubes onto non-conductive substrates. A combination of electrospraying and electrophoretic deposition techniques was used

to deposit a uniform conductive initial layer. This initial layer of CNTs thin-film (nm) was used as a conductive substrate for deposition of denser and thicker films (μm) using electrophoretic deposition. Surface coverage, uniformity, and the conductivity of the final film deposited were observed to be dependent on the quality of the underlying initial CNT film. This method of deposition eliminates the need for surface functionalization of substrates using polymer or organic layers prior to CNT deposition. Electrospraying of the initial layer also ensured a uniform coverage of the film, which proved critical for final thin-film properties. This completely solution based room temperature deposition of CNTs of this method has potential for the large scale production of high quality CNTs films .

Faraday Electrosparying

Traditional electrospraying has been increasingly used for thin-film deposition. However, its application to industrial thin-film processes are limited due to inadequate solution delivery rates and complexities arising from the scalability of typical needle electrospraying configurations. In this work we have designed and investigated an alternative method of electrospraying. Our method, for which we have adopted the term "Faraday electrospraying," emits the electrospray from an open solution surface. This is achieved by the use of Faraday waves that form on the surface of liquid when subjected to mechanical waves such as sound waves. When the solution is subjected to the external sound waves, crests and troughs (wave maxima and minima) are formed. Moreover, when a uniform high electric field (kV/cm) is applied, the crests of the solution (due to sound waves) take on a high charge density (Rayleigh Limit), causing the solution to spray. In this study, we have successfully constructed a prototype apparatus to observe these phenomena of electrospraying from the crests of a solution. Ethanol

was sprayed using this technique. This initial study showed that the rate of deposition can be controlled both via the applied electric field (E) and also applied mechanical parameters (frequency and amplitude) as found in sound waves.

7.2: Recommendations for future work

NanoGUMBOS Characterization

a) Characterization of NanoGUMBOS as active components of opto-electronics devices

In this work, we have investigated fundamental electrical characteristics of a new class of nanomaterials which have exhibited potential for use as active components of opto-electronic devices. One prospective device candidate is the solar cell which, in its "dye sensitized" form has been studied for their amenability to ionic liquids. Future work from the hybrid electronic materials/electrical engineering perspective could consist of designing devices which integrate the properties of nanoGUMBOS into a light-to-electrical energy conversion process.

b) Optimization of thin-film deposition of NanoGUMBOS using electrospraying

NanoGUMBOS formed by self-aggregation on the substrate have great potential for thin-film development. In this work we have successfully deposited [TC2][BETI] nanowires using electrospraying. Deposition of in-situ nanostructures ([TC2][BETI]) due to aggregation on the substrate makes them interesting candidates for thin-films development. As these nanostructures are formed in-situ, the size of the solution droplet can be controlled in the electrospraying, resulting in control of the size of the nanostructures. Future work could entail optimization of electrospraying apparatus for use in nanoscale materials processing.

CNTs thin-film deposition on non-conductive substrates

a) Comparative study of CNTs deposition for various non-conductive substrates

In this study CNTs are deposited on glass substrates using electrospray-assisted electrophoretic deposition (EPD). This technique can be used to deposit nanomaterials onto a variety of substrates ranging from polymers to plastics and flexible substrates. A comparative study of the initial CNT layer morphology and conductivity on a wider range of substrates (e.g. Si_3N_4, SiO_2) would contribute to the current state-of-the-art understanding of CNTs and their thin-film properties.

b) Effect of solvent evaporation dynamics on the initial layer morphology

EPD deposition of CNTs on non-conductive substrates are primarily dependent on the underlying layer deposited by the electrospraying. Electrospraying creates micro-scale droplets due to droplet fission which, in turn, are deposited onto a target to form a CNT thin-film. The evaporation dynamics of the deposited CNTs suspended in solvent droplets are critical as these phenomena depend, not only the solvent, but also the underlying substrate (target). Ultimately, the aforementioned affect the morphology of the electrosprayed film and the properties of the EPD film. Future work toward a better understanding of these evaporation dynamics would provide insight into the morphology of the resulting surface and its effect on the conductivity of the final CNTs film.

Faraday Electrospraying

a) Effect of frequency of sound waves on the generation of electrospray

In this work, Faraday waves on a solution surface are generated by the use of sound waves. For a fixed amount of solution in a container, different frequencies of sound waves create a different number of peaks (crests) in the solution; this in turn affects the number of sprays generated when an electric field is applied. Also, different frequencies of sound waves interact differently with the same material due to dampening and sound absorption. Ongoing work to better understand the effect of the frequency of a sound wave applied to solution is critical to understanding the electrospray generated and to controlling the final thin film morphology.

b) Understanding the behavior of self-assembling solution peaks at high electric fields

Electrospray is generated at the peaks (crests) of the solution due to the sound waves and uniform electric field (Rayleigh Limit). As there is a matrix of peaks simultaneously generating electrospray, there is a mutual repulsion which forces the peaks to readjust their positions in the matrix. This phenomenon is more pronounced when very high electric fields are applied and also depends on the viscosity and conductivity of the solution (kV/cm). Future work to better understand the relationship between an applied sound wave frequency and resultant self-assembling peaks (crests) will help to determine the optimal electric field needed for the formation of maximum and stable peaks (crests).

c) Study of solution viscosity and its effects on solution delivery rate

As discussed, the above solution parameters (especially the viscosity of the solution) play a critical role in the Faraday electrospraying process. Most of our study, thus far, has focused on

Newtonian fluids as these react (linearly) to the applied force and are easiest to handle in the initial investigation. However, viscosity of the liquid is a critical factor for self-adjusting peaks; more viscous solutions can withstand higher electric field before the self-adjusting of peaks occur when compared to the less viscous liquids. Future work to develop a clearer understanding of the role of solution viscosity in Faraday electrospraying will assist in better estimation of the applied electric field necessary for the maximum solution delivery rate.

7.3 Final Remarks

This dissertation has presented a comprehensive study of selected hybrid electronic materials (HEMs) in terms of their characterization and thin-film deposition. Ranging from the relatively recently discovered GUMBOS/nanoGUMBOS to the more fully characterized but "processing challenged" carbon nanotubes (CNTs, thin-films), this research has produced first-time results and innovative solutions to the literature, the scientific investigations of, and engineering developments in HEMs. As a body of original research, the work of this dissertation is a notable step in the efforts to move "beyond the transistor" in next-generation electronics.

REFERENCES

[1] M. C. Roco, "The long view of nanotechnology development: the National Nanotechnology Initiative at 10 years," in *Nanotechnology Research Directions for Societal Needs in 2020*, ed: Springer, 2011, pp. 1-28.

[2] M. Haruta, N. Yamada, T. Kobayashi, and S. Iijima, "Gold catalysts prepared by coprecipitation for low-temperature oxidation of hydrogen and of carbon monoxide," *Journal of Catalysis,* vol. 115, pp. 301-309, 1989.

[3] G. Binnig and H. Rohrer, "Scanning Tunelling Microscopy," *Helvetica Physica Acta,* vol. 55, pp. 726-735, 1982 1982.

[4] H. J. Scheel, G. Binnig, and H. Rohrer, "Atomically Flat LPE-Grown Facets Seen by Scanning Tunneling Microscopy," *Journal of Crystal Growth,* vol. 60, pp. 199-202, 1982 1982.

[5] A. Baratoff, G. Binnig, and H. Rohrer, "Scanning Tunneling Microscopy of Semiconductor Surfaces," *Journal of Vacuum Science & Technology B,* vol. 1, pp. 703-704, 1983 1983.

[6] G. K. Binnig, "Atomic-Force Microscopy," *Physica Scripta,* vol. T19A, pp. 53-54, 1987 1987.

[7] R. D. Piner, J. Zhu, F. Xu, S. Hong, and C. A. Mirkin, "" Dip-pen" nanolithography," *science,* vol. 283, pp. 661-663, 1999.

[8] R. P. Feynman, "There's plenty of room at the bottom " *Microelectromechanical Systems, Journal of,* vol. 1, pp. 60-66, 1992.

[9] p. c. Theda Daniels-Race.

[10] J. Bardeen and W. H. Brattain, "The transistor, a semi-conductor triode," *Physical Review,* vol. 74, p. 230, 1948.

[11] J. Bardeen and W. H. Brattain, "Physical principles involved in transistor action," *Physical Review,* vol. 75, p. 1208, 1949.

[12] W. Ahmed, M. J. Jackson, and I. U. Hassan, "Chapter 1 - Nanotechnology to Nanomanufacturing," in *Emerging Nanotechnologies for Manufacturing*, A. Waqar and J. J. Mark, Eds., ed Boston: William Andrew Publishing, 2010, pp. 1-15.

[13] F. C. Adams and C. Barbante, "Nanoscience, nanotechnology and spectrometry," *Spectrochimica Acta Part B-Atomic Spectroscopy,* vol. 86, pp. 3-13, Aug 1 2013.

[14] "Integrating nanotubes into electronics: Nanotechnology," *Materials Today,* vol. 7, p. 7, 3 2004.

[15] G. E. Moore, "Progress in digital integrated electronics," *IEDM Tech. Digest,* vol. 11, 1975.

[16] G. E. Moore, "Cramming more components onto integrated circuits," *Proceedings of the IEEE,* vol. 86, pp. 82-85, 1998.

[17] G. E. Moore, "Cramming more components onto integrated circuits, Reprinted from Electronics, volume 38, number 8, April 19, 1965, pp.114 ff," *Solid-State Circuits Society Newsletter, IEEE,* vol. 11, pp. 33-35, 2006.

[18] L. Giannuzzi and F. Stevie, "A review of focused ion beam milling techniques for TEM specimen preparation," *Micron,* vol. 30, pp. 197-204, 1999.

[19] P. M. Mendes, S. Jacke, K. Critchley, J. Plaza, Y. Chen, K. Nikitin, *et al.*, "Gold nanoparticle patterning of silicon wafers using chemical e-beam lithography," *Langmuir,* vol. 20, pp. 3766-3768, 2004.

[20] R. J. Blaikie, D. O. Melville, and M. M. Alkaisi, "Super-resolution near-field lithography using planar silver lenses: A review of recent developments," *Microelectronic Engineering,* vol. 83, pp. 723-729, 2006.

[21] C. A. Mack, "Fifty years of Moore's law," *Semiconductor Manufacturing, IEEE Transactions on,* vol. 24, pp. 202-207, 2011.

[22] F. Schreiber, "Structure and growth of self-assembling monolayers," *Progress in Surface Science,* vol. 65, pp. 151-257, 11 2000.

[23] A. Aviram, C. Joachim, and M. Pomerantz, "Evidence of switching and rectification by a single molecule effected with a scanning tunneling microscope," *Chemical Physics Letters,* vol. 146, pp. 490-495, 1988.

[24] A. Aviram and M. A. Ratner, "Molecular rectifiers," *Chemical Physics Letters,* vol. 29, pp. 277-283, 1974.

[25] D. K. Aswal, S. Lenfant, D. Guerin, J. V. Yakhmi, and D. Vuillaume, "Self assembled monolayers on silicon for molecular electronics," *Analytica Chimica Acta,* vol. 568, pp. 84-108, 2006.

[26] J. Kim, D. Hong, H. Lee, Y. Shin, S. Park, Y. Khang, *et al.*, "Large Scale Assembly of Pristine Semiconducting Carbon Nanotube Network-Based Devices Exhibiting Intrinsic Characteristics," *The Journal of Physical Chemistry C,* vol. 117, pp. 19721-19728, 2013.

[27] J. C. Love, L. A. Estroff, J. K. Kriebel, R. G. Nuzzo, and G. M. Whitesides, "Self-assembled monolayers of thiolates on metals as a form of nanotechnology," *Chemical Reviews,* vol. 105, pp. 1103-1169, 2005.

[28] C. Park, J. Yoon, and E. L. Thomas, "Enabling nanotechnology with self assembled block copolymer patterns," *Polymer,* vol. 44, pp. 6725-6760, Oct 2003.

[29] C. Wang, J. Zhang, K. Ryu, A. Badmaev, L. G. De Arco, and C. Zhou, "Wafer-Scale Fabrication of Separated Carbon Nanotube Thin-Film Transistors for Display Applications," *Nano Letters,* vol. 9, pp. 4285-4291, Dec 2009.

[30] A. C. Arias, J. D. MacKenzie, I. McCulloch, J. Rivnay, and A. Salleo, "Materials and Applications for Large Area Electronics: Solution-Based Approaches," *Chemical Reviews,* vol. 110, pp. 3-24, Jan 2010.

[31] J. Zhang, C. Wang, and C. Zhou, "Rigid/Flexible Transparent Electronics Based on Separated Carbon Nanotube Thin-Film Transistors and Their Application in Display Electronics," *ACS Nano,* vol. 6, pp. 7412-7419, 2012.

[32] A. G. MacDiarmid, "Synthetic Metals": A Novel Role for Organic Polymers (Nobel Lecture)," *Angewandte Chemie International Edition,* vol. 40, pp. 2581-2590, 2001.

[33] G. Kickelbick, *Hybrid materials: synthesis, characterization, and applications*: John Wiley & Sons, 2007.

[34] C. Joachim, J. Gimzewski, and A. Aviram, "Electronics using hybrid-molecular and mono-molecular devices," *Nature,* vol. 408, pp. 541-548, 2000.

[35] O. Inganäs, "Hybrid electronics and electrochemistry with conjugated polymers," *Chemical Society Reviews,* vol. 39, pp. 2633-2642, 2010.

[36] M. Caironi, T. D. Anthopoulos, Y. Y. Noh, and J. Zaumseil, "Organic and hybrid materials for flexible electronics," *Advanced Materials,* vol. 25, pp. 4208-4209, 2013.

[37] D. Vuillaume and S. Lenfant, "The metal/organic monolayer interface in molecular electronic devices," *Microelectronic Engineering,* vol. 70, pp. 539-550, 2003.

[38] K. Seshan, *Handbook of thin film deposition*: William Andrew, 2012.

[39] W. Kern, *Thin film processes II* vol. 2: Academic press, 2012.

[40] M. J. Madou, *Fundamentals of microfabrication: the science of miniaturization*: CRC press, 2002.

[41] D. S. Soane and Z. M. Soane, "Electrophoresis and photolithography," ed: Google Patents, 1998.

[42] A. Jaworek and A. T. Sobczyk, "Electrospraying route to nanotechnology: An overview," *Journal of Electrostatics,* vol. 66, pp. 197-219, Mar 2008.

[43] J. F. de la Mora, "The fluid dynamics of Taylor cones," in *Annual Review of Fluid Mechanics*. vol. 39, ed, 2007, pp. 217-243.

[44] I. Hayati, "Eddies Inside a Liquid Cone Stressed by Interfacial Electrical Shear," *Colloids and Surfaces,* vol. 65, pp. 77-84, Jul 21 1992.

[45] I. Hayati, A. I. Bailey, and T. F. Tadros, "Investigations into the Mechanism of Electrohydrodynamic Spraying of Liquids. 1. Effect of Electric-Field and the Environment on Pendant Drops and Factors Affecting the Formation of Stable Jets and Atomization " *Journal of Colloid and Interface Science,* vol. 117, pp. 205-221, May 1987.

[46] A. Jaworek, "Electrospray droplet sources for thin film deposition," *Journal of Materials Science,* vol. 42, pp. 266-297, Jan 2007.

[47] A. Jaworek, K. Adamiak, and A. Krupa, "Deposition of aerosol particles on a charged spherical collector," *Journal of Electrostatics,* vol. 40-1, pp. 443-448, Jun 1997.

[48] A. Jaworek, K. Adamiak, A. Krupa, and G. S. P. Castle, "Trajectories of charged aerosol particles near a spherical collector," *Journal of Electrostatics,* vol. 51, pp. 603-609, May 2001.

[49] A. Jaworek, A. Krupa, M. Lackowski, A. T. Sobczyk, T. Czech, S. Ramakrishna, *et al.*, "Nanocomposite fabric formation by electrospinning and electrospraying technologies," *Journal of Electrostatics,* vol. 67, pp. 435-438, May 2009.

[50] A. Jaworek, A. Krupa, M. Lackowski, A. T. Sobczyk, T. Czech, S. Ramakrishna, *et al.*, "Electrospinning and Electrospraying Techniques for Nanocomposite Non-Woven Fabric Production," *Fibres & Textiles in Eastern Europe,* vol. 17, pp. 77-81, Oct-Dec 2009.

[51] R. Kessick, J. Fenn, and G. Tepper, "The use of AC potentials in electrospraying and electrospinning processes," *Polymer,* vol. 45, pp. 2981-2984, 2004.

[52] W. J. Li, C. T. Laurencin, E. J. Caterson, R. S. Tuan, and F. K. Ko, "Electrospun nanofibrous structure: A novel scaffold for tissue engineering," *Journal of Biomedical Materials Research,* vol. 60, pp. 613-621, Jun 15 2002.

[53] J. Ayutsede, M. Gandhi, S. Sukigara, H. H. Ye, C. M. Hsu, Y. Gogotsi, *et al.*, "Carbon nanotube reinforced Bombyx mori silk nanofibers by the electrospinning process," *Biomacromolecules,* vol. 7, pp. 208-214, Jan 2006.

[54] D. C. Taflin, T. L. Ward, and E. J. Davis, "Electrified droplet fission and the Rayleigh limit," *Langmuir,* vol. 5, pp. 376-384, 1989.

[55] J. F. Delamora and I. G. Loscertales, " The Current Emitted by Highly Conductign Taylor Cones," *Journal of Fluid Mechanics,* vol. 260, pp. 155-184, Feb 10 1994.

[56] A. M. Ganancalvo, J. C. Lasheras, J. Davila, and A. Barrero, "The ELectrostatic Spray Emitted From an Electirified Conical Meniscus," *Journal of Aerosol Science,* vol. 25, pp. 1121-&, Sep 1994.

[57] R. P. A. Hartman, D. J. Brunner, D. M. A. Camelot, J. C. M. Marijnissen, and B. Scarlett, "Jet break-up in electrohydrodynamic atomization in the cone-jet mode," *Journal of Aerosol Science,* vol. 31, pp. 65-95, Jan 2000.

[58] Y. Zhang, Y. Fang, X. Zhou, and X. Dong, "Image-based hysteresis modeling and compensation for an AFM piezo-scanner," *Asian Journal of Control,* vol. 11, pp. 166-174, 2009.

[59] K. K. Leang and S. Devasia, "Feedback-linearized inverse feedforward for creep, hysteresis, and vibration compensation in AFM piezoactuators," *Control Systems Technology, IEEE Transactions on,* vol. 15, pp. 927-935, 2007.

[60] D. Croft, G. Shed, and S. Devasia, "Creep, hysteresis, and vibration compensation for piezoactuators: atomic force microscopy application," *Journal of Dynamic Systems, Measurement, and Control,* vol. 123, pp. 35-43, 2001.

[61] B. Mokaberi and A. A. Requicha, "Compensation of scanner creep and hysteresis for AFM nanomanipulation," *Automation Science and Engineering, IEEE Transactions on,* vol. 5, pp. 197-206, 2008.

[62] F. Ohnesorge and G. Binnig, "True atomic resolution by atomic force microscopy through repulsive and attractive forces," *Science,* vol. 260, pp. 1451-1456, 1993.

[63] B. Cappella and G. Dietler, "Force-distance curves by atomic force microscopy," *Surface Science Reports,* vol. 34, pp. 1-104, 1999 1999.

[64] W. Zhou and Z. L. Wang, *Scanning microscopy for nanotechnology: techniques and applications*: Springer science & business media, 2007.

[65] A. Tesfai, B. El-Zahab, D. K. Bwambok, G. A. Baker, S. O. Fakayode, M. Lowry, *et al.*, "Controllable formation of ionic liquid micro- and nanoparticles via a melt-emulsion-quench approach," *Nano Letters,* vol. 8, pp. 897-901, 2008.

[66] S. Das, D. Bwambok, B. El-Zahab, J. Monk, S. L. de Rooy, S. Challa, *et al.*, "Nontemplated Approach to Tuning the Spectral Properties of Cyanine-Based Fluorescent NanoGUMBOS," *Langmuir,* vol. 26, pp. 12867-12876, Aug 3 2010.

[67] C. Lu, S. Das, P. K. S. Magut, M. Li, B. El-Zahab, and I. M. Warner, "Irradiation Induced Fluorescence Enhancement in PEGylated Cyanine-Based NIR Nano- and Mesoscale GUMBOS," *Langmuir,* vol. 28, pp. 14415-14423, Oct 9 2012.

[68] A. Tesfai, B. El-Zahab, A. T. Kelley, M. Li, J. C. Garno, G. A. Baker, *et al.*, "Magnetic and Nonmagnetic Nanoparticles from a Group of Uniform Materials Based on Organic Salts," *ACS Nano,* vol. 3, pp. 3244-3250, Oct 2009.

[69] P. Wang, B. Wenger, R. Humphry-Baker, J. E. Moser, J. Teuscher, W. Kantlehner, *et al.*, "Charge separation and efficient light energy conversion in sensitized mesoscopic solar cells based on binary ionic liquids," *Journal of the American Chemical Society,* vol. 127, pp. 6850-6856, May 11 2005.

[70] R. Kawano, H. Matsui, C. Matsuyama, A. Sato, M. Susan, N. Tanabe, *et al.*, "High performance dye-sensitized solar cells using ionic liquids as their electrolytes," *Journal of Photochemistry and Photobiology a-Chemistry,* vol. 164, pp. 87-92, Jun 1 2004.

[71] R. D. Rogers and K. R. Seddon, "Ionic liquids - Solvents of the future?," *Science,* vol. 302, pp. 792-793, Oct 31 2003.

[72] M. Freemantle, "Designer solvents - Ionic liquids may boost clean technology development," *Chemical & Engineering News,* vol. 76, pp. 32-37, Mar 30 1998.

[73] F. J. M. Rutten, H. Tadesse, and P. Licence, "Rewritable imaging on the surface of frozen ionic liquids," *Angewandte Chemie-International Edition,* vol. 46, pp. 4163-4165, 2007 2007.

[74] D. K. Bwambok, H. M. Marwani, V. E. Fernand, S. O. Fakayode, M. Lowry, I. Negulescu, *et al.*, "Synthesis and characterization of novel chiral ionic liquids and investigation of their enantiomeric recognition properties," *Chirality,* vol. 20, pp. 151-158, 2008.

[75] J. P. Hallett and T. Welton, "Room-Temperature Ionic Liquids: Solvents for Synthesis and Catalysis. 2," *Chemical Reviews,* vol. 111, pp. 3508-3576, May 2011.

[76] K. Matsumoto, R. Hagiwara, Z. Mazej, P. Benkič, and B. Žemva, "Crystal structures of frozen room temperature ionic liquids, 1-ethyl-3-methylimidazolium tetrafluoroborate (EMImBF 4), hexafluoroniobate (EMImNbF 6) and hexafluorotantalate (EMImTaF 6), determined by low-temperature X-ray diffraction," *Solid state sciences,* vol. 8, pp. 1250-1257, 2006.

[77] W. I. S. Galpothdeniya, S. L. De Rooy, and I. M. Warner, "Optoelectronic ionic liquid sensor array," *Abstracts of Papers of the American Chemical Society,* vol. 245, Apr 7 2013.

[78] S. Hamdan, B. El-Zahab, S. Das, and I. M. Warner, "Size-control of nanoGUMBOS and importance for analytical applications," *Abstracts of Papers of the American Chemical Society,* vol. 245, Apr 7 2013.

[79] F. Huang, P. Berton, C. Lu, N. Siraj, and I. M. Warner, "Novel room temperature ionic liquid for phenolic compounds microextraction from environmental samples," *Abstracts of Papers of the American Chemical Society,* vol. 245, Apr 7 2013.

[80] P. K. S. Magut, S. Das, V. Fernand, J. Losso, K. McDonough, B. M. Naylor, *et al.*, "Biomedical applications of a group of uniform materials based on organic salts," *Abstracts of Papers of the American Chemical Society,* vol. 245, Apr 7 2013.

[81] B. P. Regmi, S. Das, and I. M. Warner, "Ionic liquid-based QCM sensor for vapor discrimination," *Abstracts of Papers of the American Chemical Society,* vol. 245, Apr 7 2013.

[82] N. Siraj, S. Das, F. Hasan, K. Kanakamedala, T. Daniels-Race, and I. M. Warner, "Evaluation of thin films based on fluorescent and conductive GUMBOS," *Abstracts of Papers of the American Chemical Society,* vol. 245, Apr 7 2013.

[83] I. J. Stavrou, L. Moore, Jr., V. E. Fernand, C. P. Kapnissi-Christodoulou, and I. M. Warner, "Facile preparation of polysaccharide-coated capillaries using a room temperature ionic liquid for chiral separations," *Electrophoresis,* vol. 34, pp. 1334-1338, May 2013.

[84] p. c. I. M. Warner.

[85] S. L. de Rooy, B. El-Zahab, M. Li, S. Das, E. Broering, L. Chandler, *et al.*, "Fluorescent one-dimensional nanostructures from a group of uniform materials based on organic salts," *Chemical Communications,* vol. 47, pp. 8916-8918, 2011.

[86] A. N. Jordan, S. Das, N. Siraj, S. L. de Rooy, M. Li, B. El-Zahab, *et al.*, "Anion-controlled morphologies and spectral features of cyanine-based nanoGUMBOS - an improved photosensitizer," *Nanoscale,* vol. 4, pp. 5031-5038, 2012 2012.

[87] D. K. Bwambok, B. El-Zahab, S. K. Challa, M. Li, L. Chandler, G. A. Baker, *et al.*, "Near-Infrared Fluorescent NanoGUMBOS for Biomedical Imaging," *ACS Nano,* vol. 3, pp. 3854-3860, Dec 2009.

[88] S. L. de Rooy, S. Das, M. Li, B. El-Zahab, A. Jordan, R. Lodes, *et al.*, "Ionically Self-Assembled, Multi-Luminophore One-Dimensional Micro- and Nanoscale Aggregates of Thiacarbocyanine GUMBOS," *Journal of Physical Chemistry C,* vol. 116, pp. 8251-8260, Apr 12 2012.

[89] T. D. Slavnova, H. Görner, and A. K. Chibisov, "Cyanine-based J-aggregates as a chirality-sensing supramolecular system," *The Journal of Physical Chemistry B,* vol. 115, pp. 3379-3384, 2011.

[90] T. D. Slavnova, H. Görner, and A. K. Chibisov, "J-aggregation of anionic ethyl meso-thiacarbocyanine dyes induced by binding to proteins," *The Journal of Physical Chemistry B,* vol. 111, pp. 10023-10031, 2007.

[91] S. Sankaran, S. Panigrahi, and S. Mallik, "Olfactory receptor based piezoelectric biosensors for detection of alcohols related to food safety applications," *Sensors and Actuators B: Chemical,* vol. 155, pp. 8-18, 7/5/ 2011.

[92] L. S. Pingree, O. G. Reid, and D. S. Ginger, "Electrical scanning probe microscopy on active organic electronic devices," *Advanced Materials,* vol. 21, pp. 19-28, 2009.

[93] A. Sarkar, K. Kanakamedala, M. Rajathadripura, N. Jagadish, P. Magut, S. de Rooy, *et al.,* "Electro-optical characterization of nanoGUMBOS," *Electronic Materials Letters,* vol. 10, pp. 775-781, 2014.

[94] A. Salomon, D. Cahen, S. Lindsay, J. Tomfohr, V. B. Engelkes, and C. D. Frisbie, "Comparison of electronic transport measurements on organic molecules," *Advanced Materials,* vol. 15, pp. 1881-1890, 2003.

[95] C. Kergueris, J.-P. Bourgoin, S. Palacin, D. Estève, C. Urbina, M. Magoga, *et al.*, "Electron transport through a metal-molecule-metal junction," *Physical Review B,* vol. 59, p. 12505, 1999.

[96] E. Tran, M. Duati, V. Ferri, K. Müllen, M. Zharnikov, G. M. Whitesides, *et al.*, "Experimental approaches for controlling current flowing through metal–molecule–metal junctions," *Advanced Materials,* vol. 18, pp. 1323-1328, 2006.

[97] A. Sarkar, K. Kanakamedala, N. N. Jagadish, A. Jordan, S. Das, N. Siraj, *et al.*, "Electro-optical characterization of cyanine-based GUMBOS and nanoGUMBOS," *Electronic Materials Letters,* vol. 10, pp. 879-885, 2014.

[98] J. Alvarez, F. Houze, J. P. Kleider, M. Y. Liao, and Y. Koide, "Electrical characterization of Schottky diodes based on boron doped homoepitaxial diamond films by conducting probe atomic force microscopy," *Superlattices and Microstructures,* vol. 40, pp. 343-349, Oct-Dec 2006.

[99] A. N. Farley, "Imaging the local electrical properties of metal surfaces by atomic force microscopy with conducting probes - Comment," *Applied Physics Letters,* vol. 70, pp. 3618-3618, Jun 30 1997.

[100] F. Houze, R. Meyer, O. Schneegans, and L. Boyer, "Imaging the local electrical properties of metal surfaces by atomic force microscopy with conducting probes," *Applied Physics Letters,* vol. 69, pp. 1975-1977, Sep 23 1996.

[101] F. Houze, R. Meyer, O. Schneegans, and L. Boyer, "Imaging the local electrical properties of metal surfaces by atomic force microscopy with conducting probes - Response," *Applied Physics Letters,* vol. 70, pp. 3619-3619, Jun 30 1997.

[102] H. Wang, X. Xu, A. Kojtari, and H.-F. Ji, "Triphenylene Nano/Microwires for Sensing Nitroaromatics," *Journal of Physical Chemistry C,* vol. 115, pp. 20091-20096, Oct 20 2011.

[103] P. Avouris, R. Martel, V. Derycke, and J. Appenzeller, "Carbon nanotube transistors and logic circuits," *Physica B-Condensed Matter,* vol. 323, pp. 6-14, Oct 2002.

[104] S. Heinze, J. Tersoff, R. Martel, V. Derycke, J. Appenzeller, and P. Avouris, "Carbon nanotubes as Schottky barrier transistors," *Physical Review Letters,* vol. 89, Sep 2 2002.

[105] S. Lastella, G. Mallick, R. Woo, S. P. Karna, D. A. Rider, I. Manners*, et al.*, "Parallel arrays of individually addressable single-walled carbon nanotube field-effect transistors," *Journal of Applied Physics,* vol. 99, Jan 15 2006.

[106] M. F. De Volder, S. H. Tawfick, R. H. Baughman, and A. J. Hart, "Carbon nanotubes: present and future commercial applications," *Science,* vol. 339, pp. 535-539, 2013.

[107] C. Niu, E. K. Sichel, R. Hoch, D. Moy, and H. Tennent, "High power electrochemical capacitors based on carbon nanotube electrodes," *Applied Physics Letters,* vol. 70, pp. 1480-1482, 1997.

[108] A. L. M. Reddy, M. M. Shaijumon, S. R. Gowda, and P. M. Ajayan, "Coaxial MnO2/carbon nanotube array electrodes for high-performance lithium batteries," *Nano Letters,* vol. 9, pp. 1002-1006, 2009.

[109] K. Hong, S. Nam, C. Yang, S. H. Kim, D. S. Chung, W. M. Yun, *et al.*, "Solution-processed organic field-effect transistors composed of poly (4-styrene sulfonate) wrapped multiwalled carbon nanotube source/drain electrodes," *Organic Electronics,* vol. 10, pp. 363-367, 2009.

[110] S. Wang, Q. Zhang, D. Yang, P. Sellin, and G. Zhong, "Multi-walled carbon nanotube-based gas sensors for NH 3 detection," *Diamond and Related Materials,* vol. 13, pp. 1327-1332, 2004.

[111] A. Sarkar, H. Wang, and T. Daniels-Race, "Surface enhanced Raman spectroscopy on silver-nanoparticle-coated carbon-nanotube networks fabricated by electrophoretic deposition," *Electronic Materials Letters,* vol. 10, pp. 325-335, 2014.

[112] L. Hu, J. Li, J. Liu, G. Grüner, and T. Marks, "Flexible organic light-emitting diodes with transparent carbon nanotube electrodes: problems and solutions," *Nanotechnology*, vol. 21, p. 155202, 2010.

[113] I. Moriguchi, R. Hidaka, H. Yamada, T. Kudo, H. Murakami, and N. Nakashima, "A Mesoporous Nanocomposite of TiO2 and Carbon Nanotubes as a High-Rate Li-Intercalation Electrode Material," *Advanced Materials*, vol. 18, pp. 69-73, 2006.

[114] T. Ebbesen and P. Ajayan, "Large-scale synthesis of carbon nanotubes," *Nature*, vol. 358, pp. 220-222, 1992.

[115] N. Grobert, "Carbon nanotubes–becoming clean," *Materials Today*, vol. 10, pp. 28-35, 2007.

[116] J. Prasek, J. Drbohlavova, J. Chomoucka, J. Hubalek, O. Jasek, V. Adam, *et al.*, "Methods for carbon nanotubes synthesis—review," *Journal of Materials Chemistry*, vol. 21, pp. 15872-15884, 2011.

[117] A. Szabó, C. Perri, A. Csató, G. Giordano, D. Vuono, and J. B. Nagy, "Synthesis methods of carbon nanotubes and related materials," *Materials*, vol. 3, pp. 3092-3140, 2010.

[118] A. Abdelhalim, A. Abdellah, G. Scarpa, and P. Lugli, "Fabrication of carbon nanotube thin films on flexible substrates by spray deposition and transfer printing," *Carbon*, vol. 61, pp. 72-79, Sep 2013.

[119] L. Hu, D. S. Hecht, and G. Gruner, "Carbon nanotube thin films: fabrication, properties, and applications," *Chemical Reviews*, vol. 110, pp. 5790-5844, 2010.

[120] A. R. Boccaccini, J. Cho, J. A. Roether, B. J. Thomas, E. J. Minay, and M. S. Shaffer, "Electrophoretic deposition of carbon nanotubes," *Carbon*, vol. 44, pp. 3149-3160, 2006.

[121] I. Corni, M. P. Ryan, and A. R. Boccaccini, "Electrophoretic deposition: from traditional ceramics to nanotechnology," *Journal of the European Ceramic Society*, vol. 28, pp. 1353-1367, 2008.

[122] O. O. Van der Biest and L. J. Vandeperre, "Electrophoretic deposition of materials," *Annual Review of Materials Science*, vol. 29, pp. 327-352, 1999.

[123] L. Besra and M. Liu, "A review on fundamentals and applications of electrophoretic deposition (EPD)," *Progress in materials science*, vol. 52, pp. 1-61, 2007.

[124] H. Negishi, N. Oshima, K. Haraya, K. Sakaki, T. Ikegami, Y. Idemoto, *et al.*, "Preparation of thin and dense lanthanum cobaltite coating on porous tubular alumina supports by electrophoretic deposition," *Nippon Seramikkusu Kyokai Gakujutsu Ronbunshi*, vol. 114, pp. 36-41, 2006.

[125] L. Besra, C. Compson, and M. Liu, "Electrophoretic deposition on non-conducting substrates: the case of YSZ film on NiO–YSZ composite substrates for solid oxide fuel cell application," *Journal of Power Sources,* vol. 173, pp. 130-136, 2007.

[126] T. Talebi, M. H. Sarrafi, M. Haji, B. Raissi, and A. Maghsoudipour, "Investigation on microstructures of NiO–YSZ composite and Ni–YSZ cermet for SOFCs," *International Journal of Hydrogen Energy,* vol. 35, pp. 9440-9447, 2010.

[127] A. Sarkar and D. Hah, "Electrophoretic deposition of carbon nanotubes on silicon substrates," *Journal of Electronic Materials,* vol. 41, pp. 3130-3138, 2012.

[128] A. Sarkar and T. Daniels-Race, "Electrophoretic Deposition of Carbon Nanotubes on 3-Amino-Propyl-Triethoxysilane (APTES) Surface Functionalized Silicon Substrates," *Nanomaterials,* vol. 3, pp. 272-288, 2013.

[129] J. Desoto, A. Sarkar, and T. Daniels-Race, "A study of electrophoretic deposition (EPD) of carbon nanotubes on insulator substrates," in *Proc. 80th. South Eastern Section of American Physical Society, American Physical Society, Western Kentucky University, Kentucky, USA (2013).* 2013.

[130] I. B. Rietveld, K. Kobayashi, H. Yamada, and K. Matsushige, "Electrospray deposition, model, and experiment: Toward general control of film morphology," *Journal of Physical Chemistry B,* vol. 110, pp. 23351-23364, Nov 23 2006.

[131] J. C. Almekinders and C. Jones, "Multiple jet electrohydrodynamic spraying and applications," *Journal of Aerosol Science,* vol. 30, pp. 969-971, Aug 1999.

[132] M. Cloupeau and B. Prunetfoch, "Electrohydrodynamic Spraying Functioning Modes - A Critical-Review," *Journal of Aerosol Science,* vol. 25, pp. 1021-1036, Sep 1994.

[133] A. M. Ganan-Calvo, J. Davila, and A. Barrero, "Current and droplet size in the electrospraying of liquids. Scaling laws," *Journal of Aerosol Science,* vol. 28, pp. 249-275, Mar 1997.

[134] I. Hayati, A. Bailey, and T. F. Tadros, " Investigations into the Mechanism of Electrohydrodynamic Spraying of Liquids . 2. Mechanism of Stable Jet Formation and Electical Forces Acting on a Liquid Cone" *Journal of Colloid and Interface Science,* vol. 117, pp. 222-230, May 1987.

[135] I. W. Chiang, B. E. Brinson, R. E. Smalley, J. L. Margrave, and R. H. Hauge, "Purification and characterization of single-wall carbon nanotubes," *Journal of Physical Chemistry B,* vol. 105, pp. 1157-1161, Feb 15 2001.

[136] H. Suzuura and T. Ando, "Chirality-dependent resistivity in carbon nanotubes," *Molecular Crystals and Liquid Crystals,* vol. 340, pp. 731-736, 2000.

[137] Y. Meng, G. Xin, J. Nam, S. M. Cho, and H. Chae, "Electrospray Deposition of Carbon Nanotube Thin Films for Flexible Transparent Electrodes," *Journal of Nanoscience and Nanotechnology,* vol. 13, pp. 6125-6129, Sep 2013.

[138] A. C. Ferrari, "Raman spectroscopy of graphene and graphite: Disorder, electron-phonon coupling, doping and nonadiabatic effects," *Solid State Communications,* vol. 143, pp. 47-57, Jul 2007.

[139] C. Vix-Guterl, M. Couzi, J. Dentzer, M. Trinquecoste, and P. Delhaes, "Surface characterizations of carbon multiwall nanotubes: Comparison between surface active sites and Raman Spectroscopy," *Journal of Physical Chemistry B,* vol. 108, pp. 19361-19367, Dec 2004.

[140] O. O. Dosunmu, G. G. Chase, W. Kataphinan, and D. H. Reneker, "Electrospinning of polymer nanofibres from multiple jets on a porous tubular surface," *Nanotechnology,* vol. 17, pp. 1123-1127, Feb 28 2006.

[141] A. L. Yarin and E. Zussman, "Upward needleless electrospinning of multiple nanofibers," *Polymer,* vol. 45, pp. 2977-2980, Apr 2004.

APPENDIX A: PERMISSION TO REPRINT FROM ACS PUBLICATIONS

Title: Room-Temperature Ionic Liquids: Solvents for Synthesis and Catalysis. 2
Author: Jason P. Hallett, Tom Welton
Publication: Chemical Reviews
Publisher: American Chemical Society
Date: May 1, 2011

PERMISSION/LICENSE IS GRANTED FOR YOUR ORDER AT NO CHARGE

This type of permission/license, instead of the standard Terms & Conditions, is sent to you because no fee is being charged for your order. Please note the following:

- Permission is granted for your request in both print and electronic formats, and translations.
- If figures and/or tables were requested, they may be adapted or used in part.
- Please print this page for your records and send a copy of it to your publisher/graduate school.
- Appropriate credit for the requested material should be given as follows: "Reprinted (adapted) with permission from (COMPLETE REFERENCE CITATION). Copyright (YEAR) American Chemical Society." Insert appropriate information in place of the capitalized words.
- One-time permission is granted only for the use specified in your request. No additional uses are granted (such as derivative works or other editions). For any other uses, please submit a new request.

If credit is given to another source for the material you requested, permission must be obtained from that source.

Title: Controllable Formation of Ionic Liquid Micro- and Nanoparticles via a Melt–Emulsion–Quench Approach

Author: Aaron Tesfai, Bilal El-Zahab, David K. Bwambok, et al

Publication: Nano Letters

Publisher: American Chemical Society

Date: Mar 1, 2008

PERMISSION/LICENSE IS GRANTED FOR YOUR ORDER AT NO CHARGE

This type of permission/license, instead of the standard Terms & Conditions, is sent to you because no fee is being charged for your order. Please note the following:

- Permission is granted for your request in both print and electronic formats, and translations.
- If figures and/or tables were requested, they may be adapted or used in part.
- Please print this page for your records and send a copy of it to your publisher/graduate school.
- Appropriate credit for the requested material should be given as follows: "Reprinted (adapted) with permission from (COMPLETE REFERENCE CITATION). Copyright (YEAR) American Chemical Society." Insert appropriate information in place of the capitalized words.
- One-time permission is granted only for the use specified in your request. No additional uses are granted (such as derivative works or other editions). For any other uses, please submit a new request.

If credit is given to another source for the material you requested, permission must be obtained from that source.

Title: Magnetic and Nonmagnetic Nanoparticles from a Group of Uniform Materials Based on Organic Salts
Author: Aaron Tesfai, Bilal El-Zahab, Algernon T. Kelley, et al
Publication: ACS Nano
Publisher: American Chemical Society
Date: Oct 1, 2009

PERMISSION/LICENSE IS GRANTED FOR YOUR ORDER AT NO CHARGE

This type of permission/license, instead of the standard Terms & Conditions, is sent to you because no fee is being charged for your order. Please note the following:

- Permission is granted for your request in both print and electronic formats, and translations.
- If figures and/or tables were requested, they may be adapted or used in part.
- Please print this page for your records and send a copy of it to your publisher/graduate school.
- Appropriate credit for the requested material should be given as follows: "Reprinted (adapted) with permission from (COMPLETE REFERENCE CITATION). Copyright (YEAR) American Chemical Society." Insert appropriate information in place of the capitalized words.
- One-time permission is granted only for the use specified in your request. No additional uses are granted (such as derivative works or other editions). For any other uses, please submit a new request.

If credit is given to another source for the material you requested, permission must be obtained from that source.

Title: Ionically Self-Assembled, Multi-Luminophore One-Dimensional Micro- and Nanoscale Aggregates of Thiacarbocyanine GUMBOS
Author: Sergio L. de Rooy, Susmita Das, Min Li, et al
Publication: The Journal of Physical Chemistry C
Publisher: American Chemical Society
Date: Apr 1, 2012

PERMISSION/LICENSE IS GRANTED FOR YOUR ORDER AT NO CHARGE

This type of permission/license, instead of the standard Terms & Conditions, is sent to you because no fee is being charged for your order. Please note the following:

- Permission is granted for your request in both print and electronic formats, and translations.
- If figures and/or tables were requested, they may be adapted or used in part.
- Please print this page for your records and send a copy of it to your publisher/graduate school.
- Appropriate credit for the requested material should be given as follows: "Reprinted (adapted) with permission from (COMPLETE REFERENCE CITATION). Copyright (YEAR) American Chemical Society." Insert appropriate information in place of the capitalized words.
- One-time permission is granted only for the use specified in your request. No additional uses are granted (such as derivative works or other editions). For any other uses, please submit a new request.

If credit is given to another source for the material you requested, permission must be obtained from that source.

APPENDIX B: PERMISSION TO REPRINT FROM ROYAL SOCIETY OF CHEMISTRY

This is an Agreement between Kalyan Kanakamedala ("You") and Royal Society of Chemistry ("Royal Society of Chemistry"). It consists of your order details, the terms and conditions provided by Royal Society of Chemistry, and the payment terms and conditions.
All payments must be made in full to CCC. For payment instructions, please see information listed at the bottom of this form.

License Number	3259690902327
License date	Oct 31, 2013
Licensed Content Publisher	Royal Society of Chemistry
Licensed Content Publication	Chemical Communications (Cambridge)
Licensed Content Title	Fluorescent one-dimensional nanostructure -es from a group of uniform materials based on organic salts
Licensed Content Author	Sergio L. de Rooy,Bilal El-Zahab, Min Li,Susmita Das,Ellen Broering, Lin Chandler,Isiah M. Warner
Licensed Content Date	Jun 15, 2011
Volume number	47
Issue number	31
Type of Use	Thesis/Dissertation
Requestor type	academic/educational
Portion	figures/tables/images
Number of figures/tables/images	3
Format	print and electronic
Distribution quantity	100
Will you be translating?	no
Order reference number	None
Title of the thesis/dissertation	Electrical Characterization of Hybrid Electonic Materials
Expected completion date	May 2014
Estimated size	100
Total	0.0 USD

This is an Agreement between Kalyan Kanakamedala ("You") and Royal Society of Chemistry ("Royal Society of Chemistry"). It consists of your order details, the terms and conditions provided by Royal Society of Chemistry, and the payment terms and conditions.
All payments must be made in full to CCC. For payment instructions, please see information listed at the bottom of this form.

License Number	3259691461661
License date	Oct 31, 2013
Licensed Content Publisher	Royal Society of Chemistry
Licensed Content Publication	Nanoscale
Licensed Content Title	Anion-controlled morphologies and spectral features of cyanine-based nanoGUMBOS – an improved photosensitizer
Licensed Content Author	Atiya N. Jordan,Susmita Das, Noureen Siraj,Sergio L. de Rooy, Min Li,Bilal El-Zahab,Lin Chandler, Gary A. Baker,Isiah M. Warner
Licensed Content Date	Jun 26, 2012
Volume number	4
Issue number	16
Type of Use	Thesis/Dissertation
Requestor type	academic/educational
Portion	figures/tables/images
Number of figures/tables/images	3
Format	print and electronic
Distribution quantity	100
Will you be translating?	no
Order reference number	None
Title of the thesis/dissertation	Electrical Characterization of Hybrid Electonic Materials
Expected completion date	May 2014
Estimated size	100
Total	0.00 USD

APPENDIX C: PERMISSION TO REPRINT FROM ELSEVIER

This is an Agreement between Kalyan Kanakamedala ("You") and Elsevier ("Elsevier"). It consists of your order details, the terms and conditions provided by Elsevier, and the payment terms and conditions.

All payments must be made in full to CCC. For payment instructions, please see information listed at the bottom of this form.

Supplier	Elsevier The Kidlington,Oxford,OX5 1GB,UK
Registered Company Number	1982084
Customer name	Kalyan Kanakamedala
Customer address	3101, Patrick F Taylor Hall, BATON ROUGE, LA 70820
License number	3258050060332
License date	Oct 29, 2013
Licensed content publisher	Elsevier
Licensed content publication	Journal of Colloid and Interface Science
Licensed content title	Investigations into the mechanisms of electrohydrodynamic spraying of liquids: I. Effect of electric field and the environment on pendant drops and factors affecting the formation of stable jets and atomization
Licensed content author	I Hayati,A.I Bailey,Th.F Tadros
Licensed content date	May 1987
Licensed content volume number	117
Licensed content issue number	1
Number of pages	17
Start Page	205
End Page	221
Type of Use	reuse in a thesis/dissertation
Portion	figures/tables/illustrations
Number of figures/tables/illustrations	2

Format	both print and electronic
Are you the author of this Elsevier article?	No
Will you be translating?	No
Title of your thesis/dissertation	Electrical Characterization of Hybrid Electonic Materials
Expected completion date	May 2014
Estimated size (number of pages)	100
Elsevier VAT number	GB 494 6272 12
Price	0.00 USD
VAT/Local Sales Tax	0.00 USD / 0.00 GBP
Total	0.00 USD

This is an Agreement between Kalyan Kanakamedala ("You") and Elsevier ("Elsevier"). It consists of your order details, the terms and conditions provided by Elsevier, and the payment terms and conditions.

All payments must be made in full to CCC. For payment instructions, please see information listed at the bottom of this form.

Supplier	Elsevier The Kidlington,Oxford,OX5 1GB,UK
Registered Company Number	1982084
Customer name	Kalyan Kanakamedala
Customer address	3101, Patrick F Taylor Hall, BATON ROUGE, LA 70820
License number	3642660297320
License date	Jun 05, 2015
Licensed content publisher	Elsevier
Licensed content publication	Surface Science Reports
Licensed content title	Force-distance curves by atomic force microscopy
Licensed content author	B. Cappella,G. Dietler
Licensed content date	1999
Licensed content volume number	34
Licensed content issue number	1-3
Number of pages	104
Start Page	1
End Page	104
Type of Use	reuse in a thesis/dissertation
Portion	figures/tables/illustrations
Number of figures/tables/illustrations	1
Format	both print and electronic
Are you the author of this Elsevier article?	No
Will you be translating?	No
Original figure numbers	figure 2
Title of your thesis/dissertation	Hybrid Electronic Materials: Characterization

	and Thin-film deposition
Expected completion date	Aug 2015
Estimated size (number of pages)	100
Elsevier VAT number	GB 494 6272 12
Price	0.00 USD
VAT/Local Sales Tax	0.00 USD / 0.00 GBP
Total	0.00 USD

This is an Agreement between Kalyan Kanakamedala ("You") and Elsevier ("Elsevier"). It consists of your order details, the terms and conditions provided by Elsevier, and the payment terms and conditions.
All payments must be made in full to CCC. For payment instructions, please see information listed at the bottom of this form.

Supplier	Elsevier The Kidlington,Oxford,OX5 1GB,UK
Registered Company Number	1982084
Customer name	Kalyan Kanakamedala
Customer address	3101, Patrick F Taylor Hall, BATON ROUGE, LA 70820
License number	3258090326490
License date	Oct 29, 2013
Licensed content publisher	Elsevier
Licensed content publication	Journal of Electrostatics
Licensed content title	Electrospraying route to nanotechnology: An overview
Licensed content author	A. Jaworek,A.T. Sobczyk
Licensed content date	March 2008
Licensed content volume number	66
Licensed content issue number	3–4
Number of pages	23
Start Page	197
End Page	219
Type of Use	reuse in a thesis/dissertation
Intended publisher of new work	other
Portion	figures/tables/illustrations
Number of figures/tables/illustrations	1
Format	both print and electronic
Are you the author of this Elsevier article?	No
Will you be translating?	No
Title of your thesis/dissertation	Electrical Characterization of Hybrid Electonic Materials

Expected completion date	May 2014
Estimated size (number of pages)	100
Elsevier VAT number	GB 494 6272 12
Price	0.00 USD
VAT/Local Sales Tax	0.00 USD / 0.00 GBP
Total	0.00 USD

APPENDIX D: PERMISSION TO REPRINT FROM SPRINGER

This is a License Agreement between Kalyan Kanakamedala ("You") and Springer ("Springer") provided by Copyright Clearance Center ("CCC"). The license consists of your order details, the terms and conditions provided by Springer, and the payment terms and conditions.

All payments must be made in full to CCC. For payment instructions, please see information listed at the bottom of this form.

License Number	3664970712562
License date	Jul 09, 2015
Licensed content publisher	Springer
Licensed content publication	Electronic Materials Letters
Licensed content title	Electro-optical characterization of cyanine-based GUMBOS and nanoGUMBOS
Licensed content author	Anirban Sarkar
Licensed content date	Jan 1, 2014
Volume number	10
Issue number	5
Type of Use	Thesis/Dissertation
Portion	Figures
Author of this Springer article	Yes and you are a contributor of the new work
Order reference number	None
Original figure numbers	figures 2,3
Title of your thesis / dissertation	Hybrid Electronic Materials, Characterization and Thinfilm depositon
Expected completion date	Aug 2015
Estimated size(pages)	100
Total	0.00 USD

This is a License Agreement between Kalyan Kanakamedala ("You") and Springer ("Springer") provided by Copyright Clearance Center ("CCC"). The license consists of your order details, the terms and conditions provided by Springer, and the payment terms and conditions.

All payments must be made in full to CCC. For payment instructions, please see information listed at the bottom of this form.

License Number	3664970986493
License date	Jul 09, 2015
Licensed content publisher	Springer
Licensed content publication	Electronic Materials Letters
Licensed content title	Electro-optical characterization of nanoGUMBOS
Licensed content author	A. Sarkar
Licensed content date	Jan 1, 2014
Volume number	10
Issue number	4
Type of Use	Thesis/Dissertation
Portion	Figures
Author of this Springer article	Yes and you are a contributor of the new work
Order reference number	None
Original figure numbers	figure 4
Title of your thesis / dissertation	Hybrid Electronic Materials, Characterization and Thinfilm depositon
Expected completion date	Aug 2015
Estimated size(pages)	100
Total	0.00 USD

APPENDIX E: LETTERS OF PERMISSION

Kalyan Kanakamedala <kalyan.kanakamedala@gmail.com> Jun 28, 2015 at 2:49 PM

To: EML <eml@kim.or.kr>
Dear Dr. Jaegab Lee, Editor-in-Chief, EML

I am the first author of the manuscript entitled, "Study of Electrospray AssistedElectrophoretic Deposition of Carbon Nanotubes on Insulator Substrates" [EML-15-108]. This article was accepted without further revision, as of July 23rd 2015, in Electronic Materials Letters. I am contacting you to request permission to use this article in my dissertation, which I am writing as we speak. Please let me know what forms and information are necessary to make this possible.

Thank you,
Kalyan Kanakamedala
PhD Candidate
Division of Electrical and Computer Engineering,
Louisiana State University

SeoYoungKang(강서영) <eml@kim.or.kr> Mon, Jun 29, 2015 at 2:30 AM
To: Kalyan Kanakamedala <kalyan.kanakamedala@gmail.com>
Dear sir,

Hello. This is Kang Seo-young from EML EDITORIAL OFFICE.

I received your E-mail well.
Regarding your manuscript ID [EML15-108],

It is allowed to use the manuscript for any purpose such as dissertation because it was already accepted.

If the article publish in online, you could search this article in the springer website.

Thanking you
If you have any questions, please contact me via E-mail
With the best regards,
Kang Seo-young
EML Editorial Office
E-mail: eml@kim.or.kr

APPENDIX F: PUBLICATIONS, TECHNICAL DISCLOSURES, AND PRESENTATIONS

Refereed Journal Articles

1. Sarkar, K. Kanakamedala, M. D. Rajathadripura, N. N. Jagadish, P. K. S. Magut, S. de Rooy, S. Das, B. El-Zahab, I. M. Warner, and T. Daniels-Race, *Electro-Optical Characterization of NanoGUMBOS*," Electronic Materials Letters, 775-781, 10(4), 2014
2. Sarkar, K. Kanakamedala, N. N. Jagadish, A. Jordan, S. Das, N. Siraj, I. M. Warner, and T. Daniels-Race, *Electro-Optical Characterization of Cyanine-Based GUMBOS and nanoGUMBOS*, Electronic Materials Letters, 879-885, 10(5), 2014
3. K. Kanakamedala, J. Desoto, A. Sarkar, T. Daniels-Race, *Study of Electrospray assisted Electrophoretic deposition of Carbon Nanotubes on Insulator Substrates,* Electronic Materials Letters (accepted as of June 2015)
4. K. Kanakamedala, S. D. Rooy, S. Das, B. El-Zahab, I. M. Warner, T. Daniels-Race, *Electrical and Optical Properties of [R6G][TPB] Nanowires* (in submission process)

Technical Disclosures

T. Daniels-Race, K Kanakamedala, C. O'Loughlin, *Faraday Electrospraying and Electrospinning*, LSU File no: 1549, 2015

Oral and Poster Presentations

1. T. Daniels-Race, K. Kanakamedala, N. N. Jagadish, S. L. deRooy, A. Jordan, S. Das, B. El-Zahab, and I. M. Warner, *Electrical Characterization of NanoGUMBOS*, Organic Microelectronics and Optoelectronics Workshop VII, San Francisco, CA, July 18-20, 2011
2. K. Kanakamedala, S. L. deRooy, S. Das, B. El-Zahab, I. M. Warner, and T. Daniels-Race, *Determination of the Current-Voltage Signatures of NanoGUMBOS,* 78th Annual Meeting of the Southeastern Section of the American Physical Society," Roanoke, VA, October 19-22, 2011
3. K. Kanakamedala, N. Siraj, M. Divakar, F. Hasan, S. Das, Susmita; I. Warner, T. Daniels-Race, *Morphology and Conductivity Studies on Carbazole Based GUMBOS Thin Films*, 79th Annual Meeting of the Southeastern Section of the APS, Tallahassee, FL, November 14- 17, 2012
4. G. King, K. Kanakamedala, H. Wang, and T. Daniels-Race, *A Study of Fluorescence Spectroscopy as Motivated by Next-Generation Nanoscale Electronic Device Development*, The LSU Undergraduate Research Conference (URC): Excite/Explore/Experiment, Louisiana State University, Baton Rouge, LA, October 26, 2012
5. N. Siraj, S. Das, F. Hasan, K. Kanakamedala, T. Daniels-Race, and I. M. Warner, *Evaluation of Thin Films Based on Fluorescent and Conductive GUMBOS*, Abstracts of Papers of the American Chemical Society 245, 2013

6. M. D. Rajathadripura, K. Kanakamedala, and T. Daniels-Race, *Characterization of Surface Morphology of Biopolymer Coated Substrates using Non-contact Atomic Force Microscopy*, 16th International Conference on Non-Contact Atomic Force Microscopy, Hyattsville, MD, August 5-9, 2013
7. K. Kanakamedla, T. Daniels-Race, *Alternative method of Electrospraying for scalable deposition of nanomaterials,* 81st Annual Meeting of the Southeastern Section of the American Physical Society," Columbia, SC, November V-59, p-18, 2014

VITA

Kalyan Chakravarthy Kanakamedala was born to Rajeswari and Nageswara Rao, in Nelipaka Banjar, Telangana, a southern state of India. He grew up in Aswapuram, Telangana and did his schooling in Kendriya Vidyalaya, Khammam. He received his Bachelors (B.Tech, *Distinction*) in Electronics and Communication Engineering from Jawaharlal Nehru Technological University, India, in May 2008. He joined Lousiana State University, Baton Rouge to pursue his graduate studies in spring 2009. He began his Masters research under the mentorship of Dr. Theda Daniels-Race in spring 2010. He began his doctoral studies in hybrid electronic materials in fall 2011 under metorship of Dr.Theda Daniles-Race. His research interests lie in electrospraying, carbon nanotubes, large-scale thin-film deposition, emerging semiconductor materials, semiconductor processing, characterization and fabrication techniques.